ADVANCED MASTERS IN STRUCTURAL ANALYSIS
OF MONUMENTS AND HISTORICAL CONSTRUCTIONS

Master's Thesis

Alejandro Jiménez Rios

Simulation of structural behavior of masonry using discrete element modeling

UPC
UNIVERSITAT POLITÈCNICA
DE CATALUNYA

Czech Technical University

Education and Culture

Erasmus Mundus

ADVANCED MASTERS IN STRUCTURAL ANALYSIS
OF MONUMENTS AND HISTORICAL CONSTRUCTIONS

Master's Thesis

Alejandro Jiménez Rios

Simulation of structural behavior of masonry using discrete element modeling

Spain | 2016

DECLARATION

Name: Alejandro Jiménez Rios

Email: aljr_2801@outlook.com

Title of the
Msc Dissertation: Simulation of structural behavior of masonry using discrete element modeling

Supervisor(s):   Sergio Henrique Pialarissi Cavalaro, Pere Roca Fabregat

External supervisor: Ricardo Pieralisi

Year: 2016

I hereby declare that all information in this document has been obtained and presented in accordance with academic rules and ethical conduct. I also declare that, as required by these rules and conduct, I have fully cited and referenced all material and results that are not original to this work.

I hereby declare that the MSc Consortium responsible for the Advanced Masters in Structural Analysis of Monuments and Historical Constructions is allowed to store and make available electronically the present MSc Dissertation.

University: Polytechnic University of Catalonia

Date: 15/07/16

Signature:

_____

ACKNOWLEDGEMENTS

ABSTRACT

The structural simulation of masonry elements has been traditionally conducted with Finite Element Models (FEM). Studies from the literature show that these models are capable of accurately reproduce the structural behavior at a micro and macro-scale levels. Despite the good results obtained, the application of FEM implies simplifications regarding the failure modes and the constitutive laws used to represent the behavior of bricks and mortar, as well as the interface between them. Alternative methods are available nowadays for the same purpose. An example is the Discrete Element Model (DEM) that is based on a particle-particle interaction. The simple definition of the interactions in the DEM is an advantage for the simulation of masonry elements.

The objective of this master thesis is to evaluate the applicability of DEM to simulate the structural behavior of masonry at a micro and macro-scale level, reproducing the response in terms of deflections, ultimate load and failure modes.

First, a review on the literature about DEM and about its application to the analysis of masonry structures was performed. Then, experimental programs conducted by other authors were selected and taken as a reference. Next, the tests found in these experimental programs were simulated with DEM. The numerical results were compared with the experimental data in order to highlight the accuracy, advantages and drawbacks of this approach. A parametric study was as well conducted to evaluate the sensibility of the results to changes in the input parameters of the model. Finally, further research proposals are presented in order to explore in a deeper and more extended way the topics presented on this dissertation

It was found that the use of DEM to simulate the structural behavior of masonry at a micro and macro-scale level, reproducing the response in terms of deflections, ultimate load and failure modes presents quite good results. Good agreement was shown in the description of failure modes and low percentage errors (below 10 %) were found on the computation of the parameters of interest such as strength of the material and maximum resistant load.

RESUMEN

La simulación estructural de elementos de mampostería se ha realizado tradicionalmente con modelos de elementos finitos (FEM, por sus siglas en inglés). Los estudios de la literatura muestran que estos modelos son capaces de reproducir con precisión el comportamiento estructural a micro y macro-escala. A pesar de los buenos resultados obtenidos, la aplicación de FEM implica simplificaciones con respecto a los modos de falla y a las leyes constitutivas utilizadas para representar el comportamiento de ladrillos y mortero, así como la interfaz entre ellos. Métodos alternativos están disponibles hoy en día para el mismo propósito. Un ejemplo es el Método de los Elementos Discretos (DEM, por sus siglas en inglés) que se basa en una interacción partícula-partícula. La definición simple de las interacciones en el DEM es una ventaja en la simulación de elementos de mampostería.

El objetivo principal de esta tesis es evaluar la aplicabilidad de DEM para simular el comportamiento estructural de la mampostería a un nivel de micro y macro-escala, y reproducir la respuesta del material en términos de desplazamientos, carga última y modos de falla.

En primer lugar, se realizó una revisión de la literatura sobre el DEM y sobre su aplicación al análisis de estructuras de mampostería. A continuación, un programa experimental llevado a cabo por otros autores fue seleccionado y tomado como referencia. Después, las pruebas de laboratorio realizadas en dicho programa experimental se simularon con DEM. Los resultados numéricos obtenidos se compararon con los datos experimentales con el fin de poner en relieve la precisión, ventajas y desventajas del enfoque DEM. Se llevó a cabo además un estudio paramétrico para evaluar la sensibilidad de los resultados a los cambios en los parámetros de entrada del modelo. Finalmente, una serie de propuestas para futuras investigaciones es presentada con el fin de explorar más a detalle y de forma extendida los temas tratados en la presente tesis.

Se encontró que el uso de DEM para simular el comportamiento de la mampostería a niveles micro y macro-escala, reproduciendo la respuesta en términos de desplazamientos, carga última y modos de falla, presenta buenos resultados. Concordancia en la descripción de los modos de falla y valores bajos de errores porcentuales (debajo del 10 %) fueron encontrados en el cálculo de los parámetros de interés como lo son la resistencia de los materiales y la carga última soportada.

TABLE OF CONTENTS

LIST OF FIGURES

LIST OF TABLES

1. INTRODUCTION

Cultural (or architectural) heritage involves monuments, groups of buildings and sites which are of outstanding universal value from the point of view of history, art or science (UNESCO, 1972). The conservation of cultural heritage involves all the efforts designed to understand it, know its history and meaning, ensure its material safeguard and, as required, its presentation, restoration and enhancement (ICOMOS, 1994).

Its importance is based on the fact that all cultures and societies are based in their own and diverse forms of tangible and intangible heritage. It represent "an irreplaceable source of spiritual and intellectual richness". It was stablished by UNESCO that "the cultural heritage of each is the cultural heritage of all" and that the different cultural expressions of each society deserve the acknowledgment and respect form all the other pairs. Conservation of cultural heritage should always be supported and encouraged in order to preserve such social values (ICOMOS, 1994).

Furthermore, cultural heritage represent nowadays a key point for attracting tourism and for the generation of wealth. The building industry and tourism represents about 15-20% of the GNP in Europe. As the built environment ages, conservation of existing buildings and infrastructure is receiving more and more attention, reaching an average value of 1/3 of the market in Europe. Being monuments and historical centers main attractors for tourism, their conservation is not only a social demand but also an economical one (SAHC, s.f.).

Due to its nature and history, cultural heritage structures cannot be studied with the use of modern legal codes and standards. That is why a series of principles and guidelines have been presented by the ISCARSAH committee in order to stablish rational methods of analysis and repair appropriate for such cases. In its general criteria principles it stablished the following steps that need to be followed in order to best study and intervene on heritage structures (ISCARSAH, 2003):

- Inspection
- Diagnosis
- Intervention
- Control

Diagnosis involves the identification of causes of damage and decay and the characterization of the present condition of the structure (SAHC, 2015-2016). The diagnosis step can be divided into two main branches: qualitative and quantitative. The qualitative part consist of the historical research of the structure and its present condition inspection. Whereas that the quantitative one consist of monitoring and structural modeling (see Figure 1). Historical research, present condition inspection as well as monitoring provide empirical evidence to the study of the structure. On the other hand,

structural modeling is based on hypothesis. All these phases of study allow to conclude about the condition of the building and infer about possible optimal interventions.
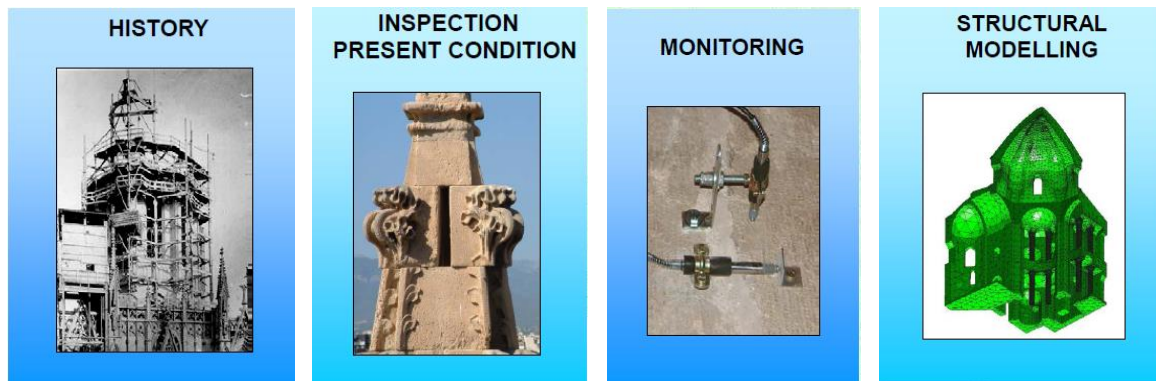
Figure 1: Stages of the diagnosis of historical constructions (SAHC, 2015-2016).

Structural modeling contributes with the simulation of the performance of the structure subjected to past, present and future actions (SAHC, 2015-2016). It is carried out through a process in which basically a physical problem is simplified into a mathematical one with the use of a series of assumptions and hypothesis. Then the mathematical problem can be solved either analytically or numerically. Finally results such as displacements, ultimate load capacity and failure mechanisms among others can be interpreted and used for several purposes like safety evaluation and design of the intervention on cultural heritage structures. Figure 2 shows this process in a graphical way.
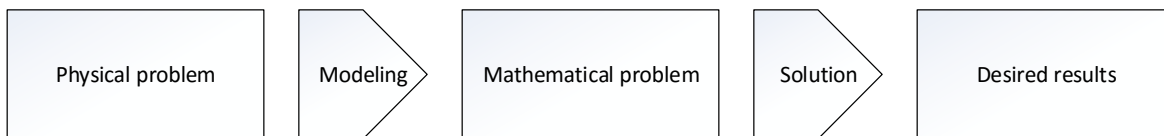
Figure 2: Structural modeling process.

It is on this key stage of the conservation of cultural heritage (structural modeling) that this dissertation tries to make a contribution. By proposing the application of an alternative technique to approach from a different angle a common engineering conservation problem. It may present certain benefits depending on the specific characteristic of different case studies. Nevertheless, since the range that heritage structures encompass from the point of view of the huge variety of materials and uncountable structural elements, trying to cover all of them will be an impossible task. That is why this work is limited to the study of modeling techniques for the simulation of the behavior of masonry. The study will only include simple one leaf brick masonry walls with mortar acting as the binder element. Both components will be modeled and discretized on 3D with its respective mechanical characteristic. The analysis will be non-linear and by the nature of the proposed approach, loads or displacements will vary on time.

1.1 Problem description

Masonry is one of the oldest construction techniques. Its manufacture process is quite simply and it can be produced with local materials. Thanks to these factors it became one of the ancient most used and widespread techniques of construction and it is still widely used in our times. It is highly durable, resistant and efficient. A great number of cultural heritage structures have been built with the use of this material.

The structural simulation of masonry elements has been traditionally conducted with Finite Element Models (FEM). Studies from the literature show that these models are capable of accurately reproduce the structural behavior at a micro and macro-scale levels. Despite the good results obtained, the application of FEM implies simplifications regarding the failure modes and the constitutive laws used to represent the behavior of bricks and mortar, as well as the interface between them. Alternative methods are available nowadays for the same purpose. An example is the Discrete Element Model (DEM) that is based on a particle-particle interaction. The simple definition of the interactions in the DEM is an advantage for the simulation of masonry elements.

DEM will be implemented to carry out a 3D detailed micro-modeling of masonry. Micro-modeling techniques aim to provide a high level of accuracy and reliability for the study of complex phenomena related to stress-strain states at a micro-scale level. The application of this method for the simulation of masonry is proposed based on the existing need for a better understanding of its microstructural behavior as remarked by (Recarey, et al., 2005). A micro-modeling approach will be followed since this is probably the most accurate tool available to simulate the real behavior of masonry. DEM application to the study of masonry is expected to provide good results since according with some authors, (Bui, et al., 2014), this is one of the best adapted tools for the study of heterogeneity materials specially to reproduce the non-linear behavior that characterize the response of this kind of material beyond the elastic phase.

1.2 Objectives

1.2.1 General objective

The general objective of this master thesis is to evaluate the applicability of DEM to simulate the structural behavior of masonry at a micro and macro-scale level, reproducing the response in terms of deflections, ultimate load and failure modes.

1.2.2 Specific objectives

In order to achieve the general objective a series of specific objectives has been stablished. Such intermediate steps helped to achieve the aim of this dissertation in an organized and concise way.

Each specific objective presented important results and allowed to evaluate the progress accomplished after each milestone of the research. The specific objectives are:

- Modify the constitutive law developed by (Smilauer, 2010) (originally used to model concrete) in order to be able to reproduce the structural behavior of masonry.
- Simulate and calibrate simple compression cube tests, compression cylinder tests and three points bending tests for both mortar and brick.
- Simulate and calibrate triplets test for composite shear behavior of masonry.
- Carry on a parametric analysis in order to study the influence of the size of the particles and the influence of simplified "2D" models (2D models are referred in this context to the simplification on the representation of the thickness of the specimens by only one layer of spheres) to describe the behavior of 3D specimens.
- Compare the results obtained by DEM simulations with those presented by (Marastoni , 2016) from experimental campaigns and FEM simulations.

1.3   Methodology

First, a review on the literature about DEM and about its application to the analysis of masonry structures was performed. Several papers presented on the last years by different authors about masonry modelling were found and summarized into a table with the most important characteristics of every different approach. This allowed us to identify the gaps of knowledge in the field and propose an alternative to study the behavior of masonry. General and specific objectives were stablished at this stage of the dissertation as well.

Then, an experimental program conducted by other authors was selected and taken as a reference. A research developed at the Department of Construction Engineering of the Polytechnic University of Catalonia (UPC) and presented by (Canella, 2014) and (Marastoni , 2016) was picked out. Besides from experimental results, (Marastoni , 2016) carried out a FEM analysis of the behavior of masonry therefore allowing us to make a comparison between the three procedures (DEM and FEM simulations as well as experimental results).

Next, the tests found in these experimental programs were simulated with DEM. The numerical results were compared with the experimental data as well as with the FEM simulations as mentioned before in order to highlight the accuracy, advantages and drawbacks of DEM approach.

A parametric study was also conducted to evaluate the sensibility of the results to changes in the input parameters of the model. The influence of the spheres size as well as the influence on the thickness reduction of specimens (in order to reduce computational cost) was analyzed.

Finally conclusions were deduced and stablished based on all the previous steps. Answers to the general and specific objectives, stablished at the state of the art stage, are also provided on this final point. The followed methodology is presented in Figure 3.
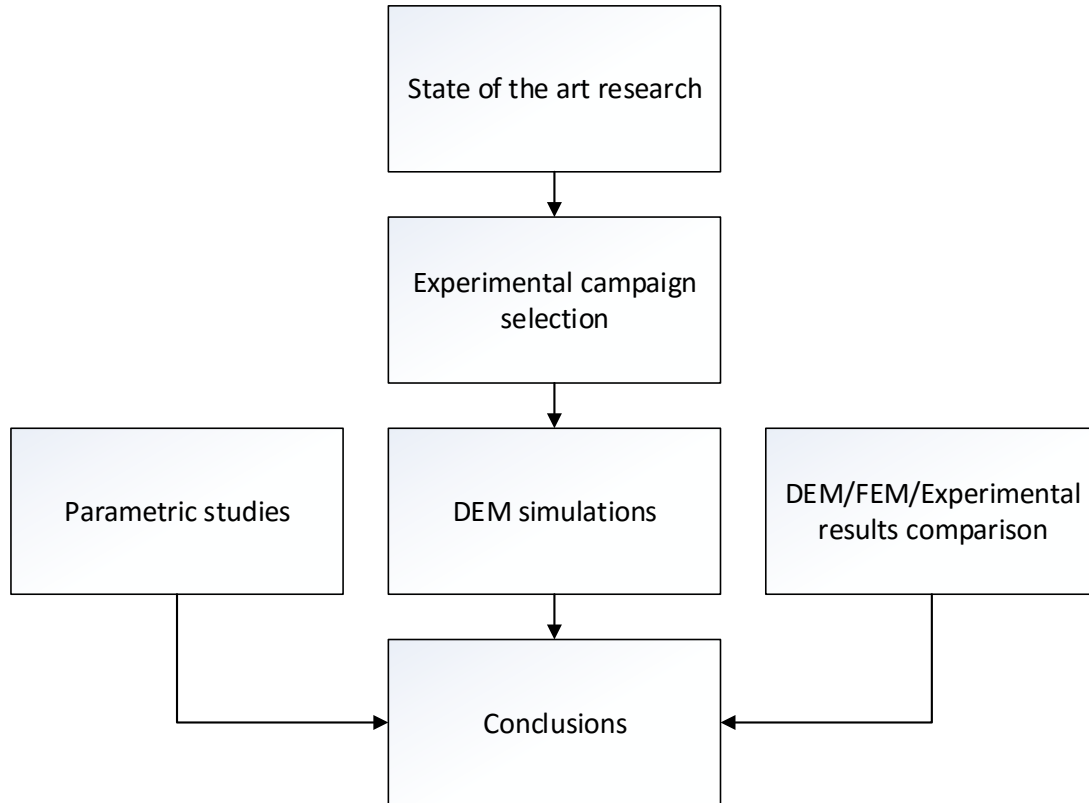
Figure 3: Methodology flowchart.

1.4   Outline of the document

This document is simply composed of five chapters. The first one deals with the general introduction in which problem, objectives and followed methodology are described.

On the second chapter the state of the art research conducted is presented. Basic concepts about the structural behavior of masonry as well as the available modeling techniques to describe such structures are introduced in this chapter. Since this dissertation deals with DEM, more details will be shown about DEM aspects and its different modeling strategies. Finally, a concise literature review has been summarized in a table in order to mention the most advanced projects developed by different researches concerning masonry modeling topics. Based on the lack of information found about certain modeling strategies it was decided to carry on a 3D detailed micro-modeling of masonry with the use of DEM.

Chapter three presents the theoretical framework behind the DEM and its application on Yade (open source software used to carry out the simulations of this thesis). All the concepts presented there are taken from (Smilauer, 2010) and (Smilauer, 2015). The constitutive law used to describe the behavior of masonry is as well described on detail including a number of modification applied to it in order to adapt it to better describe the behavior of masonry since it was originally developed to model concrete.

The main job performed during this dissertation is included on chapter four. It consist in the presentation of the experimental campaign taken as reference from (Canella, 2014) and (Marastoni , 2016), the description of the carried out numerical simulations with DEM as well as the parametric analysis, comparison of results between DEM, FEM and experimental campaign results and the conclusions stablished after this work.

Chapter five includes the presentation of general conclusions regarding both specific and general objectives as well as the future research perspectives proposals in order to explore in a deeper and more extended way the topics presented on this dissertation.

2.   STATE OF THE ART

2.1   Introduction

In this chapter basic general ideas about masonry will be presented. A broad discussion about the structural behavior of masonry as well as the nowadays available modeling techniques will be shown in section 2.2 and section 2.3 respectively. Further insight on DEM features is shown in section 2.4. This three sections have an introductory role in order to better locate and understand the information found and presented on the state of the art research section.

Section 2.5 presents a concise literature review summarizing in a table the most advanced projects developed by different researches concerning masonry modeling topics Finally a discussion about the before mentioned analyzed aspects will be given in section 2.6.

2.2   Masonry structural behavior

Masonry is a composed material integrated by units and binder. Units can be represented by stone, bricks, adobe or combination of such elements. Binder is usually present in the form of mortar, either lime or cement mortar, but in some cases, usually in stone masonry, there is no binder and it is designated as dry masonry. As for any composite material, the mechanical properties of masonry depend on the properties of its components. Bricks have an important role especially under crushing and tensile cracking failure modes. Whereas that mortar joints act as weakness planes under shear loads (Vasconcelos, s.f.).

It is a material with good compression strength but with almost negligible tensile capacity. It presents a brittle failure in tension and a frictional failure mode when it is subjected to shear forces. It is an anisotropic material which means that its mechanical characteristics change based on the orientation of the applied loads. Accurate and efficient simulation of masonry response is still a challenge and needs further experimental and theoretical developments (Roca, et al., 2010).

Figure 4 shows the general behavior of masonry under tension, compression, pure shear and combined compression-shear stresses. When masonry is loaded under pure tension the failure appears as a crack on the tangential direction of the applied force. Whereas that for compression stresses cracks usually appear parallel to the direction of the load. When subjected to shear, masonry usually fails in the interface between the mortar and the bricks. If compression is applied while shearing, the shear strength of masonry is increased considerably due to the increment on the friction forces among its different components (SAHC, 2015-2016).
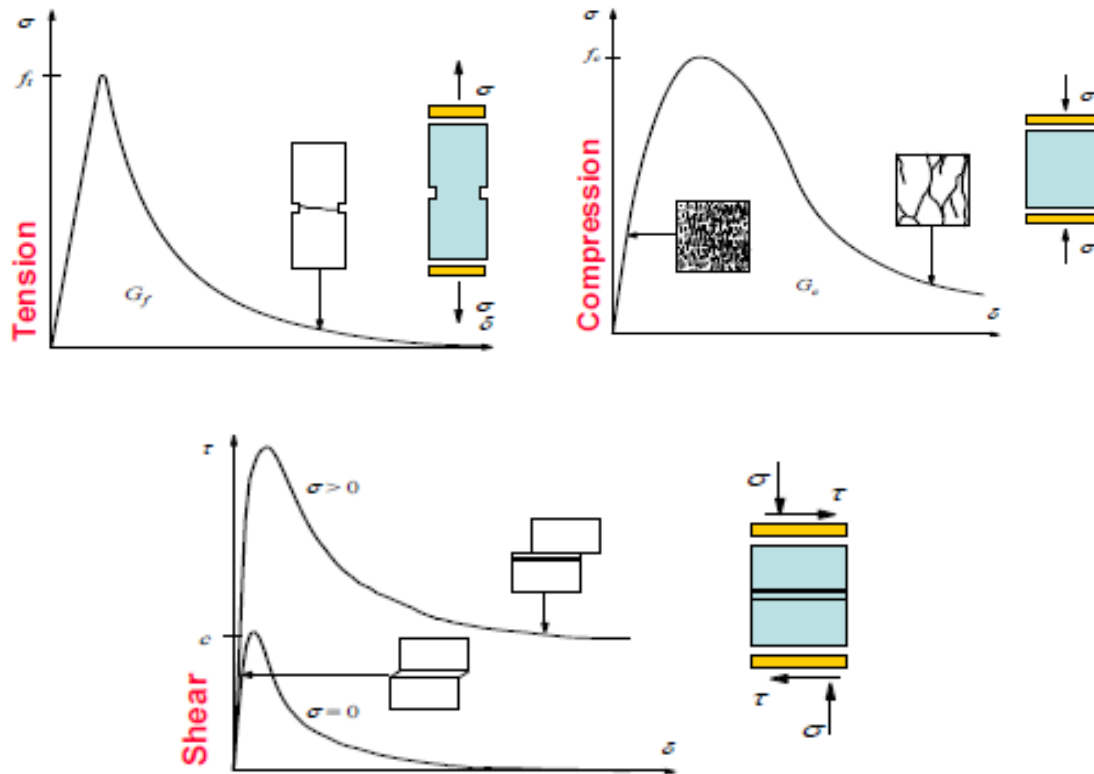
Figure 4: General behavior of masonry under tension, compression and shear stresses (SAHC, 2015-2016).

Several laboratory setups have been developed and implemented by different researchers in order to determine compression, tension, shear and flexural strength of masonry. The most common ones are presented in Figure 5. Special attention was paid on this work to the triplet test since data was available and provided from past experimental campaigns performed at UPC. This type of experiment allows to determine the ultimate load resisted by the specimen under three different levels of pre-compression and will be presented in more detail in a further section.

2.2.1   Mechanical properties of masonry components

The most important brick mechanical properties to model the behavior of masonry are its compressive and tensile strength as well as its modulus of elasticity. According to the European standards the compressive strength and the modulus of elasticity of the units can be obtained with a uniaxial compressive test. For modern materials it is common to obtain average compressive strengths of 10 MPa or higher, on the other hand, in the case of historical masonry's units, such high values are less probable to be reached (Vasconcelos, s.f.).
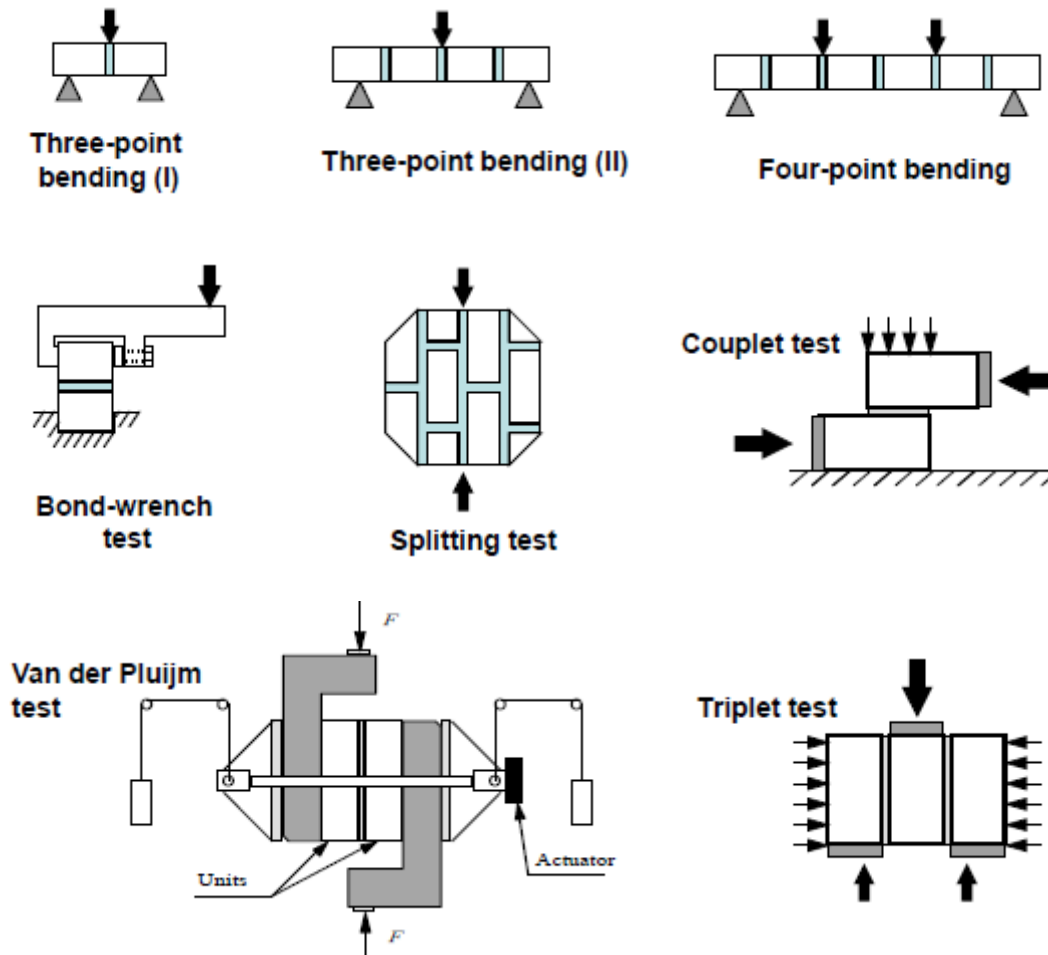
Figure 5: Typical laboratory setups to determine masonry resistance properties (SAHC, 2015-2016).

The main function of mortar in the composite behavior of masonry lays on its role to transfer stresses among the units in a more uniform way thus avoiding stress concentration that may lead to an unanticipated failure of the material. Compressive strength and bond are two important mechanical properties to describe the behavior of mortar. The last one depends on the mechanical interlocking between mortar and bricks and determine its adherence. It also has an important role on the durability of masonry (Vasconcelos, s.f.).

2.2.2 Masonry composite compressive strength f_k

This mechanical property is essential for the structural stability of masonry and also characterize its structural quality. The general stress state of masonry under compression loads is shown in Figure 6. Since generally mortar has lower modulus of elasticity than the units it presents a tri-axial compression state due to the fact that it tends to expand laterally and it is restrained by the units. Therefore the units experience a compression-lateral tension stress state as it can be seen on Figure 6. Such stress state leads to a vertical cracking of the units. This behavior has been largely observed

by experimental testing campaigns of masonry. The compressive strength of masonry is always lower than the compressive strength of bricks and higher than the compressive strength of mortar (Vasconcelos, s.f.).
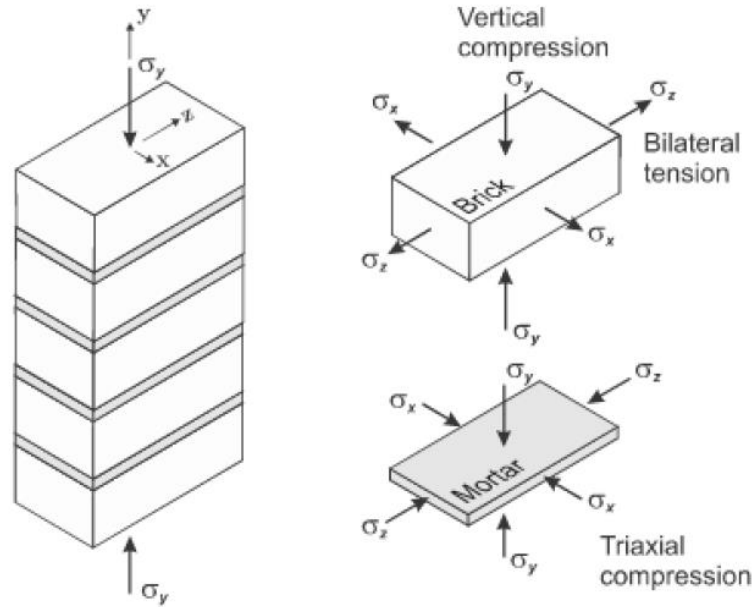
Figure 6: Stress state of masonry under uniaxial compression forces (Canella, 2014).

Eurocode 6 (EC6, 1996) provides formula (1) to compute the compressive strength of masonry, f_k based on the corresponding compressive strength of brick, f_b, and mortar, f_m:

$$f_k = K * f_b^{0.7} * f_m^{0.3}$$ (1)

Where K is a coefficient that depends on several factors (see Eurocode 6 for more details).

2.2.3   Masonry composite shear strength f$_{vk}$

When subjected to combined in-plane loading, shear and flexure resisting mechanisms characterize the response of masonry walls. Usually for low and/or high pre-compressed loading a shear resisting mechanism will develop whereas that for slender and/or low pre-compressed loading a flexural resisting mechanism is more likely to occur. Diagonal cracks, aligned with the compressive strut and open due to the presence of tensile stresses perpendicular to the strut direction, are associated to a shear resisting mechanism (Vasconcelos, s.f.). A formula to compute the shear strength of masonry is provided on equation (2) also by Eurocode 6 (EC6, 1996):

$$f_{vk} = f_{vko} + 0.4 * \sigma_d$$ (2)

Where f_{vko} is the cohesion, 0.4 is the tangent of the friction angle and σ_d is the normal stress level. Typically f_{vko} assumes a value between 0.15 and 0.3 N/mm2, and the maximum value of the shear

strength is in the range 1.0 – 1.5 N/mm2. For old masonry with weak mortars, a value of 0.05 – 0.1 N/mm2 is recommended for f_{vko}. The tangent of the friction angle should be reduce to 0.3 (irregular coursed stone) and 0.2 (rubble masonry) (SAHC, 2015-2016).

2.2.4 Masonry composite flexural strength

The flexural strength of masonry can be determined on two main directions. Such directions are shown in Figure 7. Flexural tensile strength is given by Eurocode 6 (EC6, 1996), ranging from $f_{xk1} = 0.05 - 0.20 \, N/mm^2$. When the plane of failure is parallel to the bed joints, and $f_{xk2} = 0.10 - 0.40 \, N/mm^2$, when the plane of failure is perpendicular to the bed joints. For rubble masonry f_{xk2} should be taken equal to f_{xk1}. For the Young's modulus E, a value of 1000*f_k is recommended, whereas the shear modulus G should be taken equal to $0.5 * E$ (SAHC, 2015-2016).
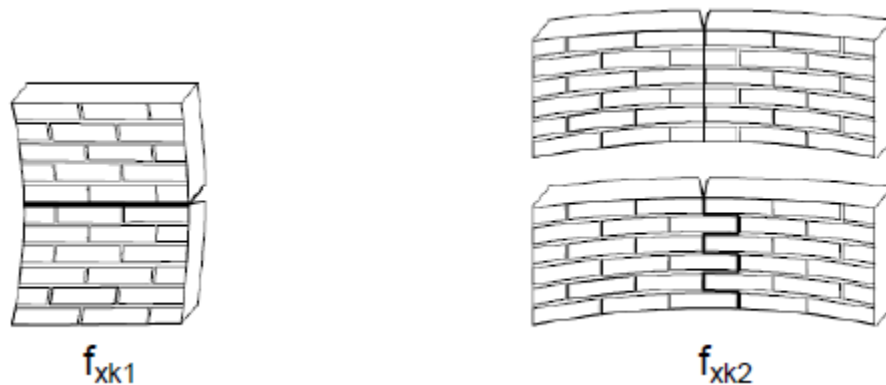
Figure 7: Principal directions to determine masonry flexural strength (SAHC, 2015-2016).

2.3 Masonry modeling techniques

Nowadays a huge variety of tools is available for the structural modeling of masonry structures. They encompass a wide range of complexity, time-cost and access for practitioners. In order to select the most adequate one according to each study case the next aspects need to be considered (SAHC, 2015-2016):

- The relationship between the tool and the sought information.
- Availability of the tool and its full understanding from the part of the designer.
- Cost, available resources and time for analysis.

The complexity of the different approaches depends on the simplifications made at material and structural level. Moreover, the study of heritage structures presents also another kind of factors that need to be taken into account in order to obtain adequate results. Such factors are (Roca, et al., 2010):

- *Geometry:* 1D, 2D or 3D dimensions (one of the minor challenges to be faced by analysis).

- *Morphology and connections:* Extremely demanding from a computational point of view. The main difficulty is to find their physical characteristics and mechanical properties by means of minimal invasive methods.

- *Actions:* Past, present and possible future actions (accidental or change of use). Load history has to be taken into account and has a paramount role on the study of heritage structures.

- *Damage and alterations:* Modeling of such factors is necessary to obtain accurate and realistic results. Such factors are usually present in heritage structures in the form of mechanical cracking and material decay.

- *History:* It is considered as a real time-scale experiment. Used to deduce the present structural state and behavior of the building. Can be used to infer qualitatively needed insufficient data.

Masonry modeling techniques can basically be grouped in three large categories; classical methods, FEM and DEM (Roca, et al., 2010). They will be described in more detail in the following sections.

2.3.1   Classical methods

Geometric and empirical rules

This rules have no scientific or rational base and were determined by observation and empirical experiences. They are based on the behavior of previous successful structures and comparison between buildings. They were normally stablished as a relationship and proportions among different geometrical parts of the structure. Notwithstanding, they succeeded in producing safe structures and such criteria is still valid nowadays. Geometric and empirical rules can be used together with more modern and sophisticated approaches in order to assess historical masonry structures (SAHC, 2015-2016).

Graphic statics and limit analysis

It is a powerful tool used nowadays. It can describe the safety level and the collapse mechanism of a structure. It is usually applied to obtain a first overall understanding of the behavior and state of the structure. Accurate formulations of the method were provided during the 19th century by Gerstner (Germany), Méry (France) and Moseley (England). Its modern formulation was stablished by Heyman in 1966 and is based on the next hypotheses:

- Masonry has null tensile strength.
- The compression strength of the material is infinite.
- Sliding between blocks is impossible.

Derived from this assumptions three theorems were stablished (named lower bound, upper bound and uniqueness theorems) in order to determine the stability of a structure (SAHC, 2015-2016).

Matrix methods

This tool is in principle only applicable to skeletal structures (2D or 3D linear members' assemblies). Nevertheless, a generalized matrix formulation for the analysis of masonry structures was developed by Roca et al. (Roca, et al., 2005). It implements curved linear elements with a variable cross-section to simulate elements such as walls and vaults. Material behavior is described as elastoplastic in compression and shear and as perfectly brittle in tension. This method partly overcome the limitations of linear elastic analysis and limit analysis and at the same time it is still computationally affordable (SAHC, 2015-2016).

Linear elastic analysis

It is a conservative approach which is not able to represent appropriately the behavior of masonry. Nevertheless, it can be used as an auxiliary tool in order to evaluate the definition of meshes, values and distributions of loads, determine reactions and get an idea of the overall results of the analysis. In fact, it is largely used due to its extended availability and relatively low computational cost (Roca, et al., 2010).

Macroelements approach

Macroelements are portions of the buildings with homogeneous constructive characteristics and structural behavior. These method is particularly suitable for existing masonry buildings in historic centers which often do not satisfy the general conditions which allow the application of common equivalent static procedures. This method uses single and combined kinematic mechanisms that involve the equilibrium of the structural macroelements in order to evaluate the ultimate capacity of the building under seismic loads (SAHC, 2015-2016).

The most common collapse mechanisms have been studied and summarized on a series of abacuses according with the different constructive typologies. Such abacuses were published on (NIKER, 2010) and some examples of façade collapse mechanisms are shown in Figure 8.
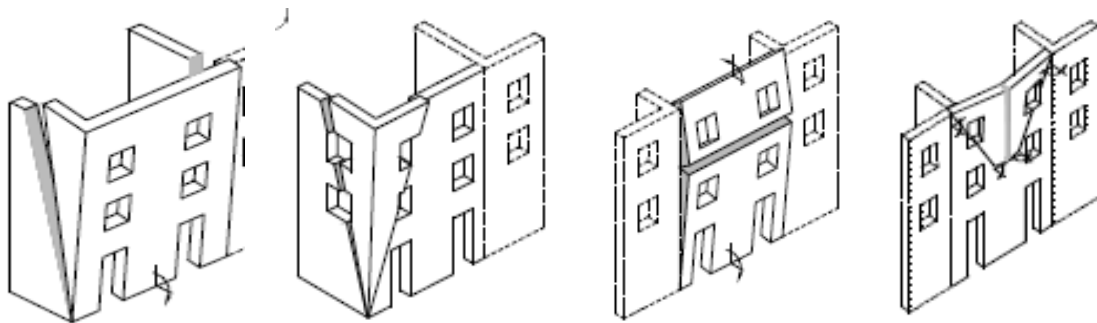
Figure 8: Examples of macroelements collapse mechanisms (NIKER, 2010).

2.3.2 FEM

Masonry FEM models can represent different levels of complexity. Figure 9 shows the several modeling strategies available nowadays. The sample of the left represents a detailed micro-modeling, the one in the middle shows a simplified micro-modeling and finally the one on the right exemplify a macro-modeling of the masonry. Going from the most complex to the simplest one respectively, details on each kind of simplification model are given on the following sections. There is no better or worse approach, each one of them is more or less suitable for different applications. Macro-models are more practice oriented and can be used when the structure is composed of solid walls with large enough dimensions in order to obtain a uniform stress-state across the element. Whereas that micro-models are more convenient to describe local behavior of particular parts of a structure and/or of structural details (Lourenco, 1998).
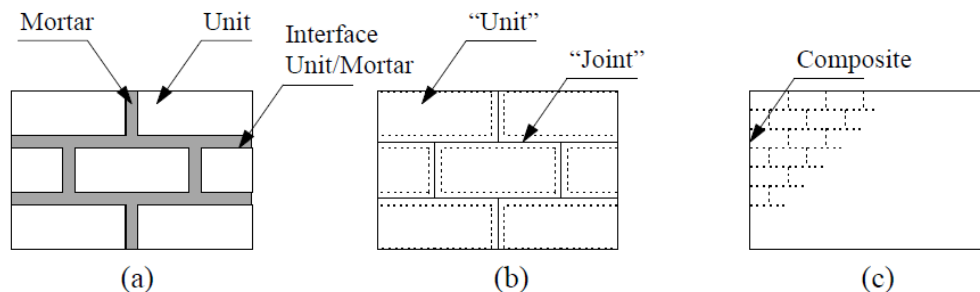
Figure 9: Modeling strategies for masonry structures: (a) Detailed micro-modeling; (b) Simplified micro-modeling; (c) Macro-modeling (Lourenco, 1998).

Macro-modeling

Homogenization techniques have to be implemented in order to apply the continuum hypothesis used to develop a simplified constitutive law. This approach is used to characterize the behavior of complete structures thanks to its lower computational cost. Mesh simplifications can be made in order to further simplify the analysis (not necessarily representing the constitutive morphology of the structural element). This method is appropriate when low accuracy-efficiency results are needed due to the fact that they are able to describe the response of masonry but unfortunately are not capable of simulate failure modes that involve the separation or sliding between different parts (Roca, et al., 2010).

Simplified micro-modeling

This strategy allows to model the brick units either as rigid or not-rigid bodies. Whereas that the mortar is modeled as zero-thickness interfaces where non-linear behavior and failure mechanisms occur. The brick units are expanded in order to conserve the original geometry of the structure. Accuracy is lost since Poisson's effect of the mortar is not included (Lourenco, 1998).

Detailed micro-modeling

Probably the most accurate tool available to simulate the real behavior of masonry. It allows to describe the local response of the material. It takes into account Young's modulus, Poisson's ratio and inelastic properties of both brick and mortar elements (Lourenco, 1998). Unfortunately this type of strategy has a relatively high computational cost and at present it is limited to the study of laboratory specimens and small structural elements. It is usually used to determine the equivalent properties of masonry and to carry on the homogenization process that later can be used in a less computational expensive macromodel (SAHC, 2015-2016).

2.3.3   DEM

The DEM is a numerical technique that allows to represent or approximate a continuum body into a series of discrete elements in order to simulate and study its micro and macro behavior.

Peter Cundall introduced this method in 1971. It was firstly intended to be used to study rock mechanics. In 1979, together with Otto Strack, they applied this new method to the study of solids (Recarey, et al., 2005). Since then, the method has been significantly improved and expanded. The contribution of different authors has provided several enhancements concerning space dimension, particle geometry, contact detection algorithms, boundary conditions, particle deformability, cohesion and fracturing and enhancements of the time integration scheme (Smilauer, 2010). According to Bui et al. "Due to the heterogeneity of masonry walls (bricks, joints and interfaces), the discrete element method (DEM) is the best adapted tool available today to study this type of structures, especially to reproduce the nonlinear behavior that appears beyond the elastic phase" (Bui, et al., 2014).

The formulation of DEM is based in two different laws. The first one is the well-known Newton's second law which describes the relationship between force, mass and acceleration. It is applied to find the displacements of the elements after the application of contact and/or external forces. The second one is a force-displacement type law, also known as a constitutive law. This second law determines the type of interaction between the bodies on the contact points and allows to calculate its strain and stress state on every time step.

There are several strategies concerning DEM simulations. All of them are based on the discretization of the structure into separate elements that are in contact with each other. They allow the finite displacement of the bodies and their rotation. Contact is modeled by a contact-point approach and new contacts between different bodies can be automatically detected (SAHC, 2015-2016). The most well-known approaches that have been applied to the modeling of masonry structures are mentioned here and described in more detail in further sections:

- FEM-DEM coupling approach

- Discontinues Deformation Analysis (DDA)

- Distinct Element Method

- DEM Particle flow approach

2.4   DEM modeling strategies

2.4.1   FEM-DEM coupling approach

Discrete-finite element methods collect different attempts of combining FEM with multi-body dynamics. Methods have been developed for the simulation of fracturing problems considering deformable blocks that may split and separate during the analysis. On the other hand, different approaches have used a fixed contact system with a small deformation framework and finite deformations concentrated in contact elements. Such methods were applied to the stability analysis of different masonry structures (Roca, et al., 2010). Other examples of the use of this strategy can be seen on the summary table presented on section 2.5 of this chapter.

2.4.2   Discontinuous Deformation Analysis (DDA)

The discontinuous deformation analysis (DDA) is a 2D method developed by Shi and Goodman for rock engineering analysis subsequently applied to masonry. Blocks are considered deformable but with a uniform strain and stress distribution. Contact is considered rigid and no interpenetration is permitted. This condition is enforced numerically by an iterative procedure at each time step (Roca, et al., 2010). An example of this strategy to the application of masonry structures is presented on (Thavalingam , et al., 2001).

2.4.3   Distinct Element Method

This approach was presented by Cundall and Strack on 1979. It discretize the structure in a series of particles modelled as separate elements. Contact between particles is detected one by one and their interaction is monitored with the use of an explicit numerical scheme. Contact forces and displacements are obtained thanks to the trace of the movements of each individual particle. Such movement of the particles and its description characterize the DEM as a dynamic method in which the speed of propagation of the particles depends on the physical properties of the discrete medium. The method assumes constant acceleration and velocities on each time step. It is necessary for the convergence of the method that the disturbances of the particles over the chosen time step are small enough in order to avoid full overlapping of the bodies (Cundall & Strack, 1979).

The main features of these method are (Roca, et al., 2010):

- No restriction of block shapes and no limitation to the magnitudes of translational and rotational displacements.
- Forces arise due to deformation.
- Accelerations are computed from the forces and moments for each block.
- Contact updating is performed when the sum of the displacements of all of the elements has exceeded a certain threshold value.

2.4.4 DEM Particle flow approach

This strategy is a simplified implementation of the DEM because it utilizes rigid disks (*2D*) or spherical particles (*3D*) to greatly simplify contact detection between elements for faster model solutions. The calculation cycle is a time-stepping algorithm that requires the repeated application of the law of motion to each particle, a force-displacement law to each contact and a constant updating of wall positions. Contacts, which may exist between two balls, or between a ball and a wall, are formed and broken automatically during the course of a simulation (Itasca, 2016).

At the start of each time step, the set of contacts is updated from the known particle and wall positions. The force-displacement law then is applied to each contact to update the contact forces based on the relative motion between the two entities at the contact and the contact constitutive model. Next, the law of motion is applied to each particle to update its velocity and position based on the resultant force and moment arising from the contact forces and any other body forces acting on the particle (Itasca, 2016).

This is the strategy applied on the present dissertation and from now on every time that DEM is mentioned it should be associated with this specific approach.

2.5 State of the art research

A state of the art research was carried out in order to identify the present knowledge on the field of structural modeling of masonry structures. Furthermore, such research helped to identify the gaps of information and the way in which this dissertation could be able to make a contribution. The most important aspects of the work of different authors on the topic are summarized and shown in Table 1. The table presents the software used to carry out the studies, the analysis dimension, the nature of the loads, the behavior and the type of structural element as well as the identification of whether a FEM-DEM coupling analysis had been performed or not. As it can be seen, most of the authors performed 2D analyses using commercial software developed by Itasca (UDEC and 3DEC). These software implements a FEM-DEM coupling method. In most of the cases a simplified micro-modeling approach was used to simulate the behavior of the masonry.

Table 1: State of the art research summary.

Reference	Software	2D/ 3D	Static/ Dynamic	Behavior	FEM-DEM	Structural element
(Reccia, et al., 2012)	Y2D	2D	-	Out of plane	Yes	Walls
(Sarhosis, et al., 2014)	UDEC	2D	Monotonic	In plane	Yes	Masonry infilled frames
(Mohebkhah, et al., 2008)	UDEC	2D	Static, monotonic	In plane	Yes	Masonry infilled frames
(Lourenco, et al., 2006)	UDEC	2D	Dynamic	Out of plane	No	Masonry blocks
(Smoljanovic, et al., 2013)	-	2D	Dynamic	In plane	Yes	Block, wall and arch
(Bui, et al., 2014)	3DEC	3D	Impact load	-	Yes	Column and arch
(Thavalingam , et al., 2001)	DIANA	2D	Static	In plane	Yes	Arch
(Zhuge, 2008)	UDEC	2D	Both	In plane	No	Wall/cable
(Lourenco & Pina-Henriques, 2006)	DIANA	2D	Static	In plane	No	Wall

Reccia et al. studied the feasibility of implementing a FEM-DEM coupling method to study the behavior of masonry structures. They assumed that blocks are infinitely rigid and mortar was modeled as zero-thickness Mohr-Coulomb type interfaces. This approach was proposed due to the fact that DEM allows to describe the separation between blocks and a simplified micro-modeling is less computational expensive in comparison with a detailed one. They compared and validated their results with simplified Giuffre's models. The obtained results were reliable and showed the feasibility of this method to describe out of plane behavior of masonry.

Following basically the same assumptions that Reccia et al. to model masonry elements, Sarhosis et al. studied the behavior of masonry infilled steel frames. They validated their model against an experimental test and used it to carry out a sensitivity study to explore the effects of multiple window openings arbitrary located along the masonry panel. Similar studies were performed by Mohebkhah et al.

Smoljanovic et al. implemented as well a FEM-DEM coupling approach but this time to describe the behavior of dry stone masonry. They achieve accurate results and demonstrated the potential of the FEM-DEM method to represent in a realistic way the response of such type of masonry. Their analysis was not only performed under monotonic load but also under cyclic and seismic loads.

Bui et al. performed similar studies using the 3DEC software developed by Itasca in order to study the 3D behavior of masonry assemblies (Bui, et al., 2010) and (Bui & Limam, 2012). In later papers they proposed a technique to indirectly identify the dynamic characteristics (natural frequencies and

mode shapes) of masonry structures using the DEM and making and impact analysis (Bui, et al., 2014).

Zhuge used the UDEC software to analyze the behavior of unreinforced masonry walls before and after being strengthened with a steel cable. His analysis involved static and dynamic loads. He proved that such retrofit technique is quite effective and significantly increase the in-plane strength, ductility and energy dissipation capacity of low-rise masonry walls.

A very complete analysis was carried out by Thavalingam et al. from the different modeling technics point of view. They analyzed a masonry arch using three different approaches and then compared the obtained results that each method provided. The three different technics used are: the FEM, the discontinuous deformation analysis (DDA) and the DEM particle flow code approach (which is similar to the one that will be used in this dissertation work). Their results are presented on a graphical way on Figure 10. Normalized displacements were plotted against load for the three methods and compared with the load determined by an experiment. Even though the three of them were able to represent the failure mode of the structure, the last mentioned method was the one that predicted the collapse load with higher accuracy (112%).
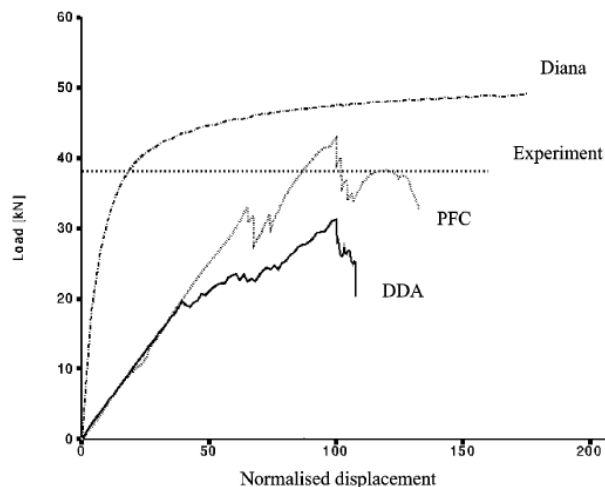
Figure 10: Comparison of load-normalized displacement diagrams (Thavalingam , et al., 2001).

Lourenco et al. studied the dynamic behavior of masonry walls as rigid blocks with the use of DEM. They proposed a new methodology to determine the needed parameters to perform DEM simulations. Their results show a very good agreement between their numerical models and the experimental data they were compared with.

Lourenco and Pina-Henriques used a discontinuum approach based on FEM including interfaces in order to represent the micro-behavior of masonry. Their model was compared with experimental and standard FEM numerical results. They concluded that advantages are presented by discontinuum

models to predict compressive strength and peak strain of masonry in comparison with continuum models.

After this state of the art research it was noticed that different aspects of the modeling of masonry were covered for different authors in their respective research. However none of them has approach the topic using the strategy proposed in this dissertation which consist in a 3D detailed micro modeling of masonry using a DEM particle flow approach.

2.6   Discussion

2.6.1   Regarding masonry structural behavior

Masonry is a heterogenic material since it is composed by bricks and mortar. Its description involves nowadays a series of assumptions and simplifications that provide accurate results for general study cases. Nevertheless, a more detailed analysis is needed if local behavior is to be described in detail.

Trying to describe the exact behavior of masonry is a quite complicated task. This is due to the difficulty that determine the individual mechanical properties of its components represent. Furthermore the composite behavior of the material also depends on the interaction between its components and this represent another degree of complexity. Even more, in the case of heritage structures, experimental campaigns are highly restricted in order to limit as much as possible the loss of cultural value. Such obstacles are being tackle in the last years with the help of new testing devices and with the high practical experience of practitioner engineers as well as with the use of new advanced modelling techniques and tools.

2.6.2   Regarding masonry modeling techniques

Being FEM and DEM the most advanced and important masonry modeling techniques, a summary of their principal characteristics, advantages and disadvantages is presented in Table 2.

Both FEM's and DEM's different strategies have important applications for the modeling of masonry structures based on the requirements and characteristics of every specific case study. Unfortunately the application of micro-modeling to entire structures is not feasible nowadays due to its high computational cost. Micromodels that try to simulate the response of the whole structure may be based on unrealistic discretizations and the obtained results may not represent accurately enough the response of the structure. Since according with some authors it is the most accurate tool available to simulate the real behavior of masonry, this kind of analysis may become the most used one in a near future due to the following reasons that will allow to mitigate its principal drawback, high computational cost:

- Improvements on the numerical methods and algorithms used on present codes.
- Computational processing capabilities enhancements.

Table 2: Summarized table of information for FEM and DEM modeling techniques.

Modeling technique	Main aspects	Advantages	Disadvantages
FEM	• Deformable blocks. • Connection between sides/faces only. • Interprenetation is possible. • Natural extension from continuum.	• Accurate representation of interface stresses. • Implicit solution. • Robustness.	• Time consuming analysis. • Difficulty to update contacts and accommodate large displacements.
DEM	• Rigid or deformable blocks (in combination with FEM). • Connection between vertices and sides/faces. • Interprenetation is possible. • Integration of the equations of motion for the blocks (explicit solution). Real damping coefficient (dynamic solution) or artificially large (static solution).	• Adequate formulation for large displacements and automatically contacts detection updates. • For deformable blocks, the mesh of each block is independent.	• A large number of contact points for accurate representation of interface stresses is needed. • Rather time consuming analysis, especially for 3D problems.

2.6.3 Regarding state of the art research

Most of the more advanced studies on the modeling of masonry structures present a 2D simplified micro-modeling with a FEM-DEM formulation method. Some other less common approaches also include the simplification of masonry partitions with rocky motion elements and very few of them attacked the problem from a particle flow strategy point of view.

Based on the lack of information about certain modeling strategies it was decided to carry out a 3D detailed micro-modeling of masonry with the use of DEM. As far as the author is concerned, this specific work has not yet been presented by any of the authors consulted or in any other publication.

This dissertation may be one of the first attempts to achieve such high level of precision and accuracy to describe the local behavior of masonry structures. A 3D detailed microanalysis using DEM to describe the response of simple one leaf brick masonry walls has been tested and the results show high degree of feasibility to model masonry structures with such kind of approach.

3. THEORETICAL BACKGROUND OF DEM

3.1 Introduction

In this chapter the theoretical development of the DEM will be presented. Since DEM consist in a loop, specific concepts regarding the theory behind the calculations will be explained step by step by the means of equations and figures. A series of important main aspects regarding the stability and efficiency of the method will be discussed as well.

The original constitutive law developed by (Smilauer, 2010) to reproduce the behavior of concrete will be described into detail. Also the modifications applied to such constitutive law in order to properly describe the behavior of masonry will be defined. Finally, conclusions regarding DEM principal features will be presented.

3.1 DEM loop

The DEM can be explained and understood as a loop due to its iterative nature. First of all bodies have to be defined as well as their shape, state, position, etc. Then, five main steps are performed (Smilauer, 2015):

- Detection of collisions between particles.
- Creation of new interactions and determination of their properties.
- Strain evaluation.
- Stress computation based on strains.
- Force application to particles in interaction.

Finally, the effect of this forces in the bodies is determined and after an increment of time (time step) the cycle starts again. All steps of the simulation loop are presented in Figure 11 and will be explained in detail in further sections.

Several open source and commercial DEM software are available nowadays. Among the commercial options, the most common ones are those developed by ITACSA such as UDEC, 3-DEC, PFC, etc. On the other hand, the most common free-access packages are DEMPack, developed at CIMNE, and Yade, open source software created at Université Grenoble I. Yade is the software used for this project and the formulation of the DEM theory presented is based on the Yade documentation. For further details or explanations see (Smilauer, 2015).
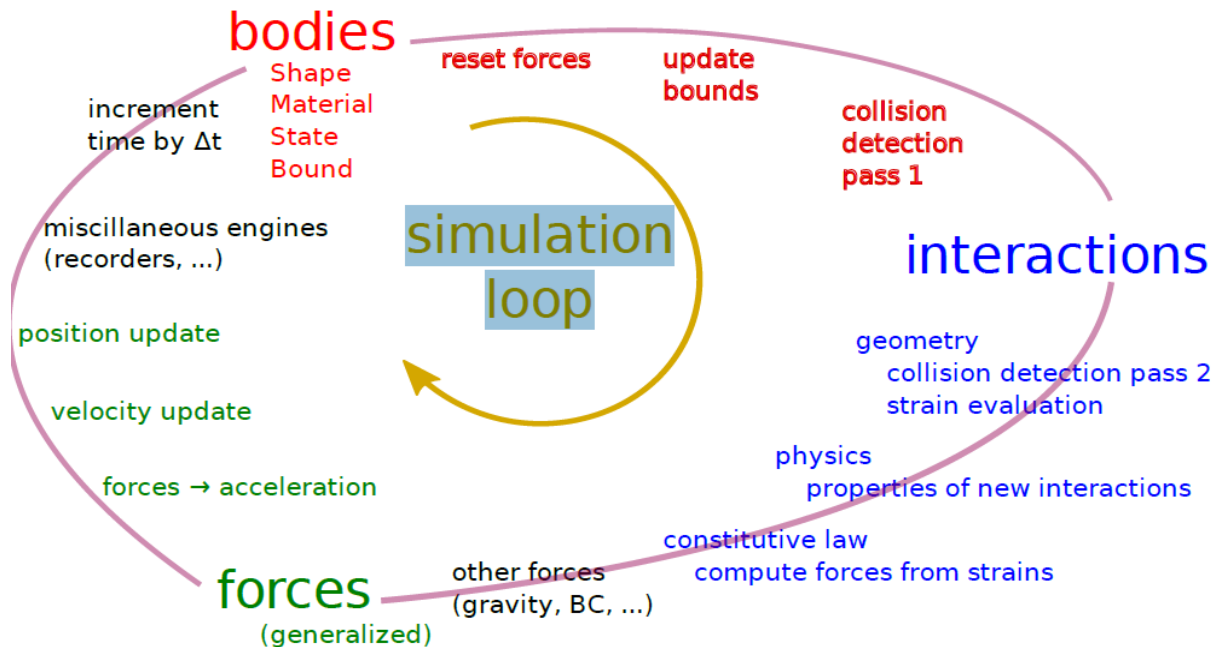
Figure 11: DEM simulation loop (Smilauer, 2015).

3.1.1 Bodies and collisions detection

The most common and easiest to handle geometry is the sphere. This is due to the fact that the contact detection only depends on its radius value and not in its rotation. Nevertheless, other shapes can also be used such as elliptical shapes, general or implicit quadratics and polygons. Also complex geometries can be modelled with the creation of clumps (group of spheres acting as a rigid body). Yade allows the creation of spheres, facets and walls but it can only simulate phenomena on 3D dimensions.

Besides from the definition of its geometry, other parameters have to be assigned to bodies such as material and state. The definition of the mechanical parameters, and therefore its correspondent constitutive law, is assigned as the material type. In Yade several kind of materials capable of describing different types of behaviors such as elasticity, plasticity, friction and cohesion can be used. The state of the body defines parameters such as its position, orientation, linear and angular velocity and acceleration.

The exact computation of collisions between bodies can be highly expensive. That is why Yade divides this step into two. The first part is called fast collision detection and the second one is called exact collision detection. The first step can be explained by taking a general pair of bodies i and j and their "exact"(in the sense of precision admissible by numerical implementation) spatial predicates (called "shape" in Yade) represented by point sets P_i, P_j the detection generally proceeds in two steps:

I.   Fast collision detection using approximate predicate $\widehat{P_i}$ and $\widehat{P_j}$; they are pre-constructed in such a way as to abstract away individual features of P_i and P_j and satisfy the condition:

$$\forall x \in R^3 : x \in P_i \rightarrow x \in \widehat{P_i} \qquad (3)$$

(Likewise for P_j). The approximate predicate is called "bounding volume" ("bound" in Yade) since it bounds any particle's volume from outside. It follows that $\left(P_i \cap P_j\right) \neq \emptyset \rightarrow \left(\widehat{P_i} \cap \widehat{P_j}\right) \neq \emptyset$ and, by applying modus Tollens:

$$\left(\widehat{P_i} \cap \widehat{P_j}\right) = \emptyset \rightarrow \left(P_i \cap P_j\right) = \emptyset \qquad (4)$$

Which is a candidate exclusion rule in the proper sense.

II.   By filtering away impossible collisions in (3), a more expensive, exact collision detection algorithm can be run on possible interactions, filtering out remaining spurious couples $\left(\widehat{P_i} \cap \widehat{P_j}\right) \neq \emptyset \wedge \left(P_i \cap P_j\right) = \emptyset$. These algorithms operate on P_i and P_j and have to be able to handle all possible combinations of shape types.

Yade uses a flat algorithm to evaluate collisions. That means that it does not create hierarchies first, but it works directly with bounding volumes Interactions. It is called the sweep and prune algorithm and operates with axi-aligned bounding boxes (Aabb) which overlap if and only if they overlap along all axes. These algorithms have roughly $O(n \log n)$ complexity, where n is the number of particles and it exploit temporal coherence of the simulation. Temporal coherence can be used to optimize simulations since it expresses the motion of particles according to physical laws and not just arbitrarily (Smilauer, 2015).

In order to achieve the stability during the integration of motion equations, an upper limit on the time step, Δt, has to be respected which limits by consequence the maximum displacement of particles during each step. The collider only evaluate possible interactions and is not run at every time step but only when a certain threshold value is reached in order to reduce the computational cost of the simulations. Such optimization is defined by the so called Verlet distances.

The sweep and prune algorithm consist on a series of Aabb which are used as $\widetilde{P_i}$; each Aabb is given by lower and upper corner $\in R^3$ (in the following, $\widetilde{P_i}^{x0}$, $\widetilde{P_i}^{x1}$ are minimum/maximum coordinates of $\widetilde{P_i}$ along the x-axis and so on). Construction of Aabb from various particle shapes (such as spheres, facets and walls) is straightforward, handled by appropriate classes deriving from bound functors.

Presence of overlap of two Aabbs can be determined from conjunction of separate overlaps of intervals along each axis (as shown in Figure 12 and described by equation (5)):

$$\left(\widetilde{P}_i \cap \widetilde{P}_j\right) \neq \emptyset \leftrightarrow \bigwedge_{w \in \{x,y,z\}} \left[\left(\left(\widetilde{P}_i^{w0}, \widetilde{P}_i^{w1}\right) \cap \left(\widetilde{P}_j^{w0}, \widetilde{P}_j^{w1}\right)\right) \neq \emptyset\right] \tag{5}$$
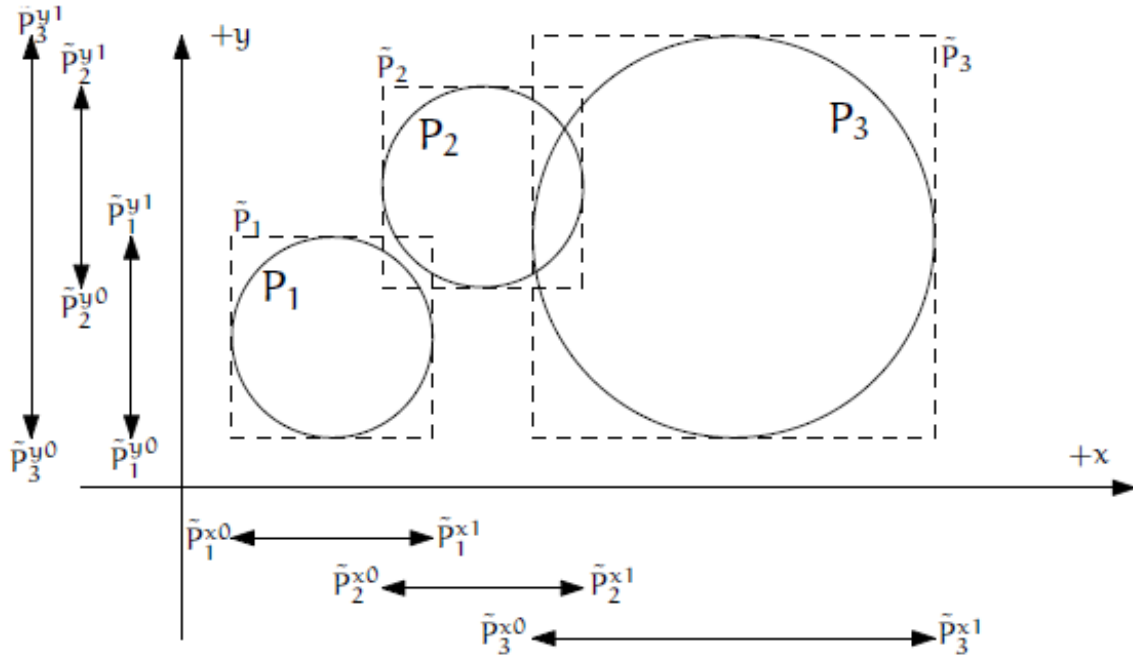
Figure 12: Sweep and prune algorithm (shown in 2D), where Aabb of each sphere is represented by minimum and maximum value along each axis. Spatial overlap of Aabbs is present if they overlap along all axes. In this case, $\widetilde{P_1} \cap \widetilde{P_2} \neq \emptyset$ (but note that $P_1 \cap P_2 = \emptyset$) and $\widetilde{P_2} \cap \widetilde{P_3} \neq \emptyset$ (Smilauer, 2015).

The collider keeps three separate lists (arrays) L_w for each axis $w \in \{x, y, z\}$

$$L_w = \bigcup_i \widetilde{P}_i^{w0}, \widetilde{P}_i^{w1} \tag{6}$$

Where i traverses all particles. L_w arrays (sorted sets) contain respective coordinates of minimum and maximum corners for each Aabb (these coordinates are called "bound" in the following); besides bound, each one of the list elements further carries an id referring to the particle it belongs to, and a flag for whether it is lower or upper bound.

In the initial step, all lists are sorted (using quicksort, average $O(n \log n)$) and one axis is used to create initial interactions: the range between lower and upper bound for each body is traversed, while bounds in-between indicate potential Aabb overlaps which must be checked on the remaining axes as well.

At each successive step, lists are already pre-sorted. Inversions occur where a particle's coordinate has just crossed another particle's coordinate; this number is limited by numerical stability of

simulation and its physical meaning (giving spatio-temporal coherence to the algorithm). The insertion sort algorithm swaps neighboring elements if they are inverted, and has complexity between $bigO\{n\}$ and $bigO\{n^2\}$, for pre-sorted and unsorted lists respectively. For this code purposes, only inversions are needed to be handle, which by nature of the sort algorithm are detected inside the sort loop. An inversion might signify:

- Overlap along the current axis, if an upper bound inverts (swaps) with a lower bound (i.e. that the upper bound with a higher coordinate was out of order in coming before the lower bound with a lower coordinate). Overlap along the other 2 axes is checked and if there is overlap along all axes, a new potential interaction is created.
- End of overlap along the current axis, if lower bound inverts (swaps) with an upper bound. If there is only potential interaction between the two particles in question, it is deleted.
- Nothing if both bounds are upper or lower.

As mentioned before an optimization on the computational cost is achieved with the use of the Verlet distances. This parameter controls the activation of the collision detection algorithm only after a certain value has been reached. This is achieved thanks to the enlargement of the predicates $\widetilde{P_i}$ in all dimensions by ΔL. Supposing that the collider run last time at step m, and the current step is n. The cumulated distance, L_{mn}, traversed by each particle between m and n is tracked by comparing the current position with the reference position from time n as $L_{mn} = |X^n - X^m|$. The collider is activated as soon as one particle gives:

$$L_{mn} > \Delta L \qquad (7)$$

3.1.2 Interaction of particles, strain and stress computations

The exact interaction between particles is calculated at each time step since it is at every time step that the new position of the bodies is updated. Special algorithms are used in Yade to determine the interactions and they are grouped on a special functor (IGeomFunctor). Besides from the geometrical interaction other properties must be as well determined. They are related with the combination of material type properties of both particles and are controlled by another functor (IPhysFunctor).

Two different stiffness variables are defined on DEM basic interactions: normal stiffness K_N and shear (tangent) stiffness K_T. It is desirable that K_N be related to fictitious Young's modulus of the particles' material, while K_T is typically determined as a given fraction of computed K_N. The K_T/K_N ratio determines macroscopic Poisson's ratio of the arrangement, which can be shown by dimensional analysis: elastic continuum has two parameters (E and ν) and basic DEM model also has two parameters with the same dimensions K_N and K_T/K_N; macroscopic Poisson's ratio is therefore determined solely by K_T/K_N and macroscopic Young's modulus is then proportional to K_N and affected by K_T/K_N.

Normal stiffness

An example of an algorithm used in Yade computes normal interaction stiffness as stiffness of two springs in serial configuration with lengths equal to the sphere radii. This is shown in Figure 13.
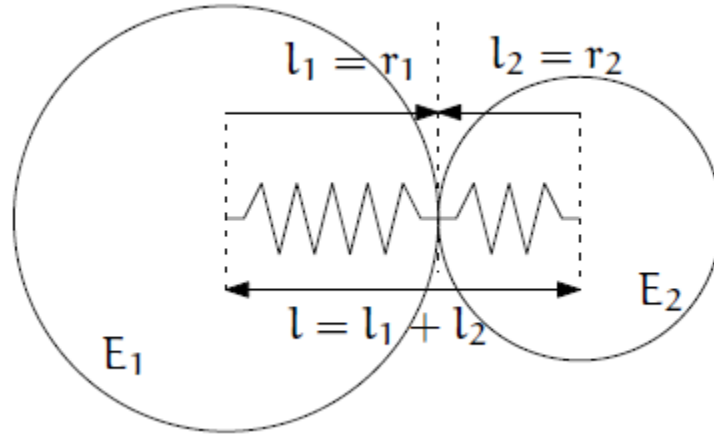
Figure 13: Series of two springs representing normal stiffness of contact between two spheres (Smilauer, 2015).

If the following definition is stablished: $l = l_1 + l_2$, where l_i are distances between contact point and sphere centers, which are initially (roughly speaking) equal to sphere radii. Change of distance between the sphere centers Δl is distributed onto deformations of both spheres $\Delta l = \Delta l_1 + \Delta l_2$ proportionally to their compliances. Displacement change Δl_i generates force $F_i = K_i * \Delta l_i$, where K_i assures proportionality and has physical meaning and dimension of stiffness; K_i is related to the sphere material modulus E_i and some length $\widetilde{l_\iota}$ proportional to r_i. Microscopic normal stiffness K_N can be calculated following the relationships shown for equation (8) to equation (9).

$$\Delta l = \Delta l_1 + \Delta l_2 \tag{8}$$

$$K_i = E_i * \widetilde{l_\iota} \tag{9}$$

$$K_N * \Delta l = F = F_1 = F_2 \tag{10}$$

$$K_N * (\Delta l_1 + \Delta l_2) = F \tag{11}$$

$$K_N \left(\frac{F}{K_1} + \frac{F}{K_2} \right) = F \tag{12}$$

$$K_1^{-1} + K_2^{-1} = K_N^{-1} \tag{13}$$

$$K_N = \frac{K_1 * K_2}{K_1 + K_2} \tag{14}$$

$$K_N = \frac{E_1 * \widetilde{l_1} * E_2 * \widetilde{l_2}}{E_1 * \widetilde{l_1} + E_2 * \widetilde{l_2}}$$

(15)

The most common way to calculate the interaction properties is assuming $\widetilde{l_i} = 2 * r_i$. Some formulations define an equivalent cross-section A_{eq}, which in that case appears in the $\widetilde{l_i}$ term as $K_i = E_i * \widehat{l_i} = E_i(A_{eq}/l_i)$. Such is the case for the concrete constitutive law model developed by Smilauer (Smilauer, 2010) and presented on a further section of this dissertation. It is important to remark this property since for this research this parameter has been modified. Smilauer computes the equivalent area according to equation (16):

$$A_{eq} = \pi * \min(r_1, r_2)^2$$

(16)

For reasons given above, no pretense about equality of particle-level E_i and macroscopic modulus E should be made. This parameters are often confused but in reality can have different values. For further explanation on this situation consult (Oñate, et al., 2012)

Other parameters

Non-elastic parameters differ for various material models. Usually, though, they are averaged from the particles' material properties, if it makes sense. In the original constitutive law used on this dissertation and developed by Smilauer, this averaging process is not even taken into account due to the fact that it was originally developed to describe interactions between particles of the same material. Furthermore, it was only applied to particles of the same size. On the other hand, interactions between cohesive and non-cohesive materials was taken into account. This aspect is also important to be remarked since a modification presented hereafter was made in order to be able to calibrate the "interface" properties between mortar and brick spheres. "Interface" in this context is refer to the interaction of particles with different material properties, in this dissertation case, mortar- brick particles interactions.

Strain evaluation

In the general case, mutual configuration of two particles has 6 degrees of freedom (DoFs) just like a beam in 3D space: both particles have 6 DoFs each, but the interaction itself is free to move and rotate in space (with both spheres) having 6 DoFs itself; then 12 - 6 = 6. The different DoFs can be seen in Figure 14. Normal strain appears if there is a difference of linear velocity along the interaction axis (n), shearing originates from the difference of linear velocities perpendicular to n and from the part of $\omega_1 + \omega_2$ perpendicular to n, twisting is calculated by the part of $\omega_1 - \omega_2$ parallel with n, and finally bending comes from the part of $\omega_1 - \omega_2$ perpendicular to n.
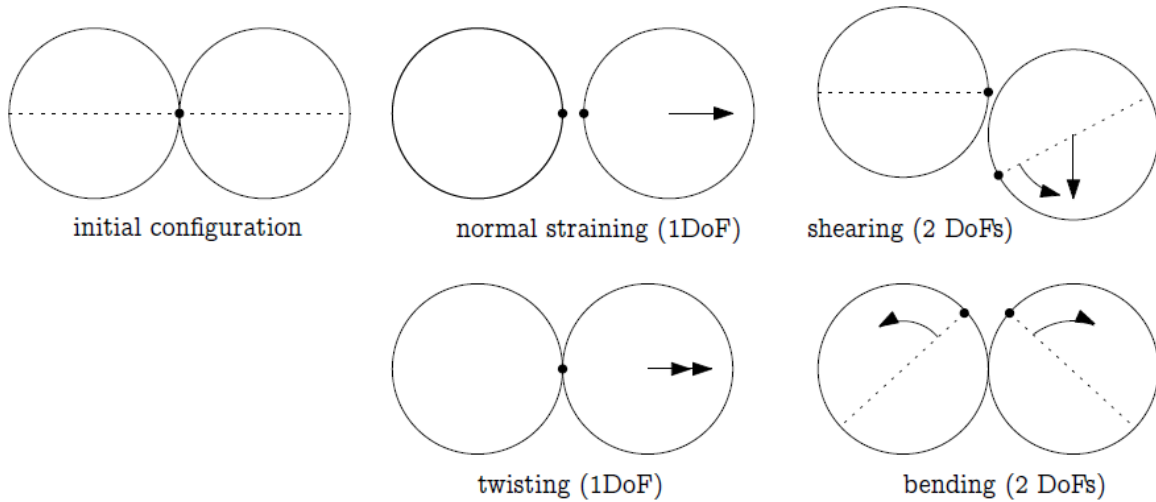
Figure 14: Degrees of freedom of configuration of two spheres (Smilauer, 2010).

Most of the constitutive laws implemented on Yade does not take into account twisting and bending degrees of freedom. Usually only normal and shear strain are defined and have an influence on the DEM simulation's results.

When two spheres get in contact in order to compute the strain certain geometrical parameters need to be determined. In this case the initial centers $\bar{C}_1$ and $\bar{C}_2$, the correspondent radius r_1 and r_2 as well as the distance, d_0, also called equilibrium distance, are obtained based in Figure 15 and on equations (17) to (19).

$$d_0 = |\bar{C}_2 - \bar{C}_1| \qquad\qquad (17)$$

$$d_1 = r_1 + \frac{d_0 - r_1 - r_2}{2} \qquad\qquad (18)$$

$$d_2 = d_0 - d_1 \qquad\qquad (19)$$

d_0 is used to convert absolute displacements to dimensionless strain, and it is also the distance where there is neither repulsive nor attractive force between spheres.

Distances d_1 and d_2 define reduced or expanded radius of the spheres. Interaction can also be created for spheres that do not geometrically overlap based on the interaction radius, R_I. The general condition thus reads:

$$d_0 \leq R_I * (r_1 + r_2) \qquad\qquad (20)$$
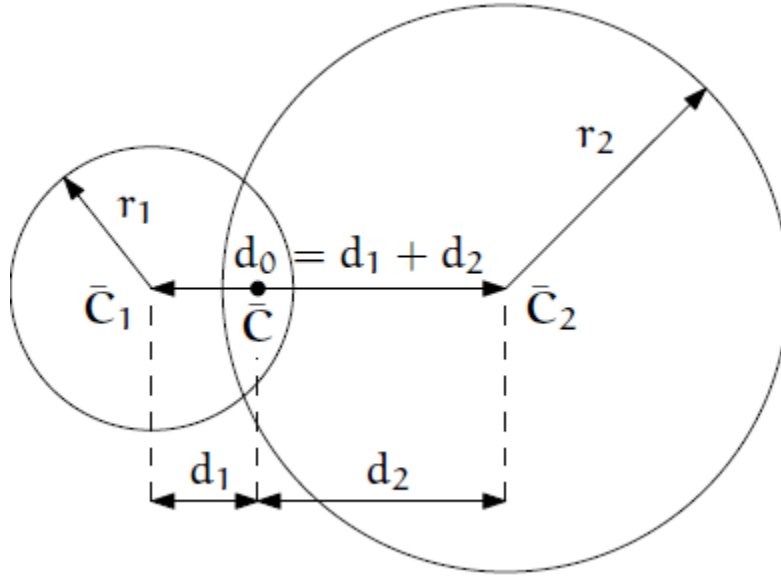
Figure 15: Geometry of the initial contact of two spheres (Smilauer, 2010).

Finally normal displacement and normal strain can be defined as:

$$u_N = \left| C_2^\circ - C_1^\circ \right| - d_0 \qquad\qquad (21)$$

$$\varepsilon_N = \frac{u_N}{d_0} = \frac{\left| C_2^\circ - C_1^\circ \right|}{d_0} - 1 \qquad\qquad (22)$$

For massively compressive simulations, it might be beneficial to use the logarithmic strain, such that the strain tends to $-\infty$ (rather than -1) as centers of both spheres approach. Otherwise, repulsive force would remain finite and the spheres could penetrate through each other. Therefore equation (22) is modified as:

$$\varepsilon_N = \begin{cases} \log\dfrac{\left| C_2^\circ - C_1^\circ \right|}{d_0} & if \ \left| C_2^\circ - C_1^\circ \right| < d_0 \\[4mm] \dfrac{\left| C_2^\circ - C_1^\circ \right|}{d_0} - 1 & otherwise \end{cases} \qquad\qquad (23)$$

Nonetheless, using a logarithmic function has as disadvantage the fact that effectively infinite rigidity can be reached and it causes instability in the simulation. In order to cope with this problem Δt has to be dynamically adjusted and Yade provides a stiffness-based time-stepper in order to achieve such purpose.

Shear displacement and shear strain are easily computed thanks to the design and implementation of the so called Total algorithm designed by Smilauer (for more details about it consult (Smilauer, 2010)). Thus these parameters are defined by:

$$u_T = p'_{02} - p'_{01} \qquad\qquad (24)$$

$$\varepsilon_T = \frac{u_T}{d_0} \qquad\qquad (25)$$

Where p'_{01} and p'_{02} represent contact planes of the „unrolled„ sphere's surface initial locally maped points.

Stress evaluation

Stresses (and forces) on both spheres can be computed once the strain on a contact has been determined. While the strain evaluation will be similar to algorithms described in the previous section, stress evaluation itself depends on the nature of the material being modeled. In DEM generally, some constitutive laws are expressed using strains and stresses while others prefer displacement/force formulation. The computation of stresses for the constitutive law used on this dissertation will be presented on a further section.

3.1.3 Forces and position updates

Position and orientation as well as velocity and acceleration of each particle are computed on every time step during this stage of the loop. Each particle accumulates generalized forces (forces and torques) from the contacts in which it participates. These generalized forces are then used to integrate motion equations for each particle separately.

To compute the new position of a sphere on every time step a leapfrog scheme is used starting with equation (26), and finally obtaining equation (27)(for more details consult (Smilauer, 2010)).

$$ü° = \frac{F}{m} \qquad\qquad (26)$$

$$u^+ = u^° + \dot{u}^{\oplus} * \Delta t \qquad\qquad (27)$$

Where ü° represents acceleration on the current time step, F the cumulate forces acting on the sphere and m the particle's mass. u^+ indicates the new position of the sphere on the next step and $\dot{u}^{\oplus}$ represents the velocity at the intermediate next step.

To obtain the new particle's orientation, q^+, an analogous procedure is followed (see (Smilauer, 2010)) and thus:

$$q^+ = \Delta q * q° \qquad\qquad (28)$$

Where $q°$ represents the orientation in the present time step and Δq the change on the orientation.

3.2 Other aspects

3.2.1 Numerical damping

In simulations of quasi-static phenomena, it is desirable to dissipate kinetic energy of particles. Since most constitutive laws do not include velocity-based damping, it is possible to use artificial numerical damping. The basic idea is to decrease forces which increase the particle velocities and vice versa by $(\Delta F)_d$, comparing the current acceleration sense and particle velocity sense. This is done by a component, which makes the damping scheme clearly non-physical, as it is not invariant with respect to coordinate system rotation; on the other hand, it is very easy to compute. This component is computed on Yade with equation (29).

$$\frac{(\Delta F)_{dw}}{F_w} = -\lambda_d sgnF_w \left(\dot{u}_w^\ominus + \frac{\ddot{u}_w^\circ * \Delta t}{2} \right), \quad w \in \{x, y, z\} \tag{29}$$

3.2.2 Stability considerations

In order to ensure stability for the explicit integration scheme, an upper limit is imposed on Δt:

$$\Delta t_{cr} = \frac{2}{\omega_{max}} \tag{30}$$

Where ω_{max} is the highest eigenfrequency within the system. For single mass-pring systems $\omega_{max} = \omega$ and is easily computed as follows:

$$\omega = \sqrt{\frac{m}{k}} \tag{31}$$

For general mass-spring systems the ω_{max} happens when two connected masses are in opposite motion. The equations that determine the critical time increment in a simulation are from (32) to (34) (for more details consult (Smilauer, 2010)):

$$\Delta t_{cr} = \frac{2}{\omega_{max}} = \min_i \sqrt{2} \sqrt{\frac{m_i}{K_i}} \tag{32}$$

$$\Delta t_{cr} = \min \Delta t_{crw}, \quad w \in \{x, y, z, \} \tag{33}$$

$$K_{iw} = \sum_j K_{Nj}((1 - \xi) * n_{jw}^2 + \xi) \tag{34}$$

3.2.3 Computational cost and results indeterminism

Computational cost

The DEM computation using an explicit integration scheme demands a relatively high number of steps during simulation, compared to implicit schemes. The total computation time depends on the simulated time and on the number of particles. In order to realize the DEM scaling, if finer results are wanted and a refining of the "mesh" is done by halving the radius of the particle, the computational cost will grow 16 times.

Results indeterminism

It is naturally expected that running the same simulation several times will give exactly the same results: although the computation is done with finite precision, round-off errors would be deterministically the same at every run. While this is true for single-threaded computation where exact order of all operations is given by the simulation itself, it is not true anymore in multi-threaded computation.

The straight-forward manner of parallel processing in explicit DEM is given by the possibility of treating interactions in arbitrary order. Strain and stress is evaluated for each interaction independently, but forces from interactions have to be summed up. If summation order is also arbitrary (in Yade, forces are accumulated for each thread in the order interactions are processed, then summed together), then the results can be slightly different. As an example:

$$\frac{1}{10} + \frac{1}{13} + \frac{1}{17} = 0.23574660633484162$$

$$\frac{1}{17} + \frac{1}{13} + \frac{1}{10} = 0.23574660633484165$$

3.3 CpmMat description

The so called CpmMat is a constitutive law originally developed by Vaclav Smilauer (Smilauer, 2010) to simulate concrete behavior. This constitutive law allows to obtain quite precise results at a macroscopic level but it is formulated as a contact law at a two-particle individual level. Its definition is presented hereafter as well as the modifications performed on it in order to adapt it to better describe the behavior of masonry.

3.3.1 Cohesive and non-cohesive contacts

At the beginning of the simulation cohesive contacts are created between the spheres that interact with each other. The cohesion is maintained until a certain stress limit is reached. Such parameter is set as a damage variable called ω. The values of ω vary from 0 to 1, being 1 the value that describes a complete contact damage state or a non-cohesive contact between particles.

3.3.2 Contact parameters

The model parameters can be grouped in 5 different categories:

- Geometry
  - r = Sphere radius
  - R_I = Interaction radius
- Elasticity
  - k_N = Normal contact stiffness
  - k_T/k_N = Relative shear contact stiffness
- Damage and plasticity
  - ε_0 = Limit elastic strain
  - ε_f = Parameter of damage evolution function
  - C_{T0} = Shear cohesion of undamaged material
  - φ = Internal friction angle
- Confinement
  - Y_0 = Parameter for plastic surface evolution in compression
  - ε_s = Hardening strain in compression
  - $\widetilde{K_s}$ = Relative hardening modulus in compression
- Rate-dependence (Non-available on the open source version)
  - τ_d = Characteristic time for visco-damage
  - M_d = Dimensionless visco-damage exponent
  - τ_{pl} = Characteristic time for visco-plasticity
  - M_{pl} = Dimensionless visco-plasticity exponent

3.3.3 Normal stresses

Using damage mechanics the normal stress-strain law is formulated as follows:

$$\sigma_N = \left(1 - \omega * H(\varepsilon_N)\right) * k_N * \varepsilon_N \qquad (35)$$

The Heaviside function $H(\varepsilon_N)$ is used in order to deactivate the damage influence in compression, which physically corresponds to crack closure. A damage evolution function is applied in order to evaluate the damage variable ω:

$$\omega = g(k) = 1 - \frac{\varepsilon_f}{k} * \exp\left(-\frac{k - \varepsilon_0}{\varepsilon_f}\right) \qquad (36)$$

$$k = \max(\tilde{\varepsilon}) \qquad (37)$$

$$\tilde{\varepsilon} = \sqrt{\langle \varepsilon_N \rangle^2 + \xi_1^2 * |\varepsilon_T|^2}$$ (38)

Where $\tilde{\varepsilon}$ is the equivalent strain responsible for damage ($\langle \varepsilon_N \rangle$ signifies the positive part of ε_N) and ξ_1 is a dimensionless coefficient weighting the contribution of the shear strain ε_T to damage. Comparative studies suggest a value of $\xi_1 = 0$ thus equation (38) simplifies to $\tilde{\varepsilon} = \langle \varepsilon_N \rangle$. k is the maximum equivalent strain over the whole history of the contact.

The product $K_T * \varepsilon_0$ corresponds to the local tensile strenght at the level of one contact (in general different from the macroscopic tensile strength). ε_f is related to the slope of the softening part of the normal strain-stress diagram shown in Figure 17 and must be larger than ε_0. ε_f can be calculated according to (39).

$$\varepsilon_f = \varepsilon_0 * relDuctility$$ (39)
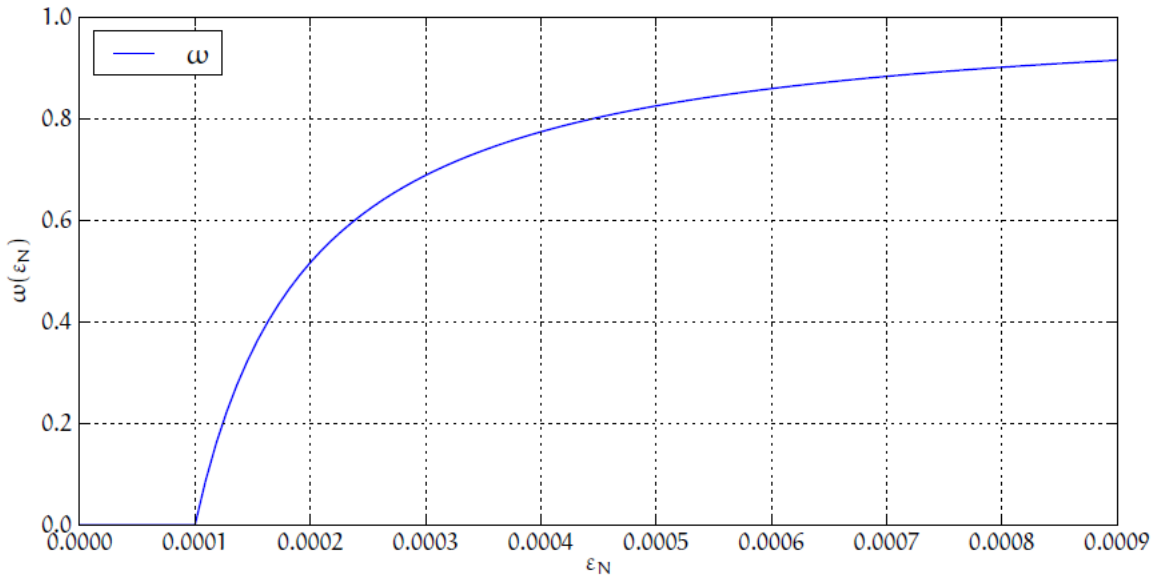
Figure 16: Damage ω evolution function $\omega = g(kD)$, where $kD = max(\varepsilon_N)$ (using $\varepsilon_0 = 0.0001, \varepsilon_f = 30 * \varepsilon_0$) (Smilauer, 2010).

Compressive plasticity

Hardening in plasticity was introduced on the constitutive law in order to better capture confinement effect. Using material parameter $\varepsilon_s < 0$, σ_s is defined as:

$$\sigma_s = k_N * \varepsilon_s$$ (40)

If $\sigma < \sigma_s$, then $\widetilde{K_s} * k_N$ is taken for tangent stiffness, $\widetilde{K_s} \in \langle 0,1 \rangle$ and plastic strain ε_N^{pl} is incremented accordingly. Such hardening behavior is shown in Figure 18.
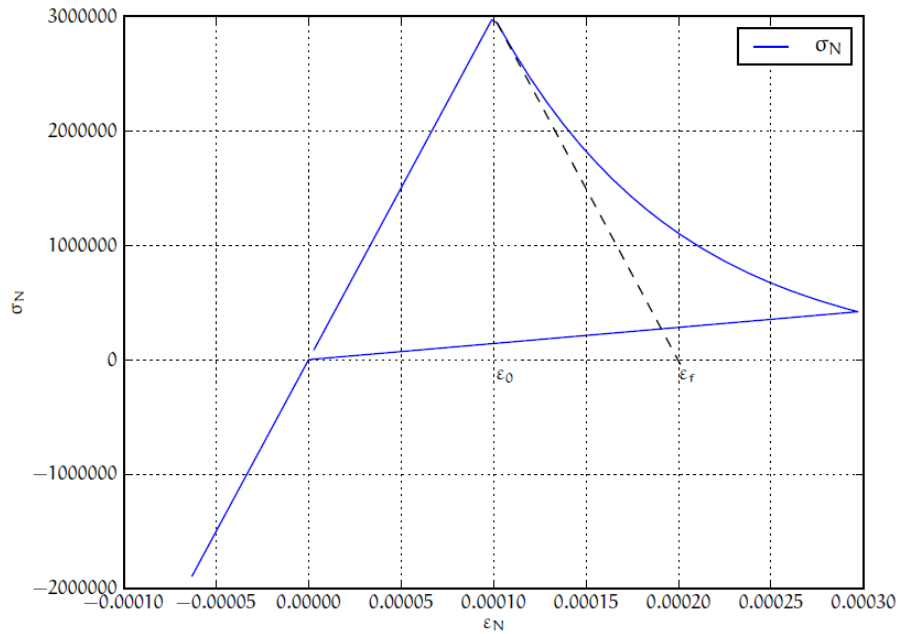
Figure 17: Strain-stress diagram in the normal direction (Smilauer, 2010).

This phenomena only occurs in compression whereas that damage only happens in tension. Thus the interaction between both is not needed to be considered. A cyclic strain-stress diagram is presented in Figure 18.
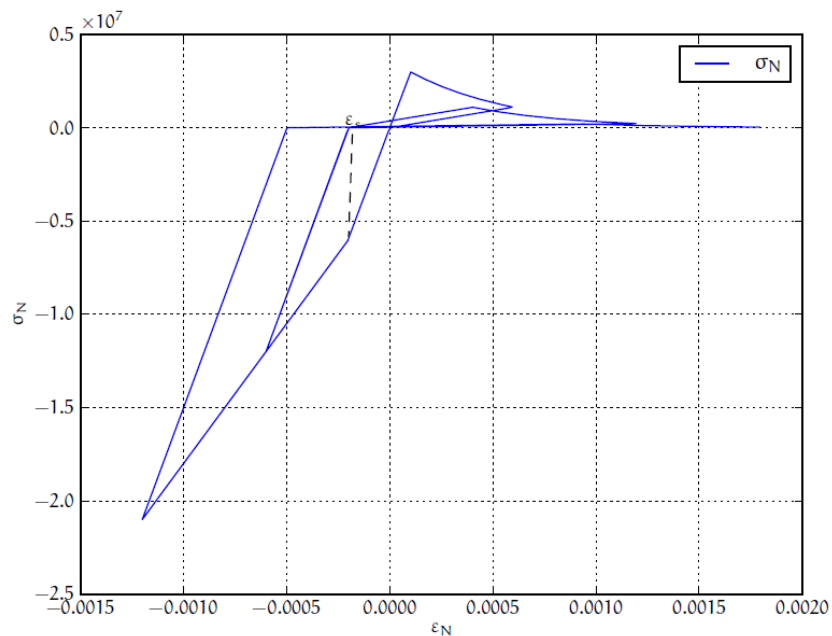
Figure 18: Strain-stress diagram in normal direction, loaded cyclically in tension and compression (Smilauer, 2010).

Visco-damage

Viscous overstress is added to the constitutive law in order to represent time-dependent phenomena. This overstress, σ_{Nv} is added to equation (35). Total strain is split into an elastic, ε_e, and a damaged part, ε_d. And since $\varepsilon_e = \sigma_N / k_N$:

$$\varepsilon_d = \varepsilon_N - \frac{\sigma_N}{k_N} \qquad\qquad (41)$$

The viscous overstress is supposed to be related to a limited rate of crack propagation, therefore:

$$\sigma_{Nv}(\dot{\varepsilon_d}) = k_N * \varepsilon_0 \langle \tau_d * \dot{\varepsilon_{Nd}} \rangle^{Md} \qquad\qquad (42)$$

Where $k_N * \varepsilon_0$ is rate-independent tensile strength (introduced only to accomplish dimensionality). The $\langle ... \rangle$ operator denotes positive part; therefore, for $\dot{\varepsilon_{Nd}} \leq 0$, viscous overstress vanishes. The normal stress equation then is modified as follows:

$$\sigma_N = \big(1 - \omega * H(\varepsilon_N)\big) * k_N * \varepsilon_N + \sigma_{Nv}(\dot{\varepsilon_d}) \qquad\qquad (43)$$

Isotropic confinement

This characteristic is included on the constitutive law in order to simulate confined compression setups. It is achieved by pre-adjusting ε_N and post-adjusting σ_N; this is based ont he assumption that the confinement value σ_0 is negative and does not cause immediate damage to contacts.

3.3.4 Shear stresses

A plastic constitutive law is applied to define shear stresses:

$$\sigma_T = k_T * (\varepsilon_T - \varepsilon_{Tp}) \qquad\qquad (44)$$

Where ε_{Tp} is the plastic strain on the contact and k_T is the shear contact modulus computed from k_N as the ratio k_T / k_N. Shear stress is limited by the yield function:

$$f(\sigma_N, \sigma_T) = |\sigma_T| - r_{pl} = |\sigma_T - (c_T - \sigma_N * \tan \varphi) \qquad\qquad (45)$$

$$c_T = c_{T0}(1 - \omega) \qquad\qquad (46)$$

Where c_{T0} and φ are the initial cohesion and internal friction angle, respectively. r_{pl} represents the radius of plasticity surface in a given σ_N plane. The plastic flow rule, presented in equation (47), is associated in the plane of shear stresses but not with respect to the normal stress.

$$\dot{\varepsilon_{Tp}} = \dot{\lambda} * \frac{\sigma_T}{|\sigma_T|} \qquad\qquad (47)$$

With $\dot{\lambda}$ being a plastic multiplier. Both yield surface and plastic flow rule are presented in Figure 19.
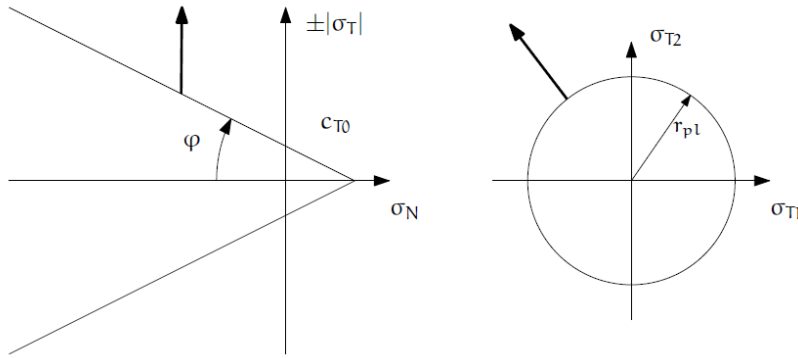
Figure 19: Linear yield surface and plastic flow rule.

In the implementation, numerical evaluation starts from current value of ε_T. Trial stress $\sigma_T^t = \varepsilon_T * k_T$ is computed and compared with current plasticity surface radius r_{pl} from (45). If $|\sigma_T^t| > r_{pl}$, the radial stress return is performed; since ε_{TP} is not stored, ε_T is updated as well in such case:

$$\sigma_T = r_{pl} * \widehat{\sigma_T} \tag{48}$$

$$\varepsilon_T' = \widehat{\varepsilon_T} * \frac{|\sigma_T|}{|\sigma_T^t|} \tag{49}$$

If $|\sigma_T^t| \leq r_{pl}$, there is no plastic slip and we simply assign $\sigma_T = \sigma_T^t$ without ε_T update.

Confinement extension

This extension to the constitutive law is introduced in order to capture a confinement effect as for the normal stress and also with the aim of prevent shear locking under extreme compression. By using a logarithmic surface in the compression part, which has C_1 continuity with the linear surface in tension; pathologic behavior around the switch point is avoided by the continuity condition and the number of new parameters is reduced as well.

$$f(\sigma_N, \sigma_T) = \begin{matrix} |\sigma_T| - (c_{T0} * (1 - \omega) - \sigma_N * \tan\varphi) & if\,\sigma_N \geq 0 \\ |\sigma_T| - c_{T0} * \left[(1 - \omega) + Y_0 * \tan\varphi * \log\left(\frac{-\sigma_N}{c_{T0} * Y_0} + 1\right)\right] & if\,\sigma_N < 0 \end{matrix} \tag{50}$$

A comparison between a linear and a logarithmic yield surface is presented in Figure 20. The speed in which the logarithmic one deviates from the linear one is determined by the dimensionless parameter Y_0.
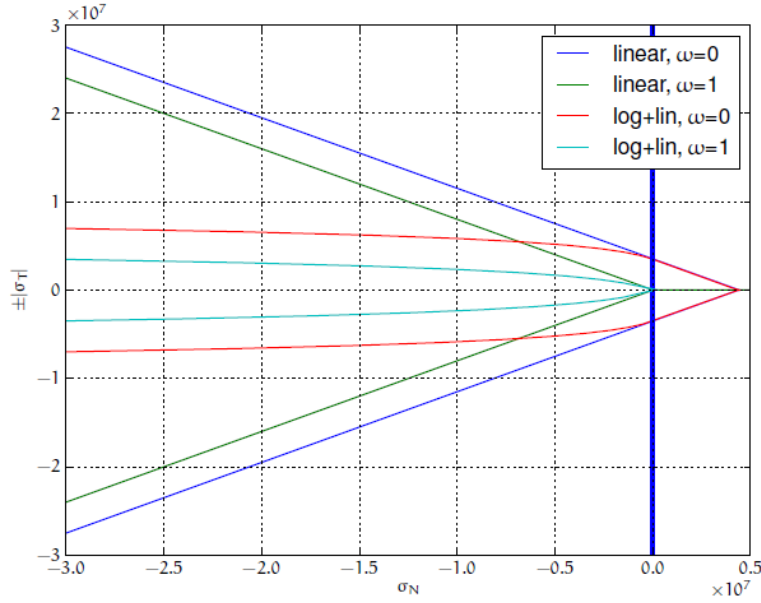
Figure 20: Comparison of linear and logarithmic (in compression) yield surfaces, for both virgin and damaged material (Smilauer, 2010).

Visco-plasticity

Similar ideas are applied for viscosity in shear as those used for the normal condition. r_{pl} is increased according to the rate of plastic flow as shown in equation (51).

$$r'_{pl} = r_{pl} + c_{T0} * \left(\tau_{pl} * \dot{\varepsilon_{Tp}}\right)^{M_{pl}} = r_{pl} + c_{T0} * \left(\tau_{pl} * \frac{\Delta \varepsilon_{Tp}}{\Delta t}\right)^{M_{pl}} \qquad (51)$$

Where τ_{pl} is the characteristic time for visco-plasticity and M_{pl} is a dimensionless exponent. The final shear stress value is obtained with formula:

$$\sigma_T = \frac{r'_{pl}}{|\sigma_T^t|} * \sigma_T^t \qquad (52)$$

3.3.5 Applying stresses on particles

The resulting normal and shear stresses (σ_N, σ_T respectively) are computed at the current contact point $C°$. The sum of the generalized forces, force and torque, is applied to each particle position $C_1°$ and $C_2°$ and if a particle has multiple interactions the generalized forces are sum on each computation step. Thus:

$$F_\Sigma = A_{eq} * (\sigma_N * n + \sigma_T) \qquad (53)$$

$$F_1 = F_\Sigma \qquad\qquad T_1 = (C° - C_1°) * F_\Sigma \qquad\qquad (54)$$

$$F_2 = F_\Sigma \qquad\qquad T_2 = -(C° - C_1°) * F_\Sigma \qquad\qquad (55)$$

3.4 CpmMat modifications

Three important modifications were applied to the original constitutive law developed by Smilauer in order to better represent the behavior of masonry. They consist on:

- *Modification on the formula to calculate A_{eq}*: The original formula to calculate this important contact parameter is repeated on equation (56) which considers the area of contact as a circle. This formula was modified to consider such area as a square and since the size of the spheres is constant (r is the same for all bodies) the used formula to calculate A_{eq} is shown in equation (57).

Since the geometry of the studied bodies is completely regular and can be discretized into perfect cubes, this modification was done in order to take into account the area that such discretization will represent but with the advantage of keep modeling spheres which simplifies the detection of contacts and thus decreases the needed computational power. Both areas are depicted in Figure 21.

$$A_{eq} = \pi * \min(r_1, r_2)^2 \qquad\qquad (56)$$

$$A_{eq} = (2 * r)^2 \qquad\qquad (57)$$

(a)   (b)
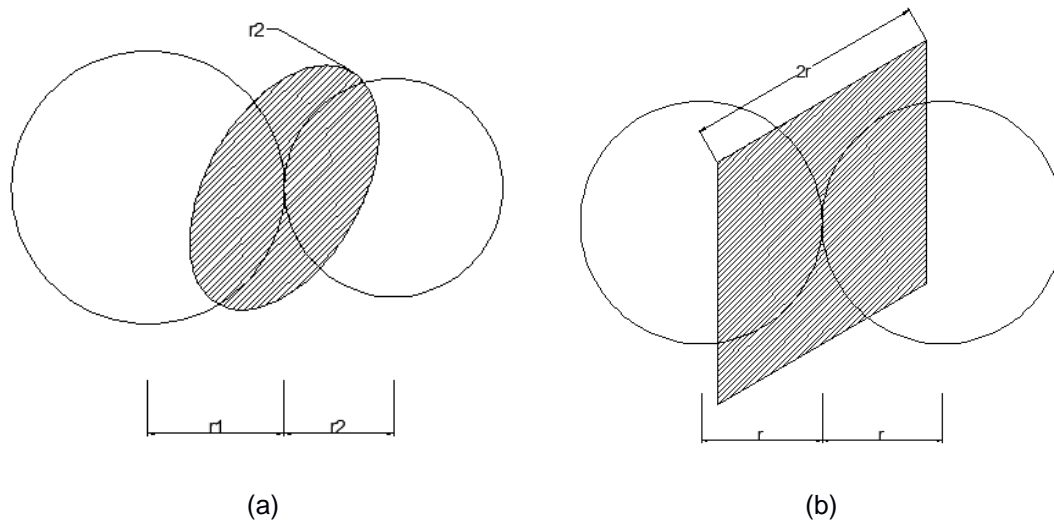
Figure 21: Sketch that represent A_{eq} at the contact point: (a) Original formula, (b) Modified formula.

- ξ_1 *different to zero*: The original constitutive law considers this parameter equal to zero and therefore simplifies the formula to compute the equivalent strain responsible for damage, $\tilde{\varepsilon}$. It was consider that the contribution of shear strain to the contact damage was of importance and therefore such simplification was rejected. Thus the formula to compute $\tilde{\varepsilon}$ is the one presented on equation (58).

$$\tilde{\varepsilon} = \sqrt{\langle \varepsilon_N \rangle^2 + \xi_1^2 * |\varepsilon_T|^2} \qquad\qquad (58)$$

- A modification to directly affect the mechanical properties of the interface was implemented. Thus the value of such variables is computed as the average value of the properties of the two different materials or can also be manually imputed or modified.

  This modification was necessary in order to provide the simulation with the necessary values for the mechanical properties of the interface. Otherwise, the code will remain limited to the computation of such parameters as the average value of the two different materials assigned to the spheres in contact. In this research, two main parameters (young and epsCrackOnset, see section 4.3.2 for more details) were modified after computation of average value by the introduction of coefficients of reduction in order to obtain the appropriate composite response of the masonry.

3.5   Conclusions

DEM method is based on a particle-particle interaction. By its nature, this is an iterative dynamic modeling technique which describes contact between bodies with the use of simple equations at every time step.

The constitutive law used allows to describe complex phenomena at every contact point between the particles. Thanks to the modifications applied to the constitutive law, originally developed to describe the behavior of concrete by Smilauer, it was possible to control key aspects for the adequate simulation of masonry.

As mentioned on 0, one of the most important drawbacks of DEM is its high computational cost. This is influenced basically for two factors; the number of particles and the simulated time. This factor, combined with the research time constrain, highly limited the scope of this dissertation and prevented us to carry out more simulation cases and achieve more precise results as it will be explained in the next chapter.

4. NUMERICAL SIMULATIONS

4.1 Introduction

In this chapter the procedure to simulate, calibrate and validate the DEM simulations will be explained. A presentation of the input parameters used in such simulations, including initial and final values, is summarized and presented in tables. The simulations performed in order to obtain the mechanical properties parameters to describe both brick and mortar response as well as the composite behavior of masonry will be described in detail.

The performed parametric analysis will be presented in order to show the influence of two important variables in the final results of the simulations (particle's size and thickness of the specimens). Finally a comparison between the DEM simulations developed during this dissertation and the results presented by (Marastoni , 2016) (FEM simulations and experimental campaign results) will be described. Conclusions of the obtained results and the discussed topics are presented at the end of the chapter.

4.2 Procedure description

In order to characterize the mechanical properties of a material, experimental techniques have to be used. Conventional macro properties are obtained by 2D and/or 3D compression, tensile and shear tests. The hypothesis of the existence of a physical relationship between micro and macro parameters can be validated through the numerical simulation at a micro-scale of such laboratory tests. This process is divided into the next steps (Recarey, et al., 2005):

- *Experimental campaign.* Determination of the macro parameters of the material thanks to the performance of laboratory tests.
- *Numerical simulation.* Use of DEM in order to simulate such laboratory tests.
- *Calibration.* Search of the appropriate values for the micro parameters in order to accurately describe the macro behavior of the material.
- *Validation.* Corroboration of the suitability of the used physical and mathematical adopted assumptions to relate micro to macro parameters and to properly describe the macro behavior of the material.

Due to the limited time to carry on this research it was decided not to perform a new experimental campaign. Instead, an existing experimental campaign developed and presented on two thesis, one of Master degree (Canella, 2014), and the second one of a PhD degree (Marastoni , 2016), was taken as reference. This campaign was performed at the Department of Construction Engineering of the Polytechnic University of Catalonia (UPC). Its aim was to obtain and validate general criteria that

enable the characterization of the mechanical properties of structural masonry components as well as the composite behavior of the material. In those researches, mechanical properties of brick and mortar (compressive strength, f_c, flexural strength, f_t, and Young's modulus, E) were determined separately by means of compression cube tests, compression cylinder tests and three points bending tests respectively. Besides, triplet tests were also carried out in order to simulate the composite behavior of masonry and determine the pick load under shear stress.

In this context, compression cube tests, compression cylinder tests and three points bending tests were simulated for both brick and mortar separately using DEM. The specimens were discretized on spheres with a constant diameter of 5 mm. This particle size was chosen in order to represent the smallest element, joint thickness on the triplets configuration (15 mm), with at least three lines of spheres, the two external lines will represent the interface with the brick spheres and the inner one will represent the mortar itself. 3D simulations were carried out following the description presented on the references, (Canella, 2014) and (Marastoni , 2016), with slight differences. The most important difference is the speed of the applied displacements. It was decided to use a speed of 7e-3 m/s instead of 7e-6 m/s in order to accelerate the simulations and optimize the process of calibration. It seemed that this modification did not affect significantly the results but in order to identify the influence of displacements speed application in the simulations a sensitivity analysis must be performed in further jobs.

The mechanical properties of both materials were calibrated taking into account the values and results obtained by (Canella, 2014) and (Marastoni , 2016) by a trial-error process. Finally, the triplet tests simulations were used to calibrate the parameters of the interface and therefore obtain a composite behavior of the material according to the results observed during the before mentioned experimental campaigns.

In order to validate DEM simulations a comparison between the experimental campaign results and the ones obtained by this technique were compared. An important aspect to take into account is the target value of one chosen parameter for each DEM simulation. Compressive strength, f_c, flexural strength, f_t, and Young's modulus, E were the selected parameters for compression cube tests, compression cylinder tests and three points bending tests respectively. On the other hand, the ultimate load reported by (Marastoni , 2016) was the target value for the triplet tests simulation. A maximum accepted error of 10 % for each case was reached except for one of them (brick flexural strength, f_t). This was an acceptable value because of the limited time, nevertheless, this small percentage error may influence in the final simulation of the triplet tests. Besides this agreement between the numerical values, appropriate fracture mode representation was also searched and achieved. Results of each stage will be presented and analyzed on the following sections.

4.3 Input parameters

4.3.1 Mortar and brick mechanical properties

All parameters included on the used constitutive law and influencing on the results were mentioned on section 3.3. Nevertheless, besides from the geometrical variables, only the next mechanical parameters can be directly controlled in the simulation:

- young
- frictionAngle
- poisson
- density
- equivStrainShearContrib
- sigmaT
- relDuctility
- epsCrackOnset

(Marastoni , 2016) proposes the numerical values presented in Table 3 to characterize both mortar and brick. Such values were taken into account and assigned to their correspondent DEM mechanical parameter in order to obtain a first approximation.

Table 3: Mechanical parameters' values for the numerical simulation presented by (Marastoni , 2016).

Mortar properties		Brick properties	
E_m [MPa]	400	E_b [MPa]	9792
v_m [MPa]	0.30	v_b [MPa]	0.17
$G_{f,m}$ [J/m^2]	100	$G_{f,b}$ [J/m^2]	100
c_m [MPa]	0.62	f_{tb} [MPa]	2.33
φ_m [°]	33.11	f_{cb} [MPa]	18.40
$f_{tm,CUT}$ [MPa]	0.34		

The calibration of the models was obtained by modifying the magnitude of the rest of the mechanical parameters and letting the values proposed by the mentioned reference unchanged. The calibrated values for the mortar are presented in Table 4. Table 5 shows the calibrated values for the brick.

Note: The values for the density were modified in order to take into account the voids on the volume caused by the discretization by means of spheres. Standard values of $2000\ kg/m^3$ and $1750\ kg/m^3$ were considered for brick and mortar respectively. Then this values were increased by a factor of 1.91 which relates the volume of a sphere circumscribed into the volume of a cube. Therefore the correspondent final value for both materials is the one shown in the mentioned tables.

Table 4: Model parameters values for mortar after calibration.

Parameter	Value	Unit
young	0.40e9	Pa
frictionAngle	33.11	°
poisson	0.30	-
density	3342.50	kg/m3
equivStrainShearContrib	0.10	-
sigmaT	0.62e6	Pa
relDuctility	1.00	-
epsCrackOnset	1.45e-4	-

Table 5: Model parameters values for brick after calibration.

Parameter	Value	Unit
young	9.80e9	Pa
frictionAngle	16.00	°
poisson	0.17	-
density	3820.00	kg/m3
equivStrainShearContrib	0.007	-
sigmaT	1.00e6	Pa
relDuctility	1.00	-
epsCrackOnset	1.00e-5	-

4.3.2 Interface mechanical properties

Triplet tests were simulating assuming the before mentioned values to describe both mortar and brick mechanical properties. Thanks to the modifications applied to the code and the constitutive law originally developed by (Smilauer, 2010), it was possible to directly assign values to the mechanical properties of the interface. $sigmaT$ and $frictionAngle$ were assigned directly since they represent

the direct properties of the interface, whereas that the rest of the values were calculated as the mean value of the two different materials in interaction.

Thus, assuming E_m represent the value of young of the mortar and E_b the value of the same parameter for the brick, we have that E_i representing the average value of young of the interface is equal to:

$$E_i = \frac{E_m + E_b}{2} \qquad\qquad (59)$$

And the same was applied for $poisson$ and $epsCrackOnset$. Interface parameter's values are presented in Table 6.

Table 6: Model parameters values for interface after calibration.

Parameter	Value	Unit
sigmaT	1.00e5	Pa
frictionAngle	15.00	°
poisson	0.235	-
young	5.10e9	Pa
epsCrackOnset	7.75e-5	-

In order to calibrate the composite behavior of the masonry two different reduction factors were introduced. Those factors modified the calculated value of the interface mechanical properties $young$ and $epsCrackOnset$. Values for such reduction factors and the final values used for these mechanical parameters during the final simulation are presented in Table 7.

Table 7: Reduction factors for young and epsCrackOnset of the interface and final value used for each variable.

|	Reduction factor	Final value used
young	0.00028	14.28e5 (Pa)
epsCrackOnset	0.0001	7.75e-9 (-)

4.4 Mortar

4.4.1 Compression cube tests

Hydraulic lime mortar was produced and tested. When the three points bending tests, described on a further section, were performed the failure of the specimens produced two different prisms. The fragments obtained from that test were recovered and tested to obtain the compression strength of the mortar following the EN 1015-11:2007 standard. The dimensions of such specimens were about 80x40x40 mm and they were loaded with loading plates of 40x40 mm dimensions. An average flexural strength of $f_{cm} = 2.45\ MPa$ was determined by (Canella, 2014) and (Marastoni , 2016). Figure 22 shows the geometry of both the experimental campaign specimen and the set-up of the DEM simulation.
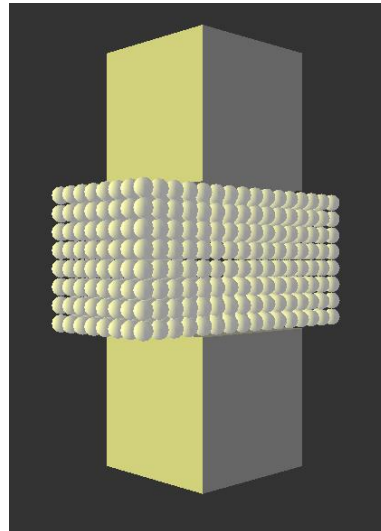
(a)	(b)

Figure 22: Mortar compression cube tests; (a) Experimental set-up (Canella, 2014), (b) Geometry of the DEM simulation model.

The results of the DEM simulation are presented in Figure 24. The value obtained for the compressive strength, f_{cm}, was 2.29 MPa. Which gives an error equal to 6.53 % in comparison with the value reported by (Canella, 2014) and (Marastoni , 2016). Figure 23 presents the failure of the specimens on the experimental campaigns. If it is compared to Figure 24 it can be noticed that both DEM and experimental failures are in agreement.
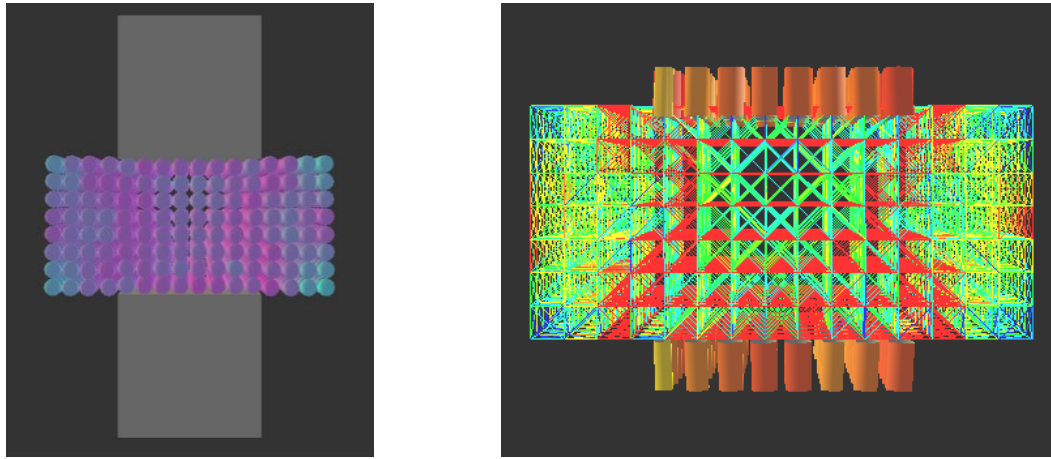
Figure 23: Mortar compression cube test failure (Canella, 2014).

4.4.1   Compression cylinder tests

Although (Marastoni , 2016) does not mention the procedure he followed in order to determine the Young's modulus of mortar he proposes a value of $E_m = 400\ MPa$. It is assumed that he followed the standard EN-12390-13:2013 in order to obtain it. This will be the reference value used on this dissertation as well. On the other hand (Canella, 2014) presents the procedure she followed according to the standard EN 12390-13:2013, which originally is aimed to test concrete cylinders, to characterize high strength mortar. Pictures presented hereinafter are only intended to provide visual guidance but it has to be clarified that they do not correspond to the evaluation of the referenced mortar taken into account on this dissertation. Figure 25 shows the geometry of both the experimental campaign specimen set-up and of the DEM simulation model.

The results of the DEM simulation are presented in Figure 27. The value obtained for the Young's modulus, E_m, was 366.48 MPa. Which gives an error equal to 8.38 % in comparison with the value reported by (Canella, 2014) and (Marastoni , 2016). Figure 26 shows the failure presented on the high strength mortar after being tested on the laboratory. Similar failure modes are observed for the DEM simulation model. Even though not direct comparison can be stablished since they represent different materials.

(a)

(b)
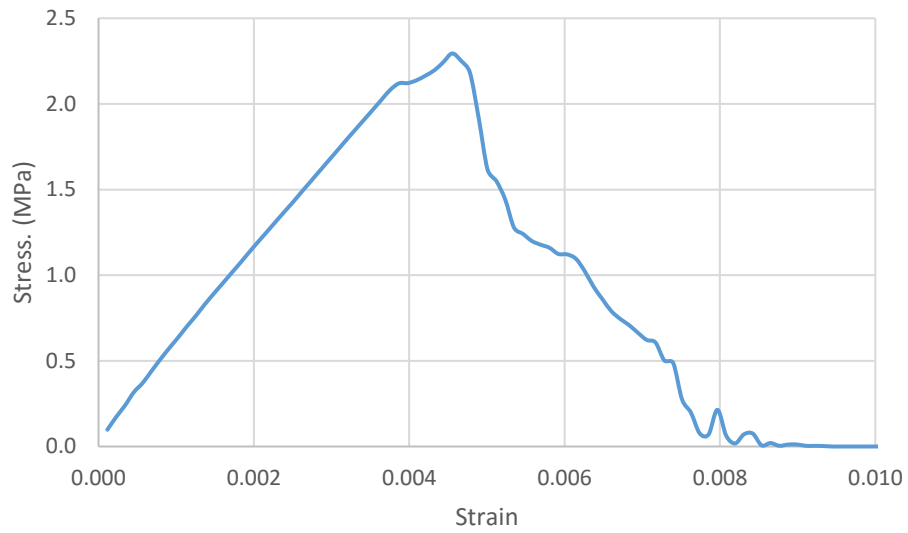
(c)

Figure 24: Mortar compression cube test DEM simulation results; (a) Displacements, (b) Contact damage, (c) Graph stress-strain.
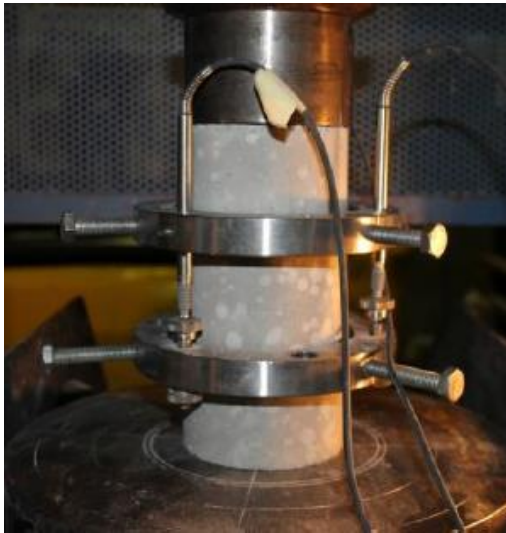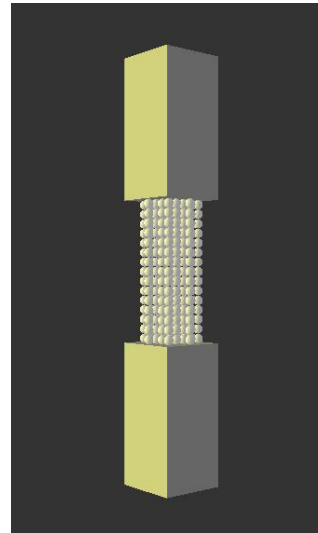
(a) (b)

Figure 25: Mortar compression cylinder test; (a) Experimental set-up (Canella, 2014), (b) Geometry of the DEM simulation model.
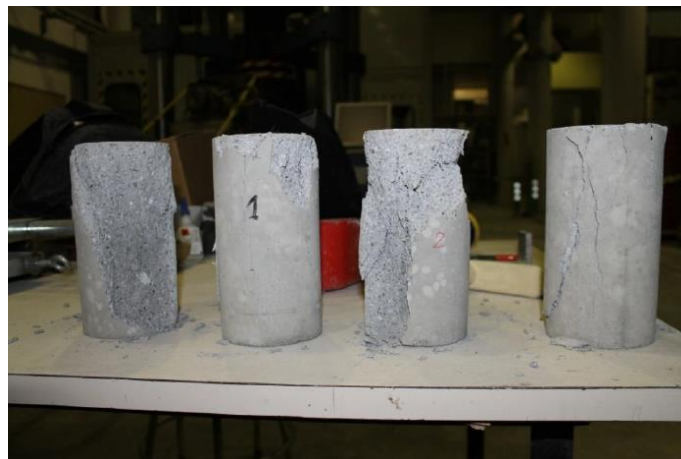
Figure 26: High strength mortar compression cylinder tests failures (Canella, 2014).

(a)

(b)

(c)
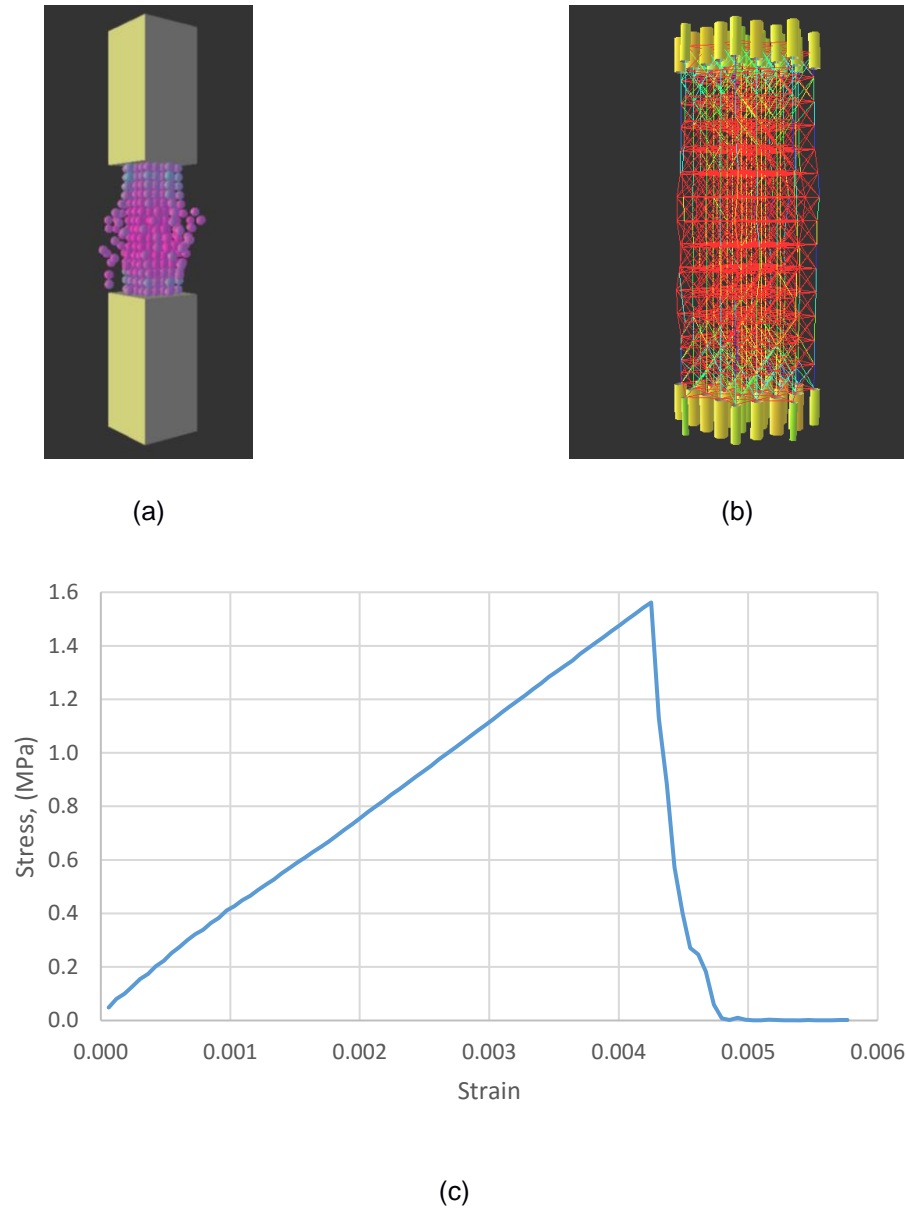
Figure 27: Mortar compression cylinder test DEM simulation results; (a) Displacements, (b) Contact damage, (c) Graph stress-strain.

4.4.1 Three points bending tests

Whereas that cube and cylinder compression test were useful to determine compressive strength, f_c, and Young's modulus, E, the three points bending tests allowed to compute the value of the flexural strength, f_t, of the masonry components. The general set-up of the three points bending test is shown in Figure 28.
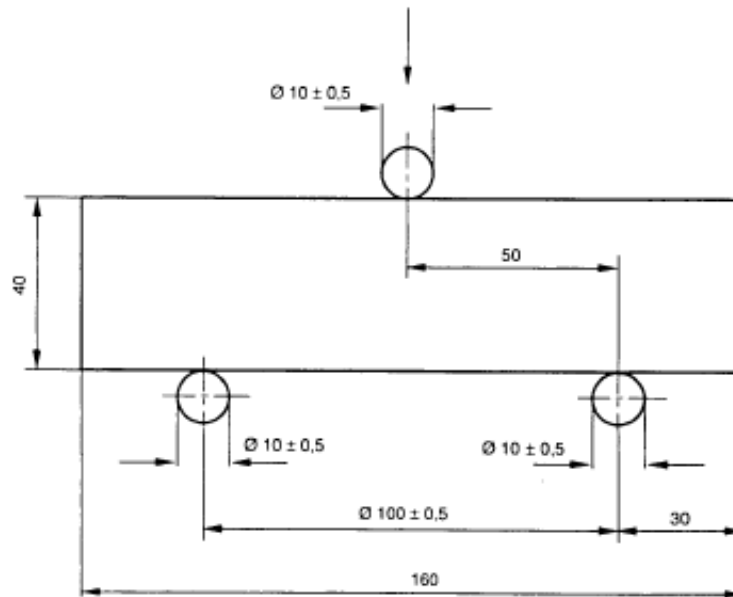
Figure 28: Flexural strength test (dimensions in mm) (EN 1015-11, 1999).

Prismatic samples with 160x40x40 mm dimensions were prepared under strict laboratory conditions and following the procedure specified in the EN 1015-11:2007 standard. Three specimens were tested after 270 days they were built under load control at a constant rate of 10 N/s and the flexural strength of the material was determined. The average value obtained by (Canella, 2014) and (Marastoni , 2016) was $f_{tm} = 0.37\ MPa$. Figure 29 shows the geometry of both the experimental campaign specimen set-up and of the DEM simulation model.
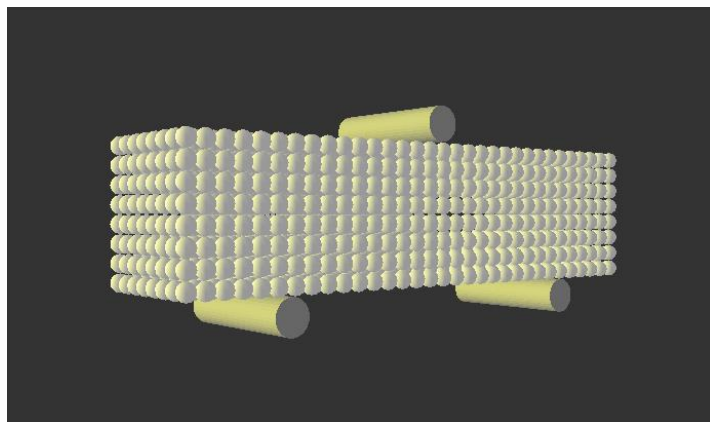
(a)   (b)

Figure 29: Mortar three points bending test; (a) Experimental set-up (Canella, 2014), (b) Geometry of the DEM simulation model.

The results of the DEM simulation are presented in Figure 31. The value obtained for the flexural strength, f_{tm}, was 0.36 MPa. Which gives an error equal to 2.7 % in comparison with the value reported by (Canella, 2014) and (Marastoni , 2016). Figure 30 shows the failure presented on the mortar specimen after being tested on the laboratory.

Special attention should be paid to the results reproduced by the DEM simulation. At an early stage a similar failure mode as that shown by the experimental campaign was reproduced in a satisfactory way. At the same step of the simulation the searched value for the flexural strength of the material was found and therefore the result was acceptable. It is interesting to note that when the simulation was taken further, a different behavior was presented by the material. After a period of almost zero variation on the stress a big increased on the stress was registered. This second stage of the simulation correspond to the creation of new contacts between the cylinder supports and the spheres of the bottom layer of the specimen. As can be seen in the results a strut like response appears and as a consequence the displacement of the load cylinder is resisted on almost pure compression by the spheres. This compression resistant response explains the increase on the pick of the graph and the new failure mode shown in the second part of the results. Since this second response was registered quite later after the principal response it will be ignored. Nonetheless, it was mentioned since as it will be shown further on the next section this cannot be ignored for the brick three points bending test.

Figure 30: Mortar three points bending test failure (Canella, 2014).

(a)

(b)
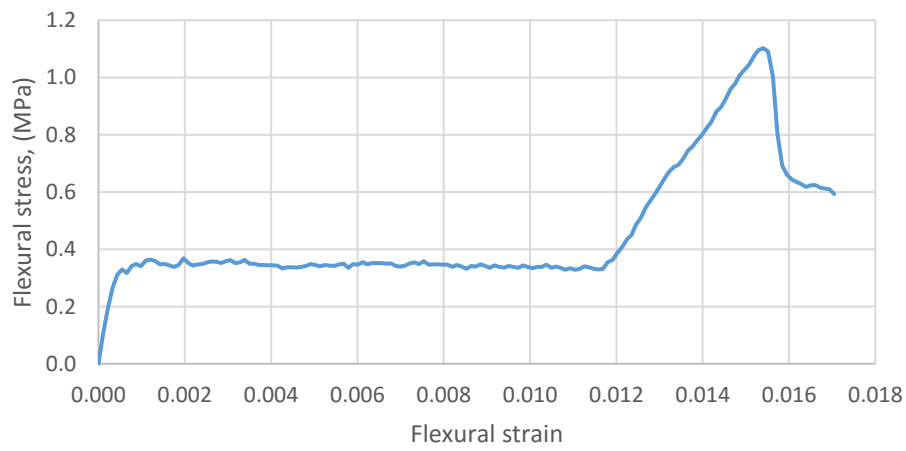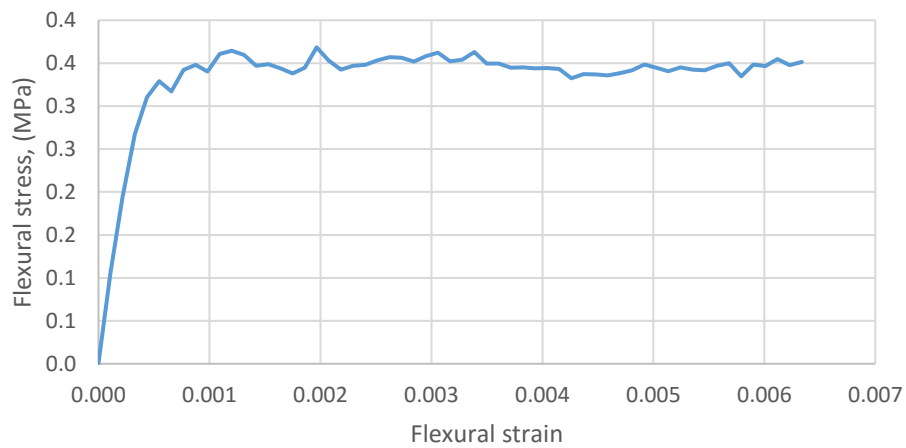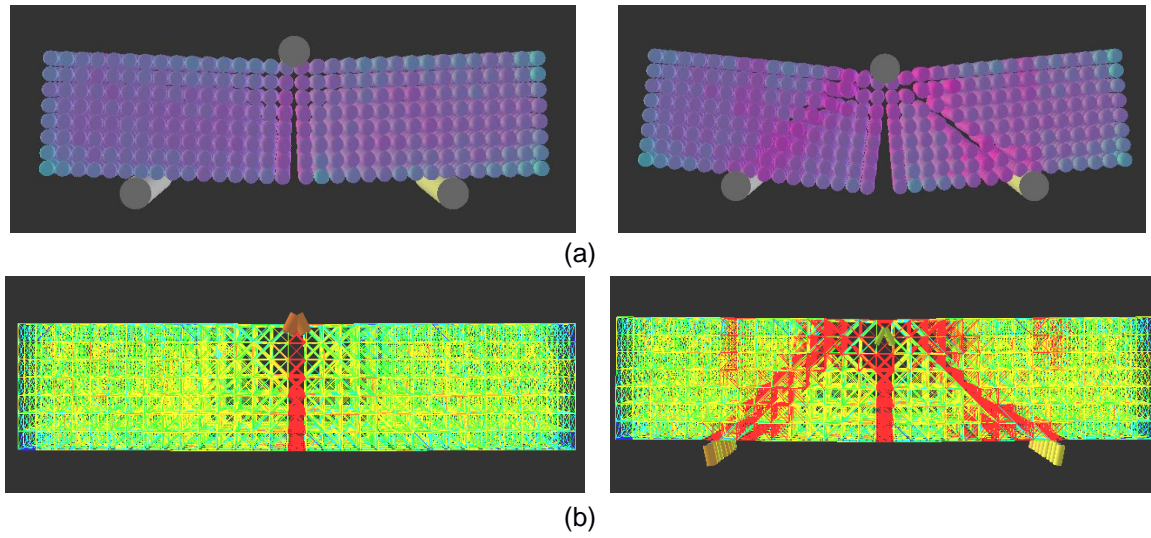
(c)

Figure 31: Mortar three points bending test DEM simulation results; (a) Displacements, (b) Contact damages, (c) Graphs stress-strain.

4.5   Bricks

4.5.1   Compression cube tests

The blocks tested were handmade fired-clay solid bricks. Specimens with 35x35x35 mm dimensions were cut from the whole bricks and tested on simple uniaxial compression under force control in order to obtain their compressive strength. Since there is no standard available to perform this test for bricks, a reference standard for mortars was taken into account, EN 1015-11:2007. An average value of compressive strength $f_{cb} = 18.40\ MPa$ was obtained by (Canella, 2014) and (Marastoni , 2016). Figure 32 shows the geometry of both the experimental campaign specimen and of the DEM simulation model.
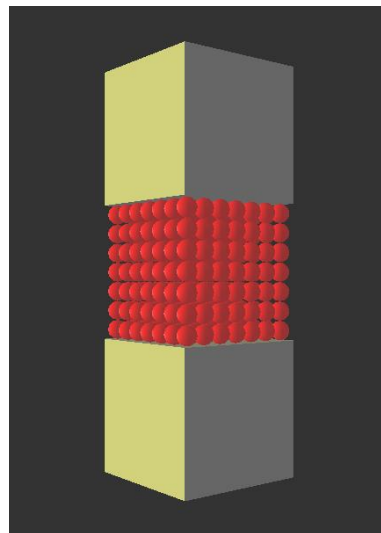
(a)   (b)

Figure 32: Brick compression cube test; (a) Specimen carved from whole brick (Canella, 2014), (b) Geometry of the DEM simulation model.

The results of the DEM simulation are presented in Figure 33. The value obtained for the compressive strength, f_{cb}, was 18.68 MPa. Which gives an error equal to 1.52 % in comparison with the value reported by (Canella, 2014) and (Marastoni , 2016). Unfortunately, no pictures of the failure of the specimen are presented on any of the mentioned references in order to be compared with the failure obtained by DEM simulation.

(a)

(b)

(c)
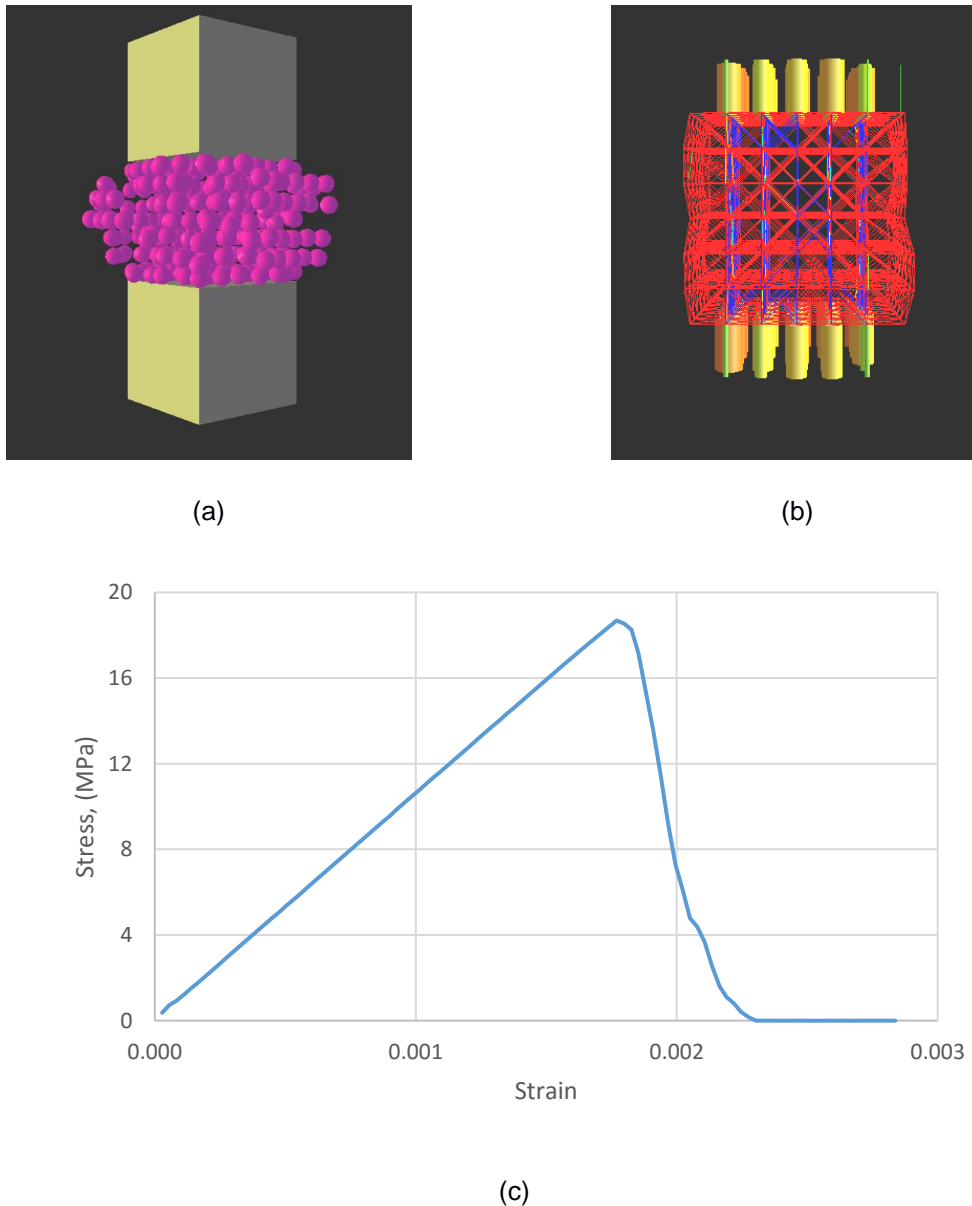
Figure 33: Brick compression cube test DEM simulation results; (a) Displacements, (b) Contact damage, (c) Graph stress-strain.

4.5.2 Compression cylinder tests

In order to compute the Young's modulus of the bricks the EN-12390-13:2013 was used (even thought this standard is stablished for concrete samples). Cylinders with 35 mm diameter and 75 mm high were cored from the bricks. Young's modulus was determined after three cycles from 30% to 60% of the failure load and the average value found was $E_b = 8106 \, MPa$ by (Canella, 2014) and (Marastoni , 2016). Brick compression cylinder tests also provided an average value for the compressive strength of the material equal to 12 MPa. Figure 34 shows the geometry of both the experimental campaign specimen set-up and of the DEM simulation model.

<center>(a)   (b)</center>
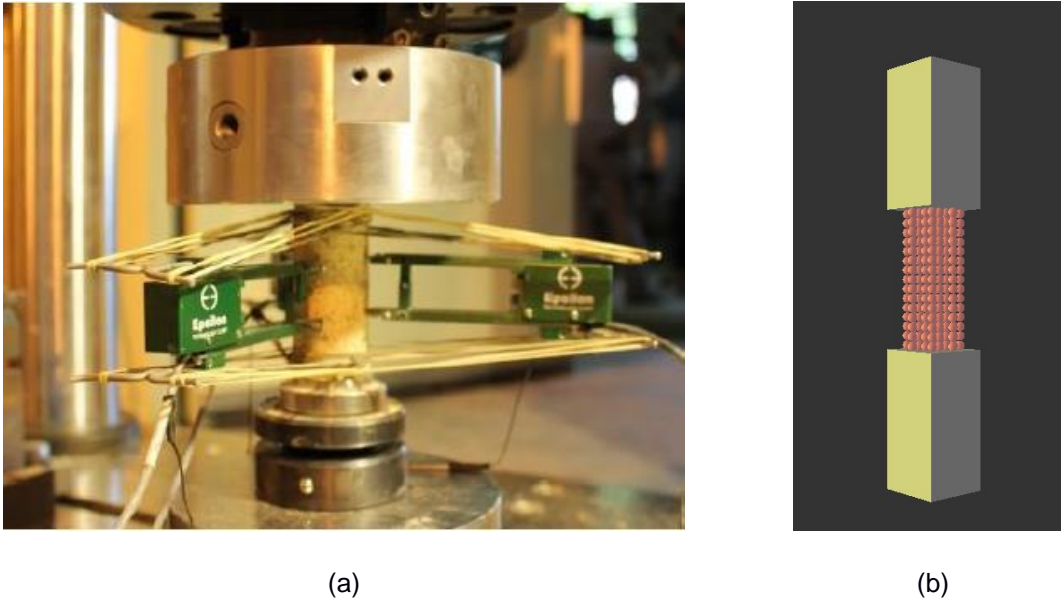
Figure 34: Brick compression cylinder test; (a) Experimental set-up (Canella, 2014), (b) Geometry of the DEM simulation model.

The results of the DEM simulation are presented in Figure 36. The value obtained for the Young's modulus, E_b, was 7606.76 MPa. Which gives an error equal to 6.16 % in comparison with the value reported by (Canella, 2014) and (Marastoni , 2016). As for the compressive strength the value found is equal to 11.95 MPa which represent an error of 0.42% in comparison with the average value presented by the mentioned references. Figure 35 shows the failure presented on the brick cylinder after being tested on the laboratory. In this case no agreement is achieved between laboratory and DEM simulation failure.

Figure 35: Brick compression cylinder test failure (Canella, 2014).

(a)   (b)

(c)
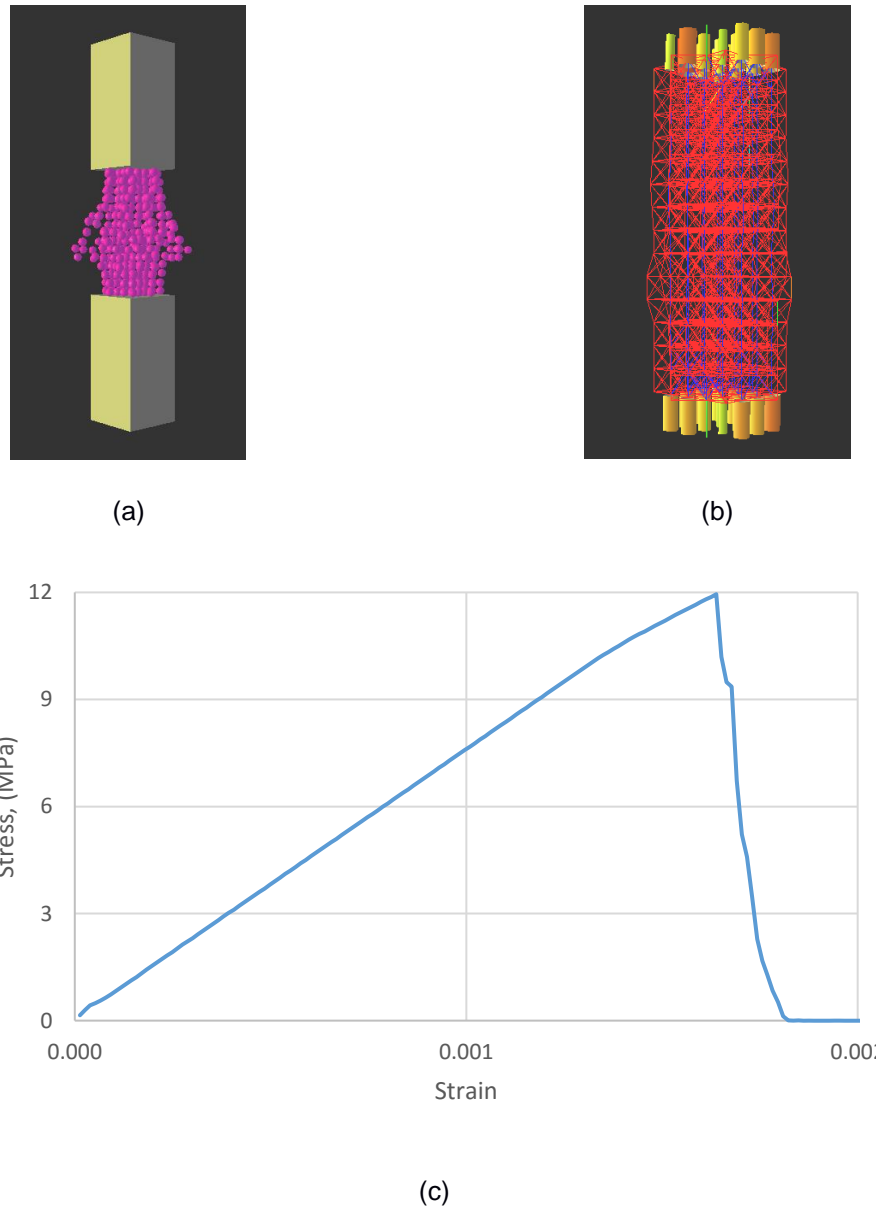
Figure 36: Brick compression cylinder test DEM simulation results; (a) Displacements, (b) Contact damage, (c) Graph stress-strain.

4.5.3   Three points bending tests

EN 1015-11:2007 which specifies the procedure to determine the flexural strength of mortars was used as reference since there is no standard available to determine this property for bricks. 160X40x40 mm prisms were cut from the whole bricks and tested following the mentioned standard. An average flexural strength for the bricks $f_{tb} = 3.63\ MPa$ was found by the before mentioned references. Figure 37 shows the geometry of both the experimental campaign specimen and of the DEM simulation model.

(a)   (b)
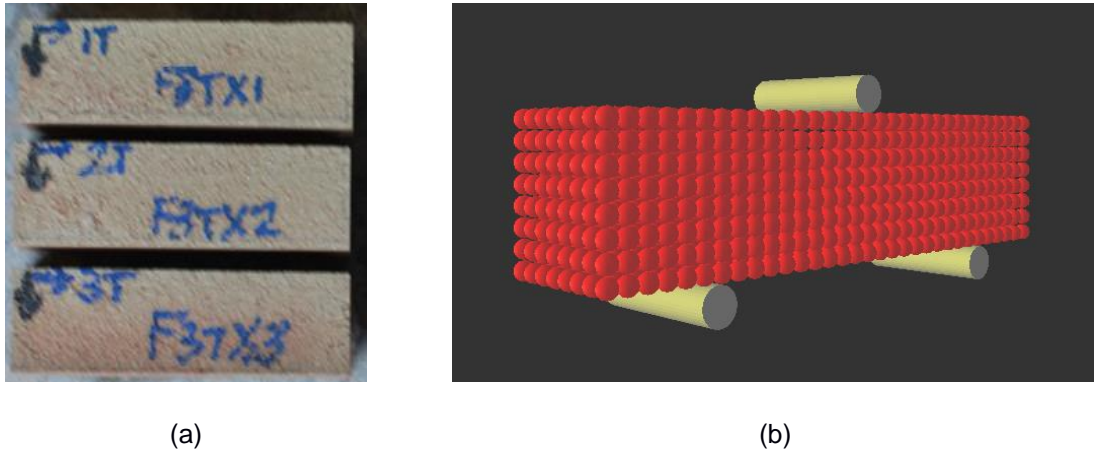
Figure 37: Brick three points bending test; (a) Specimens carved from whole brick, (b) Geometry of the DEM simulation model.

The results of the DEM simulation are presented in Figure 38. The value obtained for the flexural strength, f_{tb}, was 2.34 MPa. Which gives an error equal to 35.54 % in comparison with the value reported by (Canella, 2014) and (Marastoni , 2016). It is worth mention that this error was the biggest among all other values found and the only one above 10 % difference in comparison with the values taken from the references. Even more, unfortunately no pictures of the failure of the specimen are presented on any of the mentioned references in order to be compared with the failure obtained by DEM simulation.

Similar comments as those made for the mortar test concerning the two different simulation stages can be made about the brick simulation with the only difference that for the brick they appear immediately one after the other and is only after the second phases that a more accurate value is obtained for the flexural strength of the material. That is the reason why it is considered that the second phase cannot be ignored and the value found at the end of this phase is the one used for validation of the model.

4.1   Triplet tests

This tests were performed in order to determine the shear behavior of masonry. They were carried out following the EN 1052-3:2002 standard. Nine triplets with dimensions 145x160x305 mm were tested. The triplets consist on three bricks and two mortar joints. The average thickness of the mortar joints is considered to be 15 mm. Figure 39 shows in detailed the setup of the experiment and a 3D sketch.

(a)

(b)
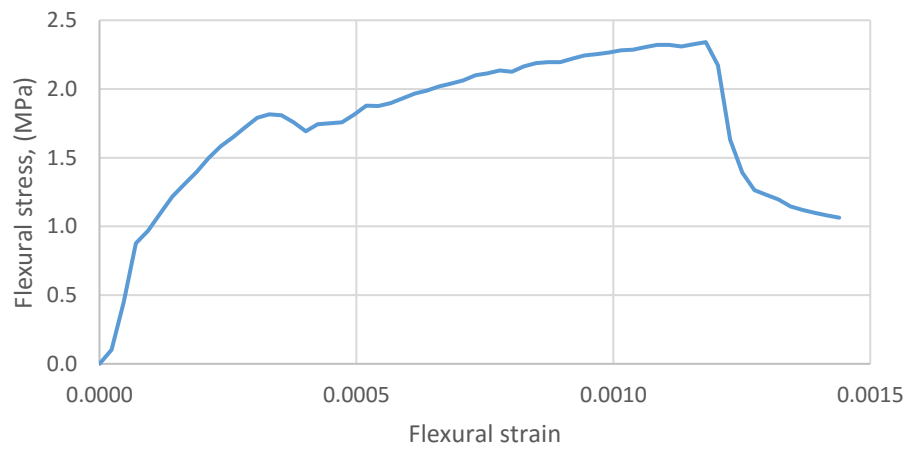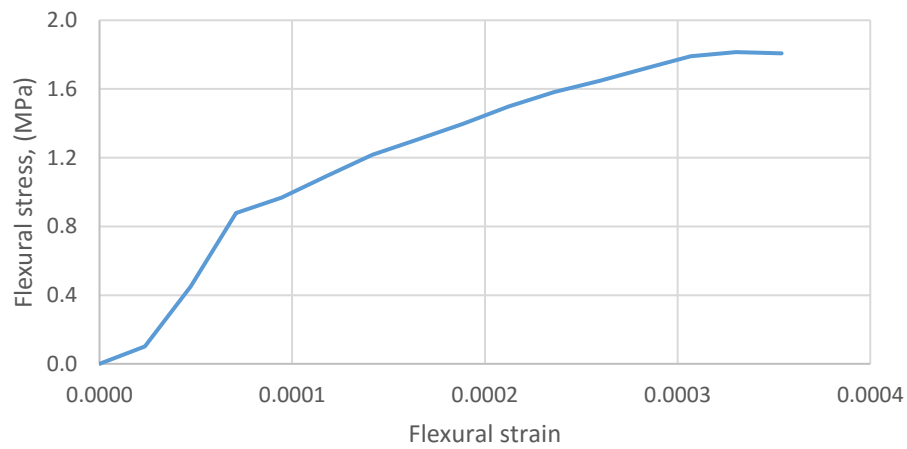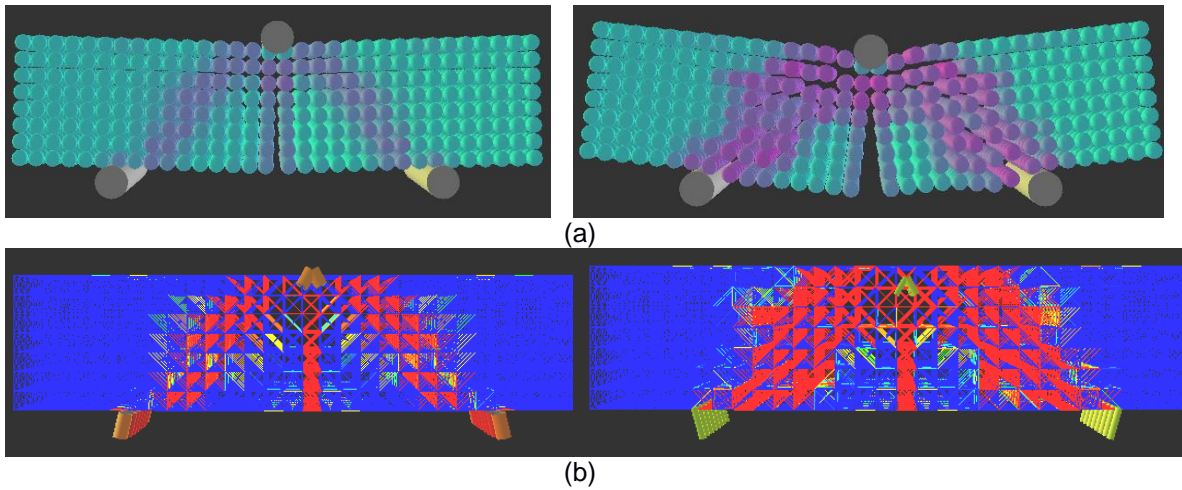
(c)

Figure 38: Brick three points bending test DEM simulation results; (a) Displacements, (b) Contact damages, (c) Graphs stress-strain.
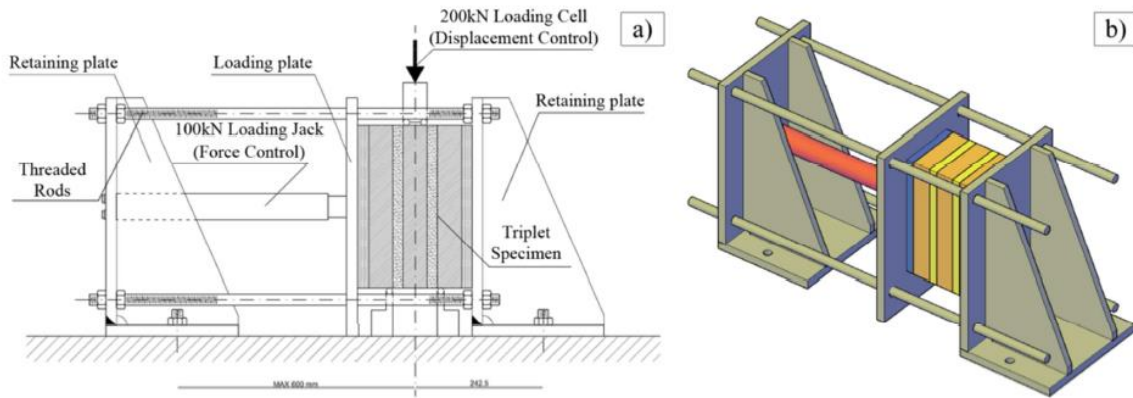
Figure 39: Experimental setup for triplet test (a) and 3D sketch (b) (Marastoni , 2016).

The nine triplets were divided into three different groups tested at different pre-compression values. Three of them were pre-compressed at 0.2 MPa, the second group was pre-compressed at 0.6 MPa and finally the last three triplets were pre-compressed at 1.0 MPa. All this procedure was followed in agreement with the before mentioned standard. The obtained load-displacement experimental curves are presented in Figure 40. It can be seen that the bigger the pre-compression pressure applied the bigger the final load resisted by the specimen.
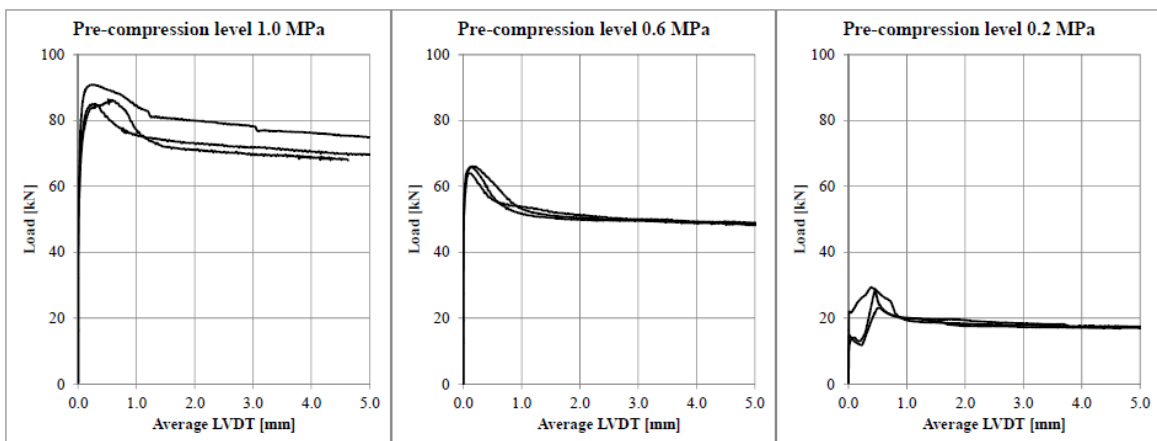
Figure 40: Triplets tests: load vs average LVDT's displacement for each step of pre-compression (Marastoni , 2016).

Figure 41 shows the geometry of both the experimental campaign set-up and of the DEM simulation model. In this dissertation only the test carried out at a pre-compression level of 0.2 MPa was reproduced since attempting to reproduce the other levels of pre-compression will result in a considerable increase of time. It should also be noted that a simplification was adopted in order to reduce the time needed to run every single simulation and therefore optimize and achieve on time the calibration goal. The maximum load reported by the mentioned references is equal to 27.09 kN for the configuration of 0.2 MPa pre-compression.

As described before the diameter of the spheres was of 5 mm, thus three spheres could be modeled on the thickness of the mortar joint. The simplification adopted consist thus in the modeling of only one layer of spheres on the thickness of the brick. Therefore this single layer represents only 1/60 times the thickness of the whole specimen. The maximum load obtained has been multiplied by a factor of 60 in order to show what will be in fact the value if the whole thickness of the specimen had been modeled. As it will be shown later, good agreement was found between the maximum load resisted by the specimen and the failure mode and those obtained by the experimental campaign presented on the before mentioned reference (Marastoni , 2016). Unfortunately, the behavior of the load-displacement graph of the described DEM simulation simplified set-up disagrees with that obtained during the experimental campaign.

(a)   (b)
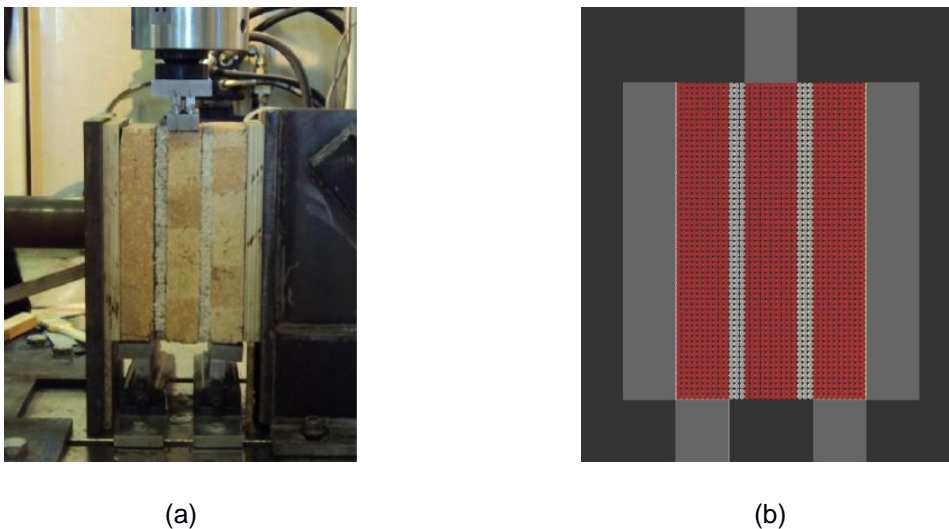
Figure 41: Mortar three points bending test; (a) Experimental set-up (Canella, 2014), (b) Geometry of the DEM simulation model.

The results of the DEM simulation are presented as a sequential series of pictures to represent displacements, contact damage and load-displacement graphs from Figure 43 until Figure 46. The value obtained for the maximum load was 27.36 kN. Which gives an error equal to 1.0 % in comparison with the value reported by (Marastoni , 2016). Figure 42 shows the failure presented on the triplet after being tested on the laboratory. It can be seen that the plan of fracture is presented within the mortar and its interface with the bricks. Pretty good agreement was achieved on the DEM simulation to represent the failure mode as can be seen specifically in Figure 43 and Figure 44, the first one showing the displacements of the spheres and the later one presenting the contact damage and therefore the fracture plan of the specimen.
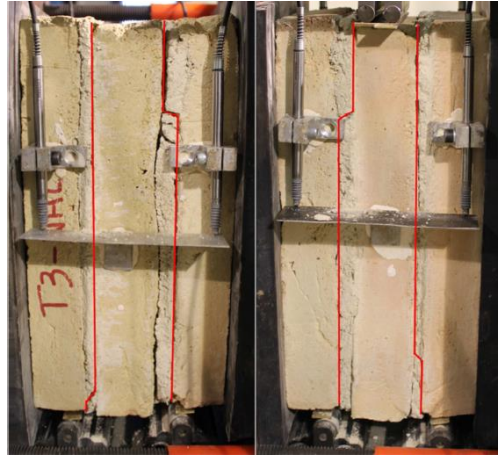
Figure 42: Typical failure of a triplet after being tested on the laboratory (Marastoni , 2016).
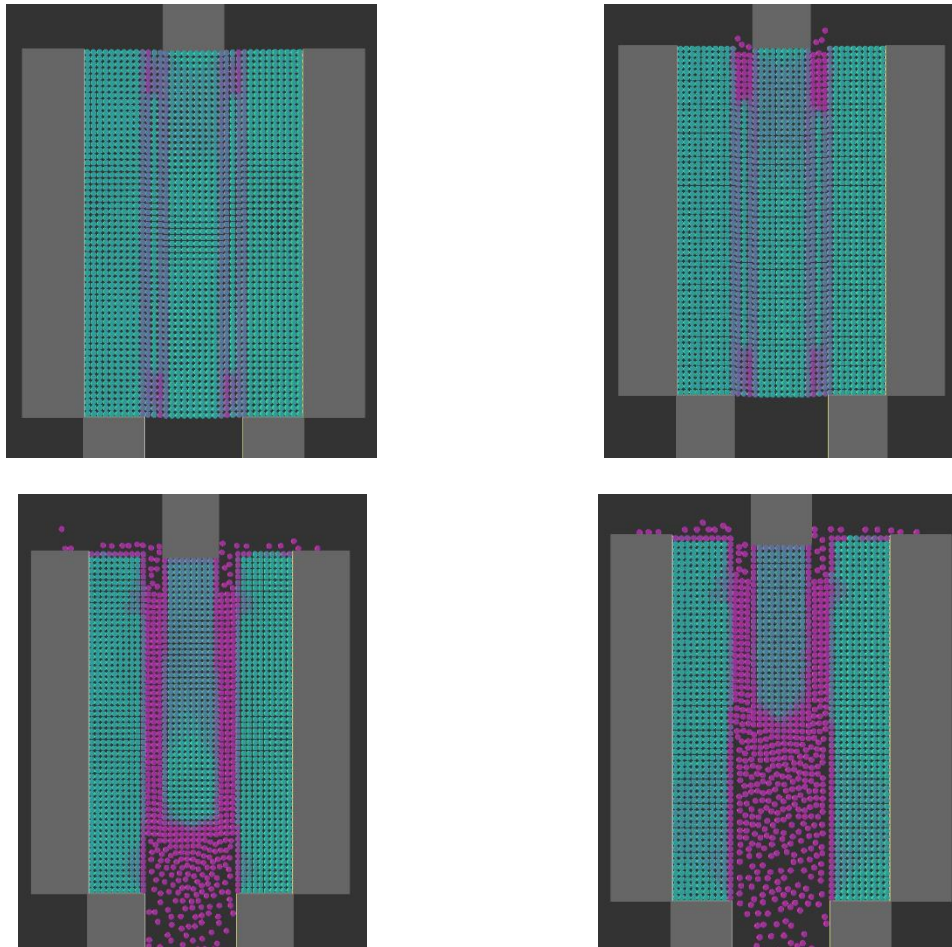
Figure 43: Sequential progression of the displacements during the triplet simulation.
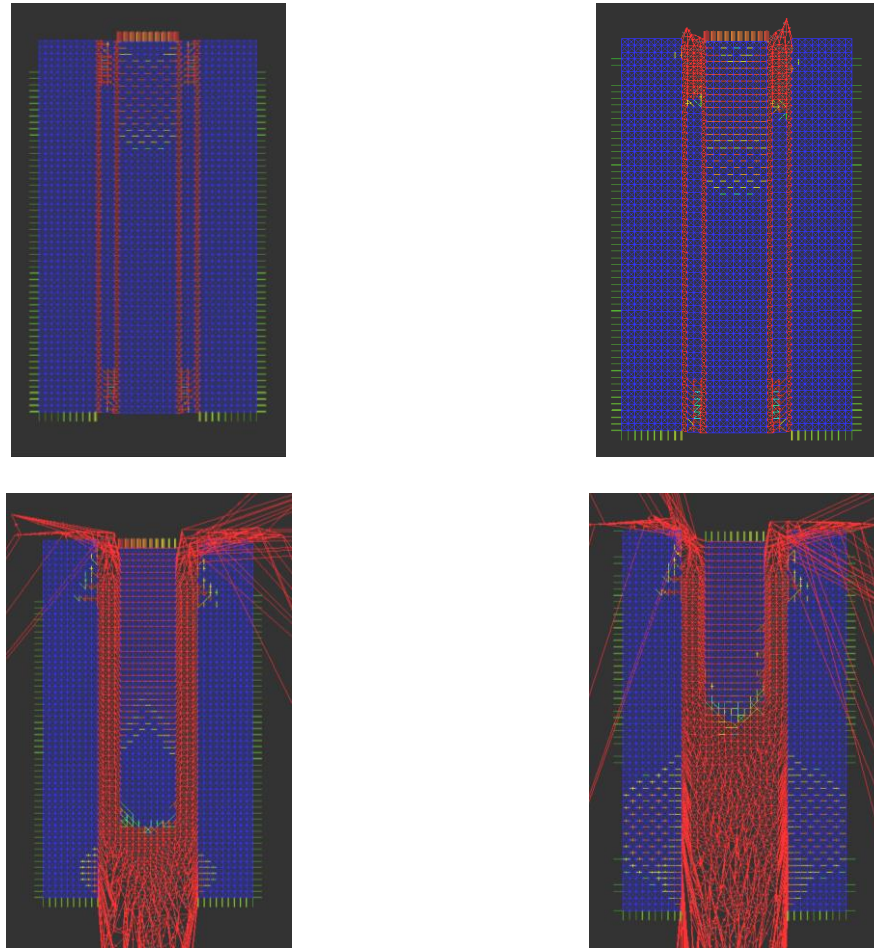
Figure 44: Sequential progression of the contact damages during the triplet simulation.

Figure 45 presents the procedure of pre-compression of the triplet on the DEM simulation. Disregarding an initial jump on the graph it can be seen that the loading was practically linear. This initial irregularity may be due to an initial rearrangement on the spheres when first got in contact with the two boxes in charge of apply the pre-compression.

Finally in Figure 46 the progression of the load-displacement graph correspondent to each of the deformation and contact damage pictures can be observed. The plot presents a similar behavior to the one obtained during the experimental campaign, that is, an initial increase on the load as the displacement increases until it reaches the maximum value where the fracture appears and subsequently a small fall on the load to finally continue in a less marked decay way due to the remaining friction contact between the particles.

Unfortunately it differs from the experimental graph. As can be seen, on DEM simulation the peak load is reached at a value correspondent to more or less 5.0 mm whereas that the pick load was reached on the experimental campaign even before only 1 mm displacement (see Figure 40).
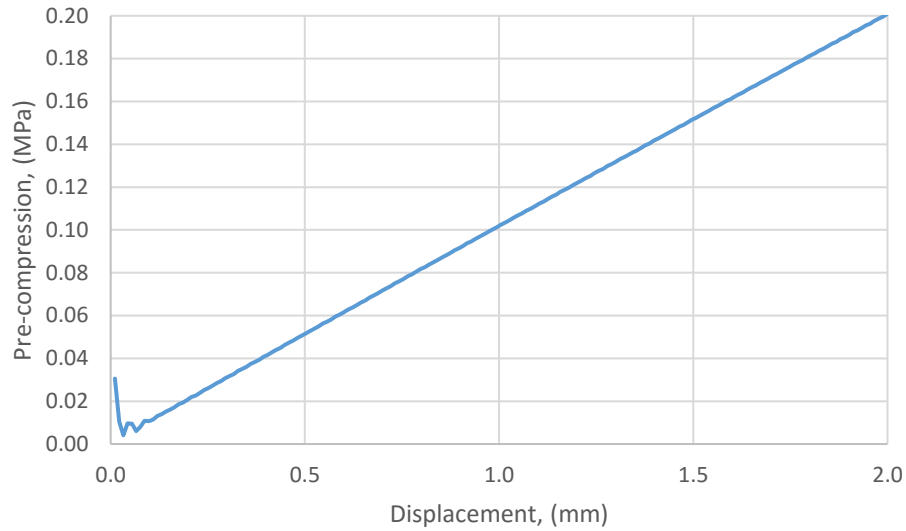
Figure 45: Pre-compression of the triplet test simulation.
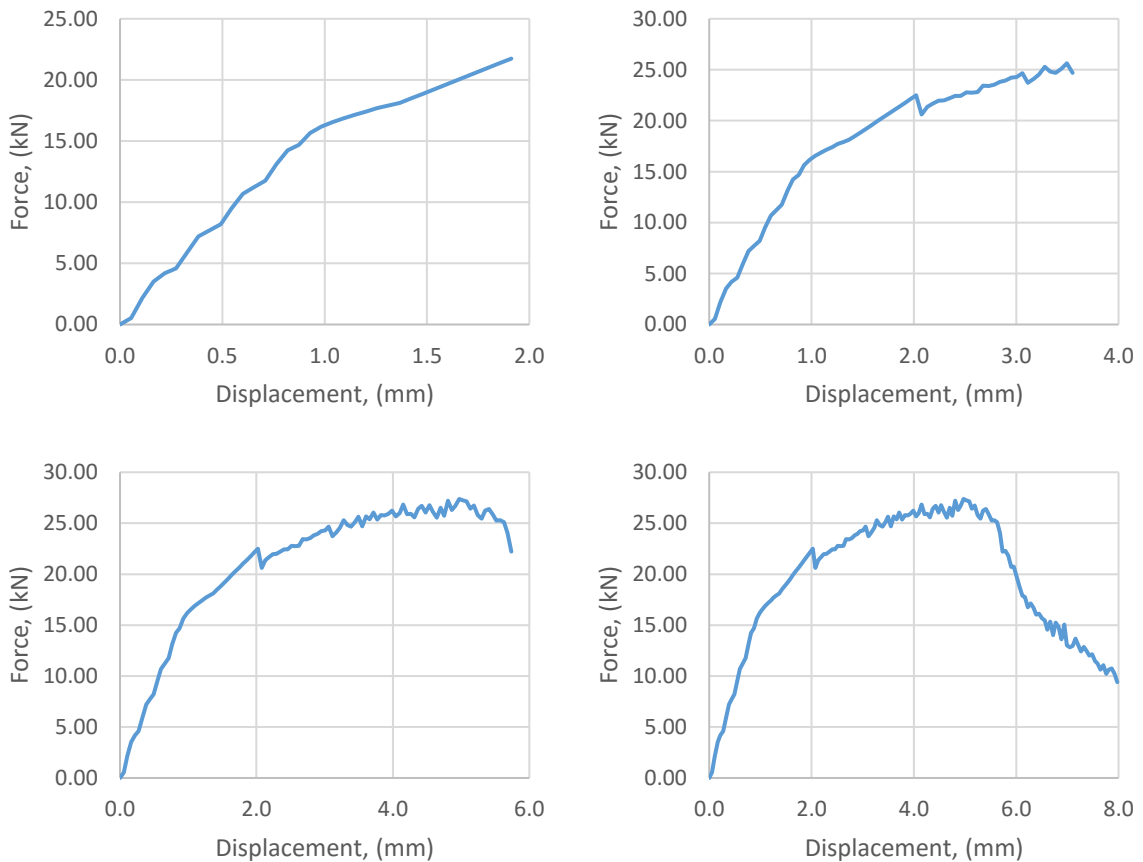
Figure 46: Sequential progression of the force-displacement graphs during the triplet simulation.

4.2   Parametric analysis

In order to evaluate the influence of certain geometrical parameters in the presented DEM simulations, two different parametric analysis were carried out. Both parametric analysis were carried out in the mortar compression cube test due to its simplicity and to the high level of accuracy obtained during the calibration of the mechanical properties of such material.

The first one concerns the spheres size. Starting from the initial sphere's diameter of 5 mm ($r = 0.0025\ m$) two steps of refinement were studied. Basically the particle radius was halved twice and then the error in the compressive strength was calculated based in the value provided by (Marastoni , 2016).

The second parametric analysis consist in the evaluation of the influence of reducing the thickness of the specimens. Basically this influence is of particular interest for this research due to the fact that the simulation of the triplet was based in the modeling of a single layer of spheres instead of the whole thickness of the brick. Such assumption permitted to obtain the final value of the resisting force by multiplying the computed force value for the correspondent relationship among the thickness of the whole specimen and the sphere size. This simplification was of paramount importance in order to achieve calibration and validation of the triplet simulation in time due to the time constraints of the development of this dissertation. Thus the thickness of the mortar compression cube was first divided by 2, then by 4 and finally by 8 (this last reduction is equal to the representation of the compression cube with only one layer of spheres, which matches the assumption used to simulate the triplet). Then the error on the compressive strength was calculated based in the value provided by (Marastoni , 2016).

4.2.1   Parametric analysis: Size of spheres

The values obtained for the compressive strength of the mortar, f_{cm}, after the variation on the size of the spheres as well as the computation of the percentage error in comparison with the target value provided by (Marastoni , 2016) are presented in Table 8. It was expected that by reducing the size of the particle more accurate results would be obtained. Nonetheless, it can be noticed that for the smallest size of spheres studied ($r = .000625\ m$) the error percentage is even bigger that for the coarser case, overpassing even the accepted limit of 10 % error.

The linear regression of the results is shown in Figure 47. The value obtained for the Pearson's lineal correlation coefficient is equal to 0.5145. This represents a moderate positive correlation between the size of the particles, r, and the compressive strength of the mortar, f_c. As for the determination coefficient, R^2, the value found is 0.2647. Which indicates that only 26.47 % of the variations in the values of f_c can be described thanks to the variation in the size of the spheres, r. This is unfortunately

a very low value to relate both variables thus showing that the inferences made based in the regression equation obtained would provide low accurate results.

Table 8: Parametric analysis (variation on the size of the spheres) results.

Mortar compression cube			
$r\ (m)$	$f_c\ (MPa)$	$f_{c\ target}\ (MPa)$	$Error\ (\%)$
0.0025	2.29	2.45	6.53
0.00125	2.36	2.45	3.67
0.000625	2.14	2.45	12.65

Figure 48 displays the values obtained of the compressive strength of the mortar, f_c, for every different size of spheres. Along with this parameter, its correspondent percentage error is also plotted. It can be noticed that contrary to what was expected the biggest error occurs when the simulation is carried out with the more refined setup, when the smallest size of spheres is used. This phenomena may be due to small irregularities in the geometry and application of the loads. The smaller the spheres the bigger the effect and the influence of such irregularities in the final results.

y = 60.571x + 2.175
R² = 0.2647
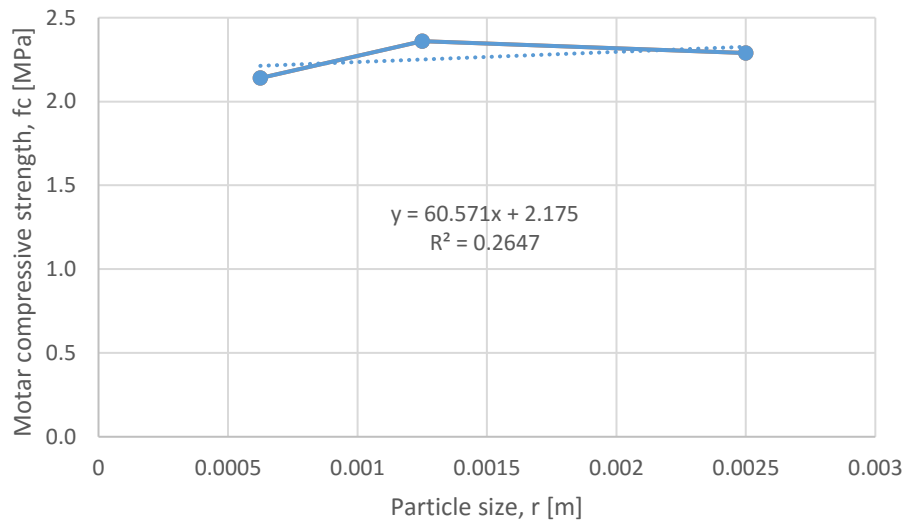
Figure 47: Linear regression of the parametric analysis (particle size influence).

Since the smaller is the size of the sphere, the more spheres are needed to model the same volume and therefore the more expensive the simulation becomes (computationally speaking) it can be concluded that the "refinement" of the model will not provide better results and time and resources can be saved by using a coarser discretization.
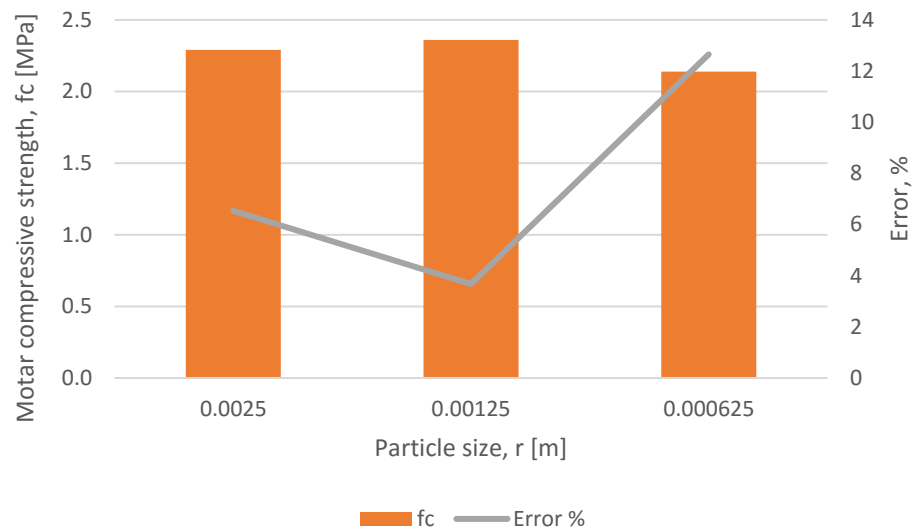
Figure 48: Error % for the values obtained of compressive strength (particle size influence).

The results of the DEM simulation are presented in Figure 50 ($r = .00125\ m$) and in Figure 51 ($r = .000625\ m$). In Figure 49 a typical failure, known as Hourglass failure, present in brittle materials subjected to uniaxial compression can be seen. It can be noticed that the displacements and contact damage reproduce by the DEM simulation are in good agreement with such kind of failure. Graphs stress-strain match as well the expected behavior of mortar under the described load conditions.

Figure 49: Typical Hourglass failure mode presented on brittle materials subjected to uniaxial compression (Canella, 2014).

(a)

(b)

(c)

(d)
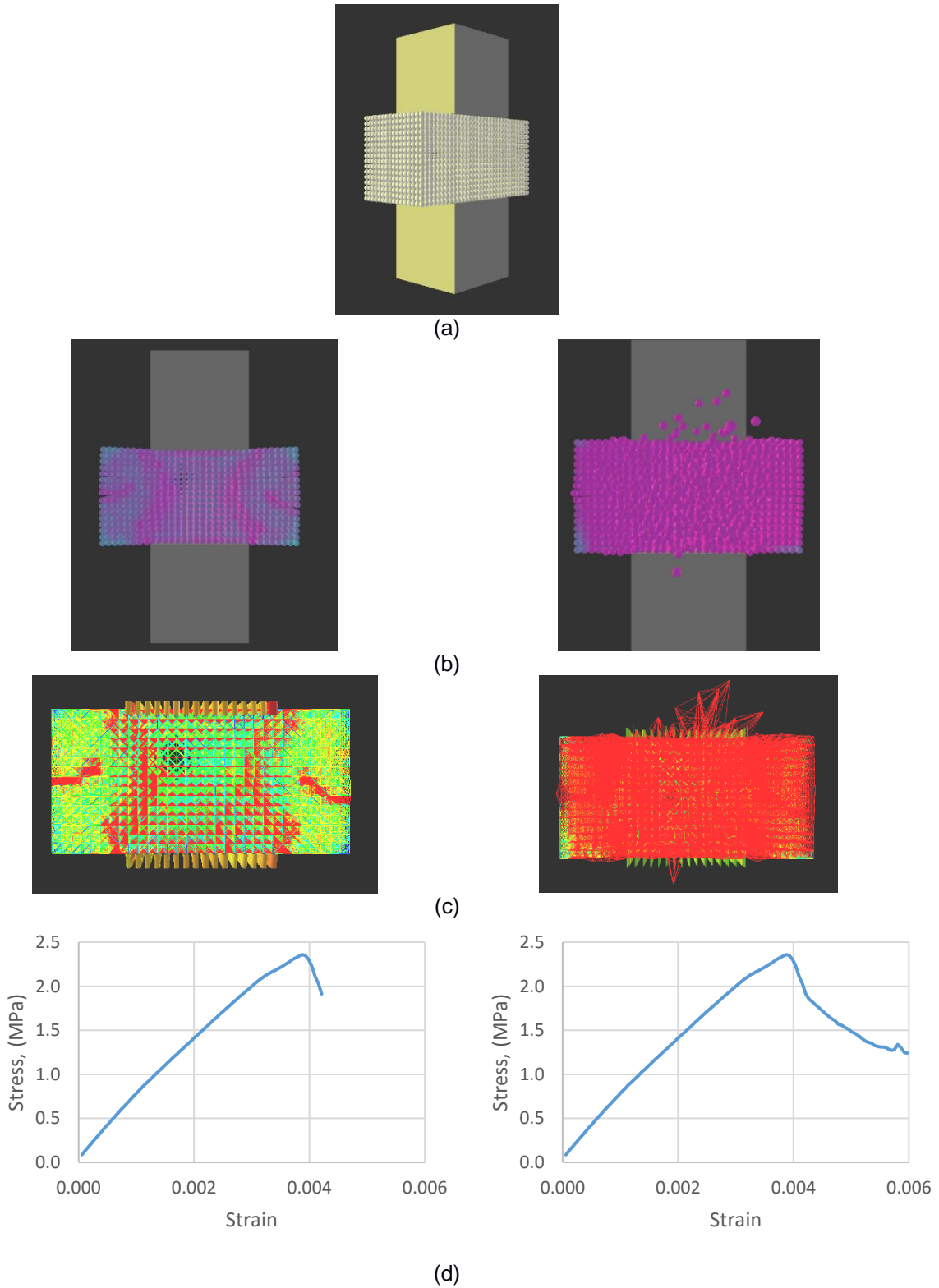
Figure 50: Mortar compression test DEM simulation results for $r = 0.00125\ m$; (a) Geometry, (b) Displacements, (c) Contact damages, (d) Graphs stress-strain.

(a)

(b)

(c)

(d)
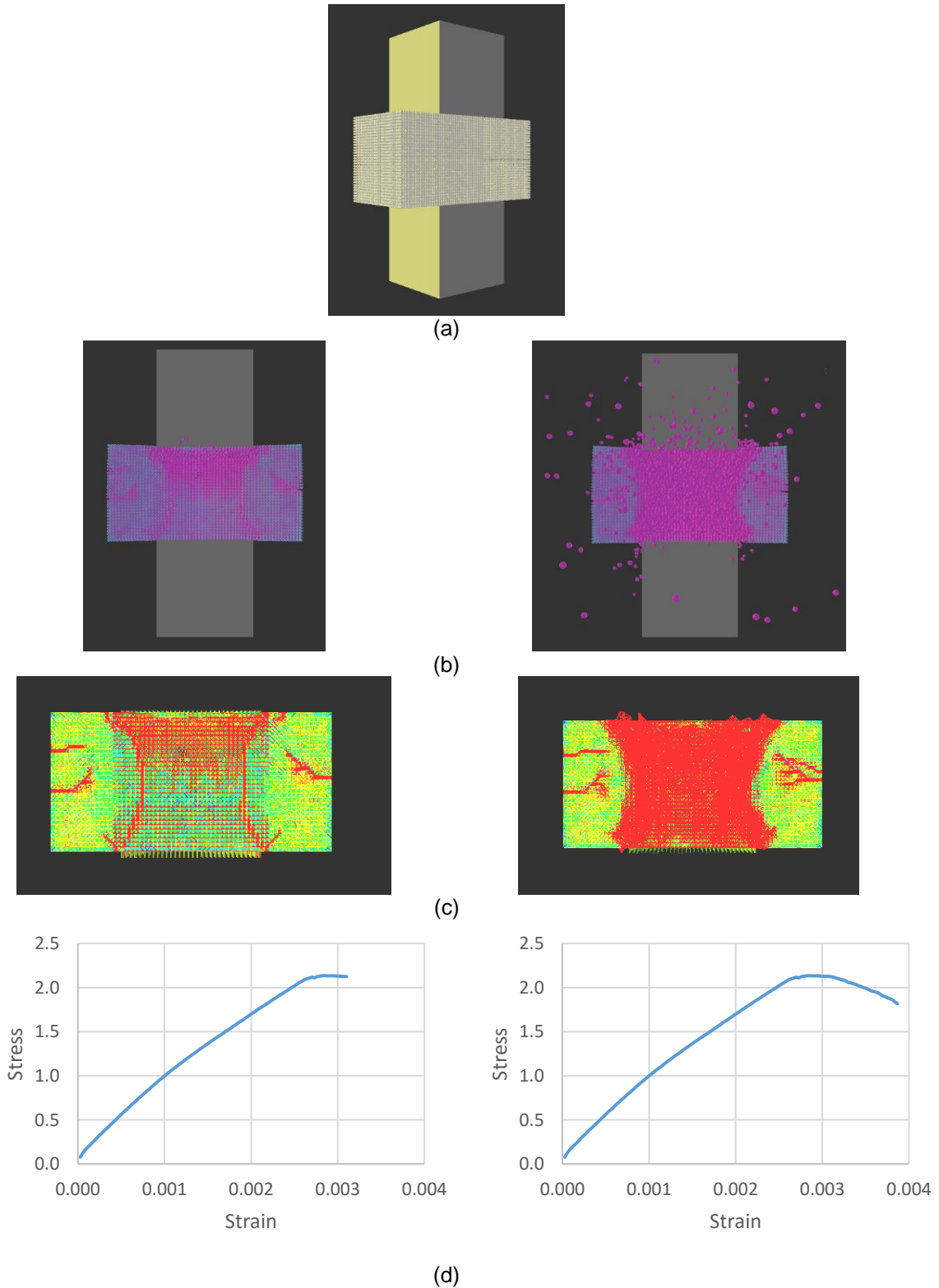
Figure 51: Mortar compression test DEM simulation results for r=0.000625 m; (a) Geometry, (b) Displacements, (c) Contact damages, (d) Graphs stress-strain.

4.2.2 Parametric analysis: Thickness reduction

The values obtained for the compressive strength of the mortar, f_{cm}, after the variation in the thickness of the specimen as well as the computation of the percentage error in comparison with the target value provided by (Marastoni , 2016) are presented in Table 9. It was expected that by reducing the thickness of the specimen the values of the compressive strength will be similar to the modeling of the whole test and that the percentage error will remain under the threshold of 10 %. Such assumptions will have validate the simplifications adopted in order to carry out the simulation of the triplet tests. Unfortunately, they were not corroborated and quite big variations on the results were observed.

Table 9: Parametric analysis (variation on the thickness of the specimen) results.

Mortar compression bricks			
$thickness/x$	f_c (MPa)	$f_{c\,target}$ (MPa)	$Error$ (%)
1	2.29	2.45	6.53
2	1.92	2.45	21.63
4	2.23	2.45	8.98
8	3.45	2.45	-40.82

The linear regression of the results is shown in Figure 52. The value obtained for the Pearson's lineal correlation coefficient is equal to 0.8919. This represents a strong positive correlation between the thickness reduction of the specimen, $thickness/x$, and the compressive strength of the mortar, $f_{cm}$. As for the determination coefficient, R^2, the value found is 0.7955. Which indicates that only 79.55 % of the variations in the values of f_{cm} can be described thanks to the variation on the thickness of the specimen, $thickness/x$. This is quite good value to relate both variables thus showing that the inferences made based on the regression equation obtained would provide accurate results.

Figure 53 displays the values obtained of the compressive strength of the mortar, f_{cm}, for every different step of thickness reduction. Along with this parameter, its correspondent percentage error is also plotted. It can be noticed that contrary to what was expected the biggest error occurs when the simulation is carried out with the simplification of using only one layer of spheres (when the thickness of the specimen is reduced by a factor equal to 8). This phenomena may be due to influence of a 3D behavior in DEM simulations. Since no spheres interact with each other out of the load plane the appropriate behavior of the material cannot be adequately described and therefore the percentage error increases drastically.

$$y = 0.1935x + 1.747$$
$$R^2 = 0.7955$$
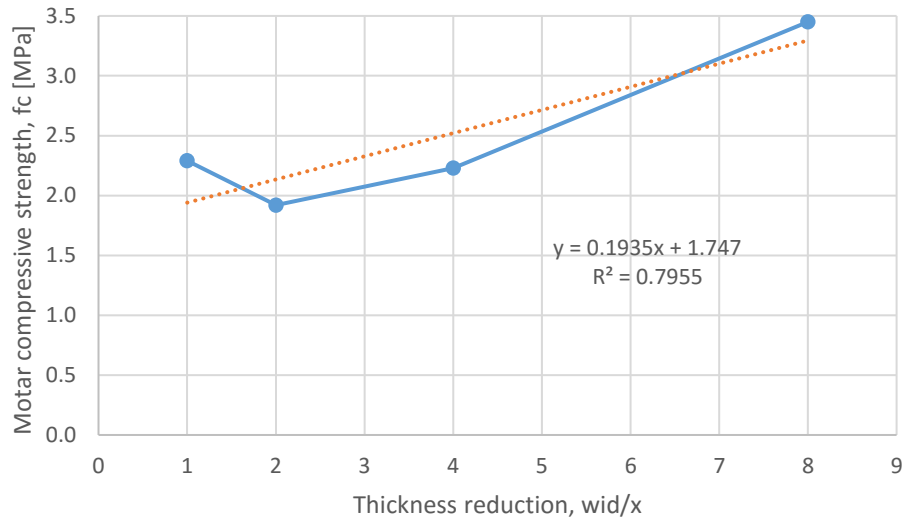
Figure 52: Linear regression of the parametric analysis (thickness reduction influence).

Even though this simplification does not provide accurate enough results, this was the only way, as justified before, to obtain calibration of the triplet tests. The main factor was as explained in last sections the high computational cost required by the DEM simulations combined with a quite strict time constraint. Further simulations need to be carried out in future research projects in which simulation of the whole thickness specimens for the triplet test must be performed. This may possibly require a readjustment on the interface mechanical properties values in order to better reproduce the behavior of masonry.
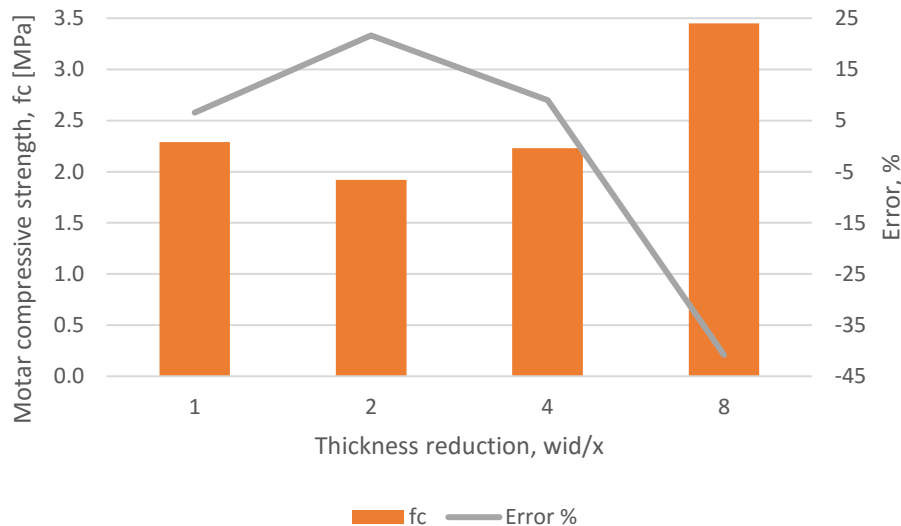
Figure 53: Error % for the values obtained of compressive strength (thickness reduction influence).

The results of the DEM simulation are presented in Figure 54 ($thickness/2$), Figure 55 ($thickness/4$) and Figure 56 ($thickness/8$). In Figure 49 a typical failure, known as Hourglass failure, present in brittle materials subjected to uniaxial compression can be seen. It can be noticed that the displacements and contact damage reproduce by the DEM simulation are not in good agreement with such kind of failure. Graphs stress-strain match in the other hand the expected behavior of mortar under the described load conditions.

(a)

(b)

(c)

(d)
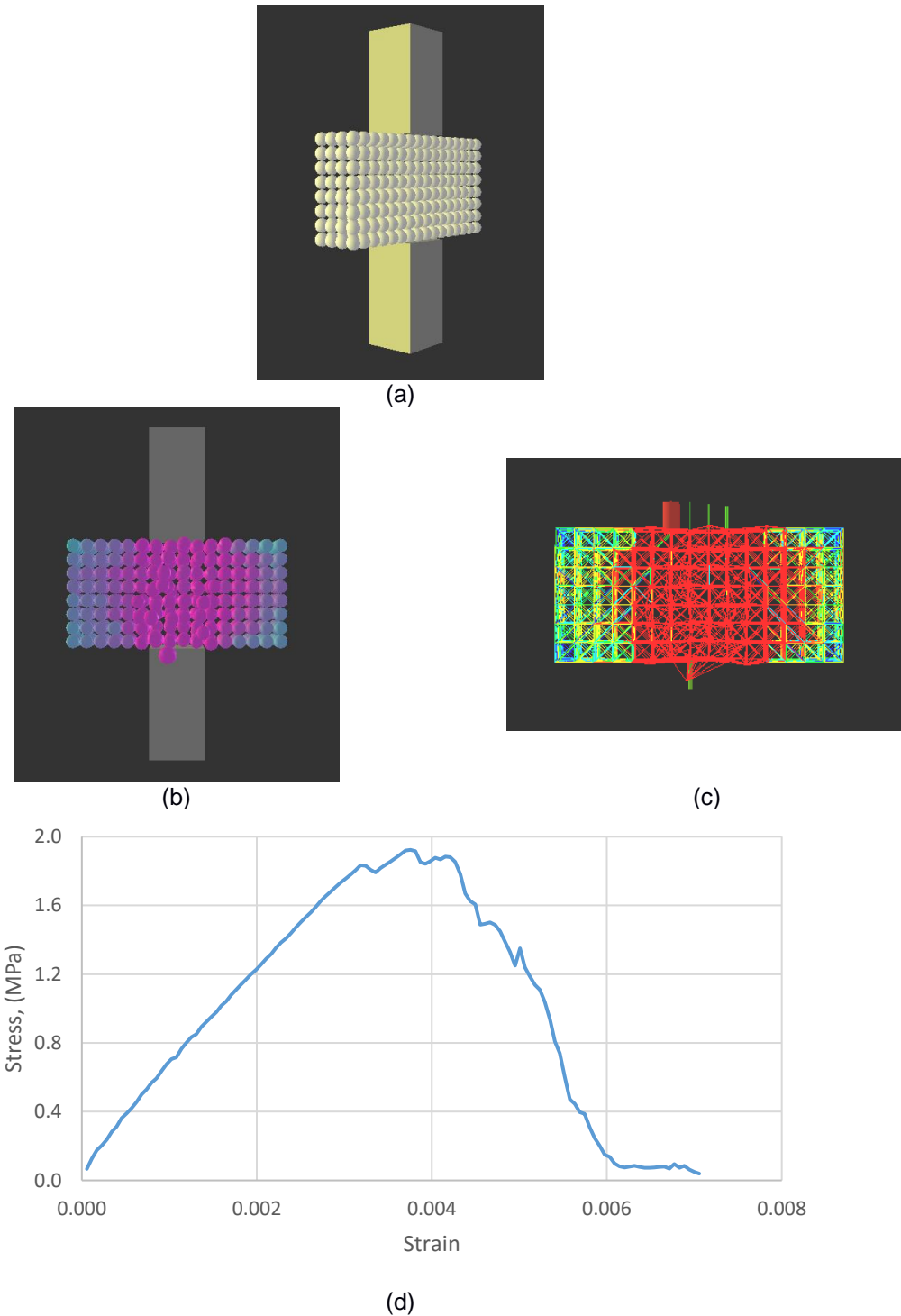
Figure 54: Mortar compression test DEM simulation results for thickness/2; (a) Geometry, (b) Displacements, (c) Contact damages, (d) Graphs stress-strain.

(a)

(b)

(c)

(d)
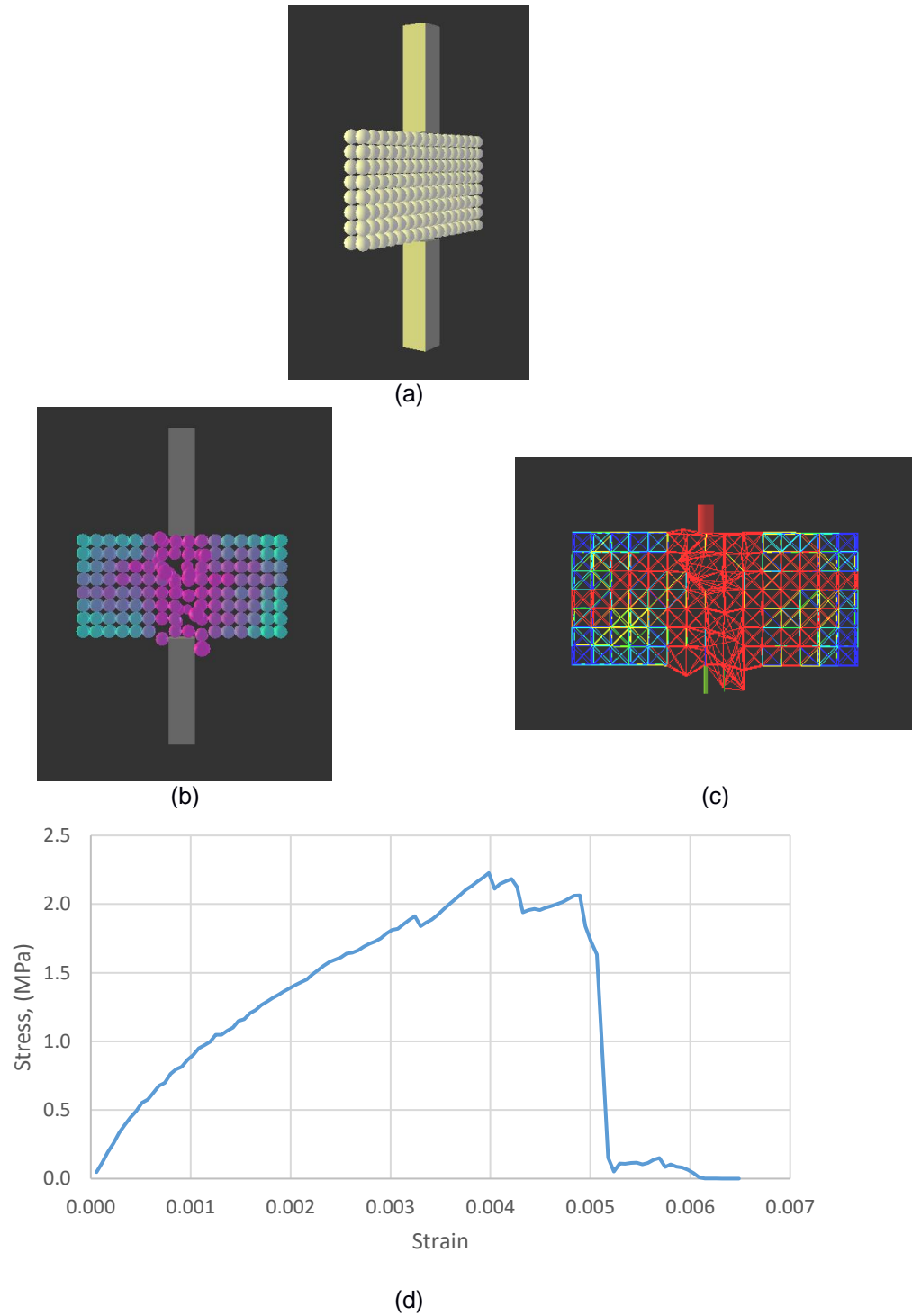
Figure 55: Mortar compression test DEM simulation results for thickness/4; (a) Geometry, (b) Displacements, (c) Contact damages, (d) Graphs stress-strain.

(a)

(b)

(c)

(d)
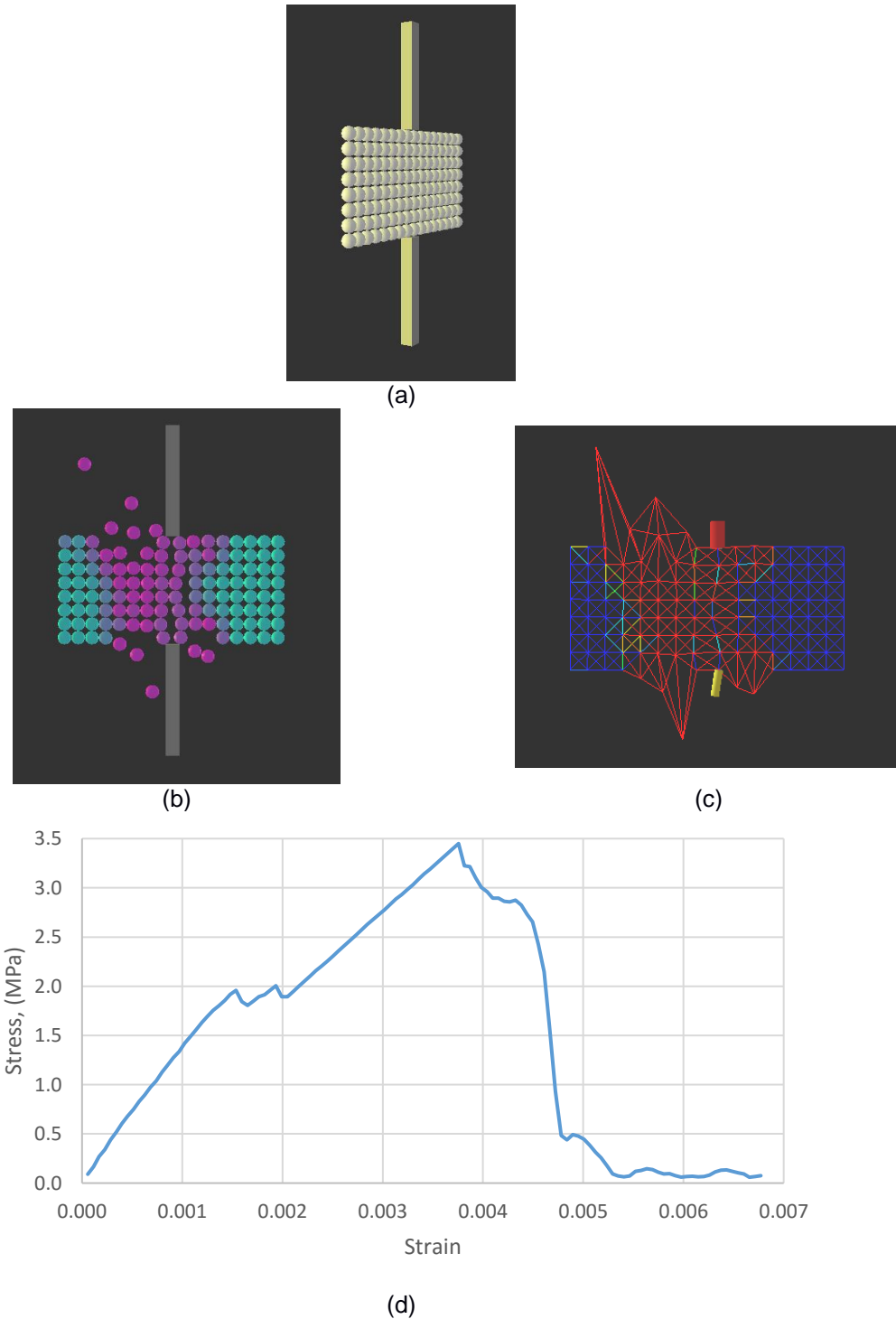
Figure 56: Mortar compression test DEM simulation results for thickness/8; (a) Geometry, (b) Displacements, (c) Contact damages, (d) Graphs stress-strain.

4.3 Comparison between DEM, FEM and experimental results

The aim of this sub-chapter is to present a contrast between the results obtained with FEM simulations, which is nowadays the most common technique for the modeling of masonry, developed by (Marastoni , 2016), and those performed with the use of DEM throughout this research. For such purposes, the triplet tests will be contrasted into detail. The values of the results obtained, the percentage error computed as well as the fracture mode depicted on both FEM and DEM simulations and on the experimental campaign are shown on the following sections.

Numerical values obtained for FEM and DEM simulations are presented in Table 10 and Table 11 respectively. In Table 10 all the results obtained by (Marastoni , 2016), for the three different levels of pre-compression (0.2, 0.6 and 1.0 MPa) and for the different FEM models (2D and 3D) as well as those found during the experimental campaign with its correspondent percentage errors, are shown. Since the DEM simulation was carried out only for a level of 0.2 MPa this is the only value (see Table 11) that can be compared. It can be seen that this simulation was able to obtain a quite accurate result, only 1.0 % error, which is more than 50 times smaller in comparison with the value obtained for the same case with both 2D and 3D FEM simulations.

Table 10: Experimental and numerical results obtained with FEM for ultimate loads on triplets tests (Marastoni , 2016).

Pre-compression (Mpa)	Fmax exp. (kN)	Fmax 2D (kN)	% error	Fmax 3D (kN)	% error
0.20	27.09	41.24	+ 52.00 %	40.96	+ 51.00 %
0.60	65.36	60.56	- 7.00 %	60.95	- 7.00 %
1.00	87.49	76.19	- 13.00 %	76.40	- 13.00 %

Table 11: Numerical results obtained with DEM for ultimate loads on triplets tests

Pre-compression (Mpa)	Fmax exp. (kN)	Fmax DEM (kN)	% error
0.20	27.09	27.36	- 1.00 %

On the other hand, better agreement is found in the development of the stress-strain curves for the FEM simulations than for those performed with the use of DEM. It can be seen that for both FEM simulations and experimental campaign curves the maximum load is attained even before applying

displacements of the order of 1 mm. Whereas that for the DEM simulation, such pick load is only reached after the 3 mm displacements. Behavior shown by Marastoni's curves is in perfect agreement with the general behavior of masonry under shear loads (see Figure 4) whereas that the behavior reproduced by the DEM simulations is more in agreement with the curve found on the experimental campaign. All curves show a quasi-constant load-displacement progression after have reached the pick load and suffered a subsequent small drop. This is due to the loss of cohesion and the afterwards pure contact friction of the materials and the effect of the pre-compression that prevent the elements to separate.

Similar differences in the behavior of the graphs were observed in Figure 10 by (Thavalingam , et al., 2001). It seems that in general DEM simulations describe a more ductile behavior of the failure in comparison with FEM simulations which depict a stiffer and more brittle behavior.
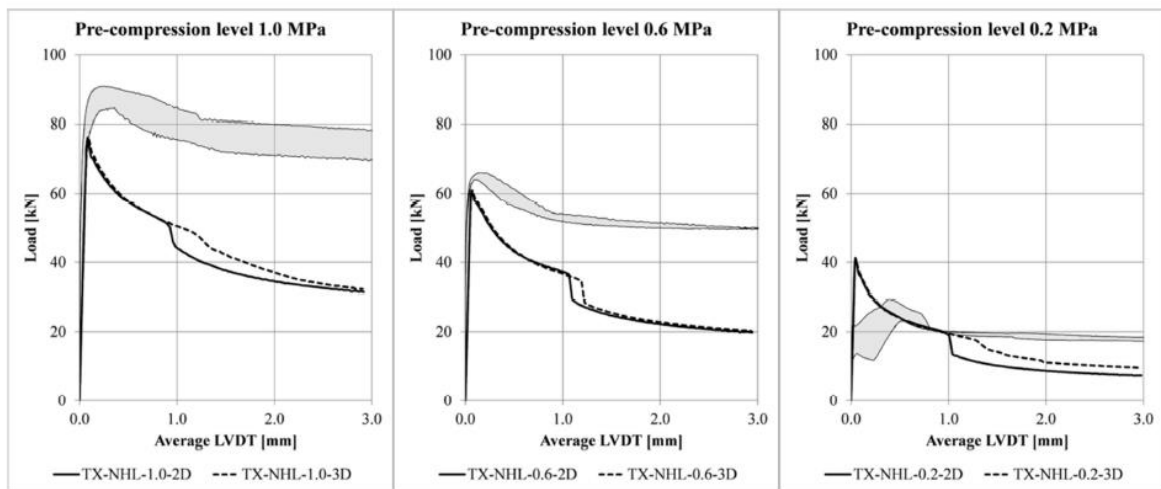
Figure 57: Numerical results obtained whit FEM compared to experimental tests for triplets (Marastoni , 2016).

As to what concerns the fracture mode, good agreement is reached for both types of simulation techniques in comparison to the one obtained on the experimental campaign. The failure appears on the interface elements and propagates vertically along the mortar. The fracture mode obtained in the laboratory can be seen in Figure 59, and the same for FEM simulation and DEM simulation in Figure 60 and Figure 61 correspondently.

Figure 58 presents the graphs described in the above paragraphs for both DEM and FEM simulations as well as for the experimental campaign results. It can easily be noticed that the behavior of FEM simulations show better agreement with the experimental campaign graphs that the one obtained by DEM. On the other hand the value of the maximum load attained is better match with DEM than with FEM simulations.
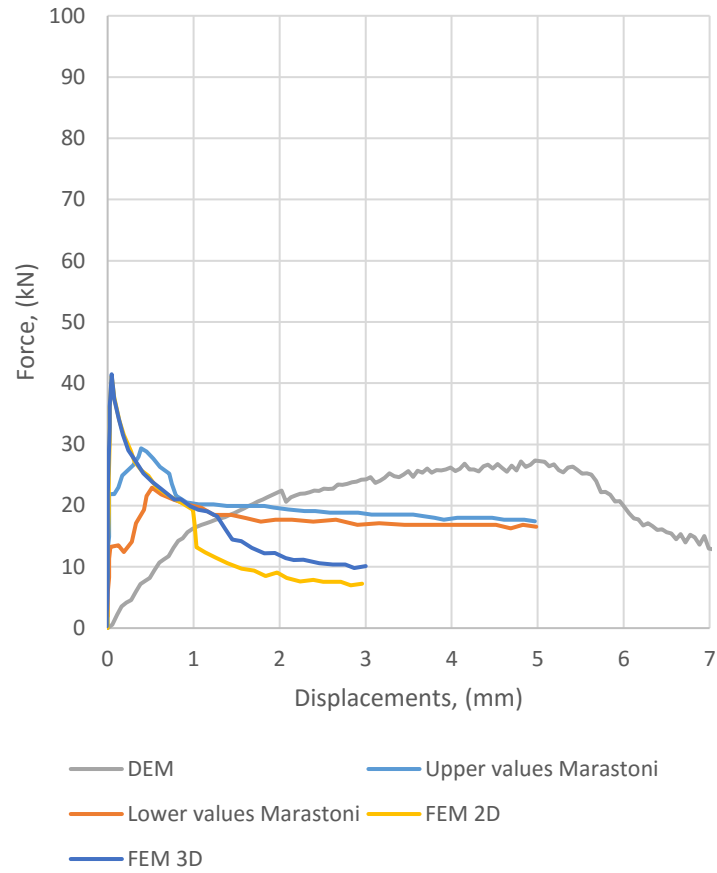
Figure 58: Numerical results comparison.

Figure 59: Experimental failure for triplets shear tests: internal crack formation (Marastoni , 2016).

step 38
Contour Fill of DAMAGE.

step 48
Contour Fill of DAMAGE.

step 53
Contour Fill of DAMAGE.

Damage d

1.00
0.89
0.78
0.67
0.55
0.44
0.33
0.22
0.11
0.00

step 54
Contour Fill of DAMAGE.

step 122
Contour Fill of DAMAGE.

step 123
Contour Fill of DAMAGE.
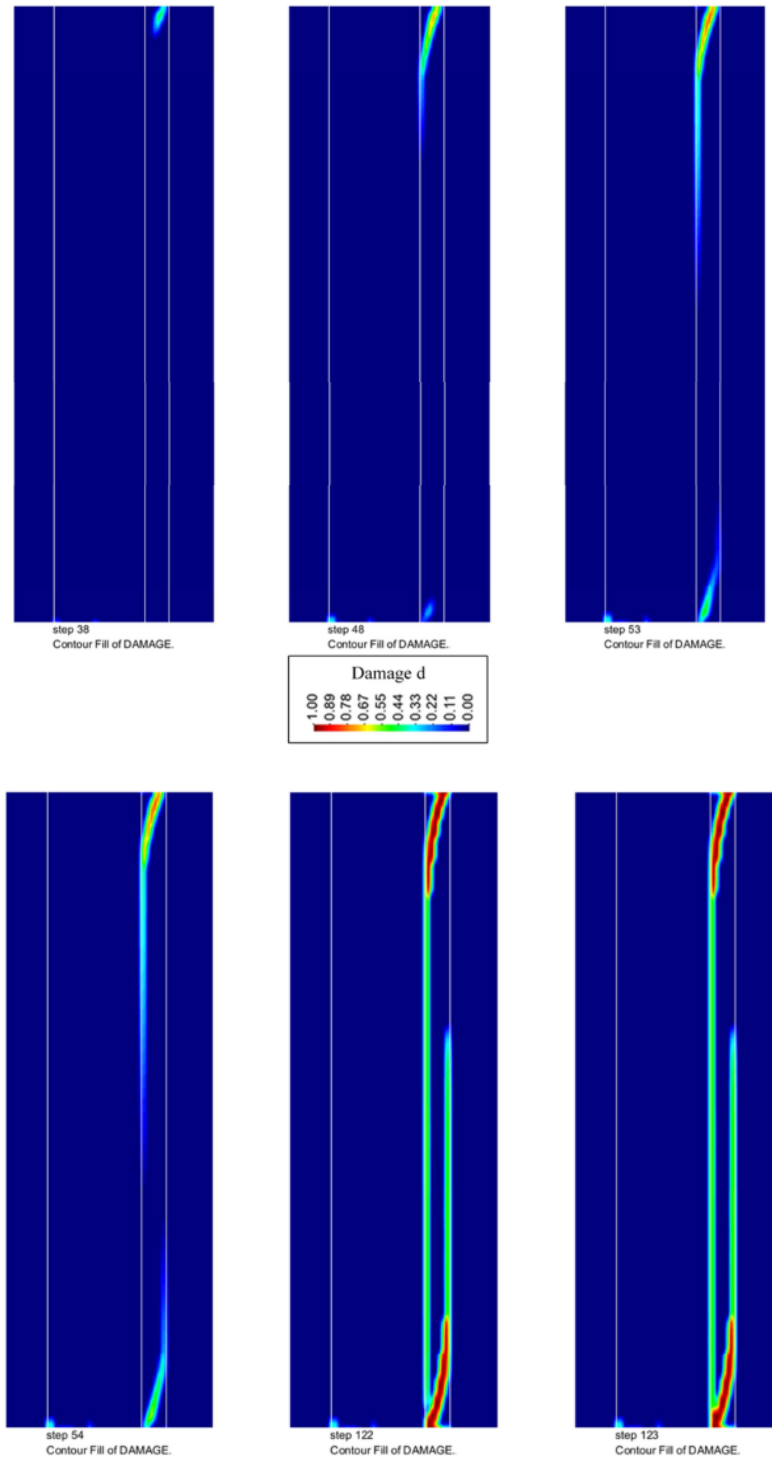
Figure 60: Damage contours for FEM simulation at different steps (Marastoni , 2016).
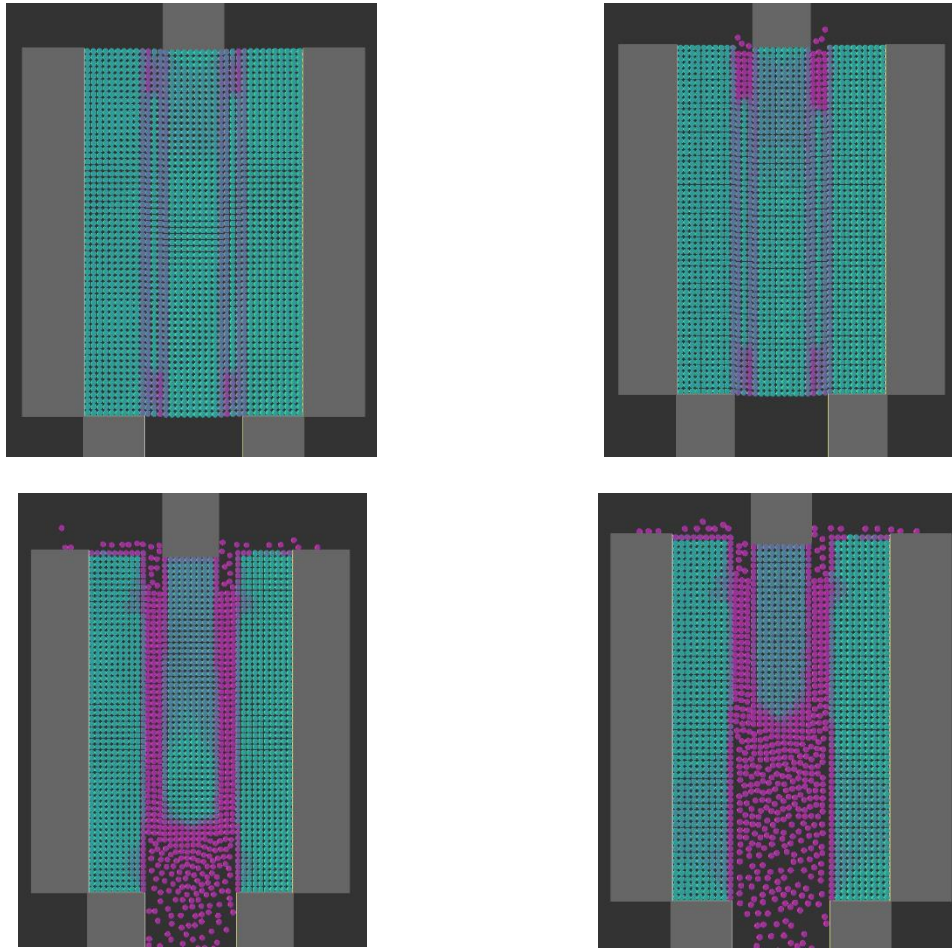
Figure 61: Sequential progression of the displacements during the triplet simulation (repeated).

4.4 Conclusions

4.4.1 Regarding compression cube tests

- *Mortar*: Percentage error smaller than 10 % was found (6.53 %) on the obtainment of the compressive strength of the material. Good agreement between experimental campaign and simulation was reproduce concerning the failure mode of the specimen.

- *Bricks*: Percentage error smaller than 10 % was found (1.52 %) on the obtainment of the compressive strength of the material. Unfortunately, no comparison could be carried out in order to contrast the failure mode between experimental campaign and simulation due to the lack of photographic evidence.

4.4.2 Regarding compression cylinder tests

- *Mortar*: Percentage error smaller than 10 % was found (8.38 %) on the obtainment of the Young's modulus of the material. Good agreement between experimental campaign and

simulation was reproduce concerning the failure mode of the specimen. Even though not direct comparison can be stablished since they represent different materials.

- *Bricks*: Percentage error smaller than 10 % was found (6.16 %) on the obtainment of the Young's modulus of the material. As for the compressive strength the error was as well within the acceptable range (0.42 %). In this case no agreement is achieved between laboratory and DEM simulation failure mode.

4.4.3   Regarding three points bending tests

- *Mortar*: Percentage error smaller than 10 % was found (2.7 %) on the obtainment of the flexural strength of the material. Good agreement between experimental campaign and simulation was reproduce concerning the failure mode of the specimen.

- *Bricks*: This is the only variable with a variation above the error threshold stablished of 10 % (35.54 %) in the obtainment of the flexural strength of the material. Unfortunately, no comparison could be carried out in order to contrast the failure mode between experimental campaign and simulation due to the lack of photographic evidence.

4.4.4   Regarding Triplet tests

Percentage error smaller than 10 % was found (1.0 %) on the obtainment of the maximum load resisted by the masonry specimen. Pretty good agreement was achieved on the DEM simulation to represent the failure mode. On the other hand the graph obtained differs significantly from the experimental one.

4.4.5   Regarding parametric analysis

- *Particle size influence*: The value obtained for the Pearson's lineal correlation coefficient represents a moderate positive correlation between the size of the particles, r, and the compressive strength of the mortar, f_c. As for the determination coefficient a quite small value was found (0.2647) thus showing that the inferences made based on the regression equation obtained would provide low accurate results.

    On the other hand, displacements and contact damage reproduce by the DEM simulation are in good agreement with typical failure of brittle materials subjected to uniaxial compression. Graphs stress-strain match as well the expected behavior of the material.

- *Thickness reduction influence*: The value obtained for the Pearson's lineal correlation coefficient represents a strong positive correlation between thickness reduction of the specimen $thickness/x$, and the compressive strength of the mortar, f_c. As for the determination coefficient a quite big value was found (0.7955) thus showing that the inferences made based on the regression equation obtained would provide accurate results.

On the other hand, displacements and contact damage reproduce by the DEM simulation in this case are not in agreement with typical failure of brittle materials subjected to uniaxial compression. Graphs stress-strain tough match the expected behavior of the material.

On the other hand, the assumptions that would have validate the simplifications adopted in order to carry out the simulation of the triplet tests such as that that by reducing the thickness of the specimen the values of the compressive strength will be similar to the modeling of the whole test and that the percentage error will remain under the threshold of 10 %, were not corroborated and quite big variations on the results were observed.

Further simulations need to be carried out in future research projects modeling this time the whole thickness of the triplet. This may possibly require a readjustment in the interface mechanical properties values in order to better reproduce the behavior of masonry.

4.4.6   Regarding comparison between DEM, FEM and experimental results

DEM simulation was able to obtain a quite accurate result, only 1.0 % error, which is more than 50 times smaller in comparison with the value obtained for the same case with both 2D and 3D FEM simulations presented by (Marastoni , 2016).

Better agreement is found in the development of the stress-strain curves obtained by the FEM simulations to reproduce the general behavior of masonry under shear loads. On the other hand, the behavior reproduced by the DEM simulations is more in agreement with the curve found on the experimental campaign.

As to what concerns the fracture mode, good agreement is reached for both types of simulation techniques in comparison to the one obtained on the experimental campaign.

5. CONCLUSIONS

5.1 Introduction

In this chapter an overview of the job done will be presented as well as the respective conclusions correspondent to the initially stablished general and specific objectives. A perspective into what could be developed in future research in order to complement the concepts and topics treated during this research will be proposed as well.

5.2 Regarding general objectives

The evaluation of the applicability of DEM to simulate the structural behavior of masonry at a detailed micro scale level and obtain the expected macro-scale level behavior, reproducing the response in terms of deflections, ultimate load and failure modes presents quite good results. Good agreement was shown in the description of failure modes and low percentage errors (below 10 %) were found on the computation of the parameters of interest such as strength of the material and maximum resistant load. Therefore it can be concluded that the use of DEM to model masonry is fully applicable.

Unfortunately due to its high computational cost limitations, this approach present important restrictions regarding the size of the elements that can be simulated. So far it is constrained to the simulation of small specimens and laboratory tests. This approach can also reproduce the response of specific elements on existing structures but it is still far from being capable of model a whole structure and obtain its response to applied loads. Such limitation can be overcome in the future by means of optimization of the code algorithms and thanks to the fast progress on computational processing capabilities.

5.3 Regarding specific objectives

5.3.1 Modify the constitutive law developed by (Smilauer, 2010) in order to be able to reproduce the structural behavior of masonry.

The modifications performed to the original code were of paramount importance in order to properly reproduce the response of the materials. The inclusion of the ξ_1 parameter, which takes into account the contribution of the tangential stress to the computation of the contact damage, helped to calibrate the mechanical properties of both brick and mortar. Whereas that the modification to directly manipulate the values that describe the interface was used to calibrate the composite behavior of the masonry.

The modification done to the formula to compute A_{eq} permitted to take into account the area that a cubic discretization will represent but with the advantage of keep modeling spheres which simplifies the detection of contacts and thus decreases the needed computational resources.

5.3.2 Simulate and calibrate simple compression cube tests, compression cylinder tests and three points bending tests for both mortar and brick.

Simulation of standard laboratory tests and calibration of mechanical properties of the component materials (bricks and mortar) were carried out successfully. Good agreement in the representation of the failure modes and low percentage errors (below 10 %) were found for all target parameters except in the case of the brick flexural strength, f_{tb}.

Regarding compression cube tests

- *Mortar*: Percentage error smaller than 10 % was found (6.53 %) on the obtainment of the compressive strength of the material. Good agreement between experimental campaign and simulation was reproduce concerning the failure mode of the specimen.
- *Bricks*: Percentage error smaller than 10 % was found (1.52 %) on the obtainment of the compressive strength of the material. Unfortunately, no comparison could be carried out in order to contrast the failure mode between experimental campaign and simulation due to the lack of photographic evidence.

Regarding compression cylinder tests

- *Mortar*: Percentage error smaller than 10 % was found (8.38 %) on the obtainment of the Young's modulus of the material. Good agreement between experimental campaign and simulation was reproduce concerning the failure mode of the specimen. Even though not direct comparison can be stablished since they represent different materials.
- *Bricks*: Percentage error smaller than 10 % was found (6.16 %) on the obtainment of the Young's modulus of the material. As for the compressive strength the error was as well within the acceptable range (0.42 %). In this case no agreement is achieved between laboratory and DEM simulation failure mode.

Regarding three points bending tests

- *Mortar*: Percentage error smaller than 10 % was found (2.7 %) on the obtainment of the flexural strength of the material. Good agreement between experimental campaign and simulation was reproduce concerning the failure mode of the specimen.
- *Bricks*: This is the only variable with a variation above the error threshold stablished of 10 % (35.54 %) in the obtainment of the flexural strength of the material. Unfortunately, no comparison could be carried out in order to contrast the failure mode between experimental campaign and simulation due to the lack of photographic evidence.

5.3.3   Simulate and calibrate triplets test for composite shear behavior of masonry.

The simulation of the composite behavior of masonry as well as the calibration of the interface mechanical properties parameters was achieved with high accuracy level. Percentage error smaller than 10 % was found (1.0 %) for the maximum load resisted by the masonry specimen. Pretty good agreement was achieved on the DEM simulation to represent the failure mode. On the other hand the graph obtained differs from the experimental one.

Similar differences in the behavior of the graphs were observed in Figure 10 by (Thavalingam , et al., 2001). It seems that in general DEM simulations describe a more ductile behavior of the failure in comparison with FEM simulations which depict a stiffer and more brittle behavior.

5.3.4   Carry on a parametric analysis in order to study the influence of the size of the particles and the influence of simplified 2D models to describe the behavior of 3D specimens.

The parametric analysis performed allowed to study the influence of two variables, particles size and thickness reduction of the specimens, in the final results. Such procedure demonstrated the high susceptibility on the variation of the geometry setup of DEM simulations. Simplifications of 3D models using only one layer of spheres ("2D model") are not so straight forward as they are in FEM plane stress or plane strain equivalent simplifications (not even under symmetric geometry and load cases). Nonetheless, this was the only viable option to obtain the presented results on time. Special care must be taken when such assumptions are adopted in future simulations.

Particle size influence

The value obtained for the Pearson's lineal correlation coefficient represents a moderate positive correlation between the size of the particles, r, and the compressive strength of the mortar, f_c. As for the determination coefficient a quite small value was found (0.2647) thus showing that the inferences made based on the regression equation obtained would provide low accurate results.

On the other hand, displacements and contact damage reproduce by the DEM simulation are in good agreement with typical failure of brittle materials subjected to uniaxial compression. Graphs stress-strain match as well the expected behavior of the material.

Thickness reduction influence

The value obtained for the Pearson's lineal correlation coefficient represents a strong positive correlation between thickness reduction of the specimen $thickness/x$, and the compressive strength of the mortar, f_c. As for the determination coefficient a quite small value was found (0.7955) thus showing that the inferences made based on the regression equation obtained would provide accurate results.

On the other hand, displacements and contact damage reproduce by the DEM simulation in this case are not in agreement with typical failure of brittle materials subjected to uniaxial compression. Graphs stress-strain tough, match the expected behavior of the material.

Furthermore, the assumptions that would have validate the simplifications adopted in order to carry out the simulation of the triplet tests such as that by reducing the thickness of the specimen the values of the compressive strength will be similar to the modeling of the whole test and that the percentage error will remain under the threshold of 10 %, were not corroborated and quite big variations on the results were observed. Special care must be taken when such assumptions are adopted in future simulations.

5.3.5 Compare the results obtained by DEM with those presented by (Marastoni , 2016) from experimental campaigns and FEM simulations.

DEM simulation was able to obtain a quite accurate result, only 1.0 % error, which is more than 50 times smaller in comparison with the value obtained for the same case with both 2D and 3D FEM simulations presented by (Marastoni , 2016).

Better agreement is found in the development of the stress-strain curves obtained by the FEM simulations to reproduce the general behavior of masonry under shear loads. On the other hand, the behavior reproduced by the DEM simulations is more in agreement with the curve found on the experimental campaign.

As to what concerns the fracture mode, good agreement is reached for both types of simulation techniques in comparison to the one obtained on the experimental campaign.

5.4 Further research perspectives

In order to explore in a deeper and more extended way the topics presented on this dissertation, the following points are proposed:

- Identify the influence of the velocity of the application of loads or displacements in the simulations with by means of a sensitivity analysis.
- Optimize the mechanical properties parameters of brick and mortar in order to improve results on triplet and other kind of composite masonry behavior tests.
- Perform the rest of the pre-compression triplet tests simulations (at 0.6 and 1.0 MPa) as well as a whole thickness simulation.
- Use other type of element for discretization (cubes instead of spheres for instance) and evaluate the validity of the discretization of masonry components for each type of discrete element.

- Simulate other laboratory tests: stack masonry compression tests, Brazilian tests and whole masonry walls subjected to compression-shear loads in order to extent the use of DEM simulations to reproduce the response of masonry structures under several load conditions.

6. REFERENCES

Bui, T. T. & Limam, A., 2012. *Masonry walls under membrane or bending loading cases: experiments and discrete element analysis.* Stirlingshire, Civil-Comp Press.

Bui, T. T. et al., 2010. *Masonry walls submitted to out-of-plane loading: experimental and numerical study.* Dresden, IMS.

Bui, T. T., Limam, A. & Bui, Q. B., 2014. Characterisation of vibration and damage in masonry structures: experimental and numerical analysis. *European journal of environmental and civil engineering,* 18(10), pp. 1118-1129.

Canella, E., 2014. *Experimental characterization of the compressive behaviour of brick-lime mortar masonry..* Barcelona: UPC.

Cundall, P. A. & Strack, O. D. L., 1979. A discrete numerical model for granular assemblies. *Géotechnique,* 29(1), pp. 47-65.

EC6, 1996. *Eurocode 6: Design of masonry structures.* s.l.:s.n.

EN 1015-11, 1999. *Methods of test for mortar for masonry - Part 11: Determination of flexural and compressive strength of hardened mortar.,* s.l.: European Standard.

ICOMOS, 1964. *The Venice Charter,* Venice: s.n.

ICOMOS, 1994. *The Nara document on authenticity,* Nara: s.n.

ISCARSAH, 2003. *Recommendations for the analysis, conservation and structural restoration of architectural heritage.,* Victoria Falls: ICOMOS.

Itasca, C. G. I., 2016. *Itasca.* [Online]
Available at: http://www.itascacg.com/software/pfc/distinct-element-method
[Accessed 16 06 2016].

Lourenco, P. B., 1998. Experimental and numerical issues in the modelling of the mechanical behaviour of masonry.. In: *Structural analysis of historical constructions II.* Barcelona: CIMNE, pp. -.

Lourenco, P. B., Peña, F. & Lemos, J. V., 2006. *Modeling the dynamic behavior of masonry walls as rigid blocks..* Lisbon, s.n.

Lourenco, P. B. & Pina-Henriques, J., 2006. Masonry compression: a numerical investigation at the meso-level. *International journal for computer-aided engineering and software,* 23(4), pp. 382-407.

Marastoni , D., 2016. *Advanced minor destructive testing for the assessment of existing masonry.* Bologna: Universita di Bologna.

Mohebkhah, A., Tanimi, A. A. & Moghadam, H. A., 2008. Nonlinear analysis of masonry-infilled steel frames with openings using discrete element method.. *Journal of constructional steel research,* Volume 64, pp. 1463-1472.

NIKER, 2010. Inventory. In: *New integrated knowledge based approaches to the protection of cultural heritage from earthquake-induced risk..* s.l.:POLIMI, p. 53.

Oñate, E., Su, O., Labra, C. & Rojek, J., 2012. Comparative study of different discrete element models and evaluation of equivalent micromechanical parameters. *International journal of solids and structures,* Volume 49, pp. 1497-15717.

Recarey, C. A. et al., 2005. *Estudio de estimación de parámetros constitutivos en el método de elementos discretos o de partículas.* Barcelona: CIMNE.

Reccia, E., Cazzani, A. & Cecchi, A., 2012. FEM-DEM modeling for out of plane loaded masonry panels: a limit analysis approach. *The open civil engineering journal,* 6(1), pp. 231-238.

Roca, P., Cervera, M., Gariup, G. & Pela, L., 2010. Structural analysis of masonry historical constructions, classical and advnaced approaches.. *Archive of computational methods in engineering,* 17(3), pp. 299-325.

Roca, P., Molins , C. & Marí, A. R., 2005. Strength capacity of masonry wall structures by the equivalent frame method. *Journal of structural engineering,* Volume 131, pp. 1601-1610.

SAHC, 2015-2016. *SAHC Coursework Notes.* Prague: SAHC.

SAHC, n.d. *SAHC Website.* [Online]
Available at: http://www.msc-sahc.org/content.asp?startAt=2&categoryID=636
[Accessed 10 06 2016].

Sarhosis, V., Tsavdaridis, K. D. & Giannopoulos, I., 2014. Discrete element modelling of masonry infilled steel frames with multiple window opennings subjected to lateral load variations.. *The open construction and building technology journal,* Volume 8, pp. 93-103.

Smilauer, V., 2010. *Cohesive particle model using the discrete element method on the Yade platform.* Prague: CVUT.

Smilauer, V., 2015. *Yade documentation 2nd ed..* [Online]
Available at: http://yade-dem.org/doc/

Smoljanovic, H., Zivaljic, N. & Nikolic, Z., 2013. A combined finite-discrete element analysis of dry stone masonry structures. *Engineering structures,* Volume 52, pp. 89-100.

Thavalingam , A., Bicanic, N., Robinson, J. I. & Ponniah, D. A., 2001. Computational framework for discontinous modelling of masonry arch bridges. *Computers and structures,* Volume 79, pp. 1821-1830.

UNESCO, 1972. *Convention concerning the protection of the world cultural and natural heritage..* Paris, s.n.

Vasconcelos, G., n.d. *Masonry components,* Guimaraes: University of Minho.

Zhuge, Y., 2008. Distinct element modelling of unreinforced masonry wall under seismic loads with and without cable retrofitting. *Transactions of Tianjin University,* Volume 14, pp. 471-475.